Monthly Scientific-Technical and Production Journal

The Paton WELDING JOURNAL

March 2002 # 3

English translation of the monthly «Avtomaticheskaya Svarka» journal published in Russian since 1948

Founders: *The National Academy of Sciences of Ukraine*
The E.O. Paton Electric Welding Institute of the NAS of Ukraine, International Association «Welding»
Publisher: *International Association «Welding»*

Editorial and advertising offices:
E.O. Paton Electric Welding Institute,
International Association «Welding»,
11, Bozhenko str., 03680, Kyiv, Ukraine
Tel.: (38044) 227 67 57
Fax: (38044) 268 04 86
E-mail: journal@paton.kiev.ua
http://www.nas.gov.ua/pwj

State Registration Certificate
KV 4790 of 09.01.2001

Subscriptions:
$460, 12 issues per year,
postage and packaging included.
Back issues available

CONTENTS

HYBRID LASER-MICROPLASMA WELDING OF THIN SECTIONS OF METALS*

B.E. PATON[1], V.S. GVOZDETSKY[1], I.V. KRIVTSUN[1], A.A. ZAGREBELNY[1], V.F. SHULYM[1] and V.L. DZHEPPA[2]
[1]The E.O. Paton Electric Welding Institute, NASU, Kyiv, Ukraine
[2]Design Bureau «Yuzhnoye», Dnepropetrovsk, Ukraine

Prototype of an integrated plasmatron for microplasma, laser and laser-microplasma welding of different metals up to 3 mm thick in the automatic and manual modes was designed and manufactured. Technological cababilities of this plasmatron for welding steels, titanium and aluminium alloys in the microplasma, laser and hybrid modes were studied. The efficiency of utilisation of energy of the laser beam and microplasma arc combined in a hybrid process was proved to substantially increase. Laser-microplasma welding using the microplasma arc with alternating-polarity current pulses is shown to have a high potential for joining aluminium alloys.

Key words: *electric arc, laser beam, integrated plasmatron, microplasma, laser, laser-microplasma welding, metal penetration, space, investigations*

Combined or hybrid processes implemented by a combined use of two different heat sources, e.g. laser beam and electric arc, are receiving currently an increasingly wide acceptance. Initial investigations into laser-arc welding processes [1–5] showed that they possess a number of peculiarities which cannot be explained by simple superposition of properties of the involved heat sources if taken separately. In particular, it was found that the combined effect exerted on metals by laser and arc heat sources was accompanied by a fundamental increase in the coefficient of utilisation of energy of both heat sources and stability of movement of the arc spot over the workpiece surface. All this allows a more than 1.5 times increase in a maximum depth of penetration, as compared with the corresponding laser process, which is especially important for the cases when low-power lasers are employed, and makes it possible to improve stability and almost double the productivity of the corresponding arc process.

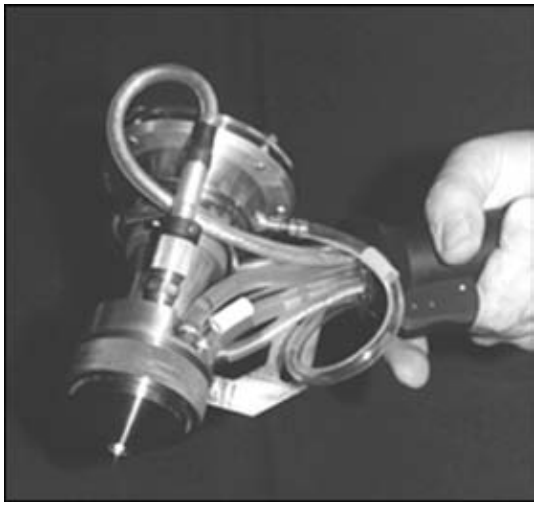

Figure 1. Integrated plasmatron for microplasma, laser and hybrid welding in automatic and manual modes

Results obtained from utilisation of the constricted (plasma) arc instead of the freely burning one in the hybrid process turned out to be much more encouraging. Two diagrams of realisation of the laser-plasma welding are known in the art — one with laser beam and plasma arc located at an angle to each other [6, 7], and the other with their coaxial arrangement [8–11]. The latter seems to be more rational, as it provides the required coaxiality of thermal and dynamic effects of the heat sources on the weld pool surface.

Unfortunately, employment of traditional plasmatrons for realisation of hybrid laser-plasma welding within the frames of the diagram under consideration is hardly possible. Coaxial arrangement of the laser beam and plasma arc requires the use of specialised devices, i.e. integrated laser-arc plasmatrons [8–10, 12], the main peculiarity of which is design of the cathode unit (refractory tubular cathode or system of pin cathodes located on the circumference) to allow focused laser radiation to be introduced into the welding zone along the axis of the plasma-shaping channel.

This article considers results of tests of a prototype of the integrated laser-arc plasmatron intended for automatic and manual welding of different metals up to 3 mm thick, as well as results of studies of technological capabilities of hybrid welding of stainless steels, titanium and particularly aluminium alloy from the standpoint of its future application under the space conditions.

Experimental equipment. The prototype of a versatile plasmatron for microplasma, laser and laser-microplasma welding in the automatic and manual modes was designed and manufactured for implementation of the process of hybrid welding of thin sections of metals (Figure 1). This device is a two-electrode plasmatron with a tungsten cathode 1.5 mm in di-

*This study was performed in collaboration with the Bremen Institute for Applied Beam Technologies (BIAS) Bremen, Germany.

ameter (for operation at straight polarity (SP)) and tungsten electrode 2.5 mm in diameter (for operation under conditions of alternating-polarity pulses of the electric current), installed inside a water-cooled casing. Electrodes are located diametrically at an angle of 21° to the plasmatron axis with a possibility of moving along their axes. The plasmatron has a replaceable plasma-shaping nozzle made from copper or molybdenum, with a diameter of the exit channel equal to 2–3 mm, and an external nozzle for shielding gas feeding.

The suggested plasmatron design allows the focused laser beam to be introduced into the welding zone along the axis of the plasma-shaping nozzle. For this purpose the casing is fitted in its upper part with an interfacing unit (Figure 2) to connect the plasmatron to the standard focusing system RSY-FM- D160Z HP/2 with an adjustable focal distance of 160±6 mm, which is connected to the light guide via the RSY-KM-B120 HPW/2 collimator. The plasmatron is designed for operation with the up to 2 kW YAG laser (size of the focal spot is 0.6–1.0 mm) at SP currents of the microplasma arc equal to 50 A and using alternating-polarity pulses of the electric current with an amplitude of 35 A.

Preliminary tests of the plasmatron in the arc mode, conducted by the E.O. Paton Electric Welding Institute using an experimental power supply, included:

- identification of conditions for excitation and maintenance of the pilot and main arcs;
- checking functioning of the plasmatron at straight and reverse polarities;
- preliminary evaluation of technological capabilities of the plasmatron in the microplasma welding mode.

With the plasma-shaping nozzle channel diameters of 2–3 mm and plasma gas (argon) flow rates of 0.5–0.8 l/min the pilot arc was ignited in a stable manner both between each of the electrodes and the nozzle and between the two electrodes (pilot arc current 5–7 A, open-circuit voltage 60 V). The best shape of the pilot arc with a plasma flame going out of the nozzle exit section was observed in its burning between the plasmatron electrodes.

At a distance from the nozzle exit section to the sample surface equal to h = 2–3 mm, the SP main arc had a stable excitation and burning at an electric current of I = 32–53 A at an arc voltage of U = = 36–29 V ($U_{o.-c}$ = 80 V). Increasing the open-circuit voltage to 100 V provided the stable excitation and burning of the main arc at a distance to the sample surface increased to 6 mm.

Samples 1.0, 1.5, 2.0 and 3.0 mm thick of stainless steel 12Kh18N9T (C — 0.12; Cr — 17.0–19.0; Ni — 8.0–10.0 wt.%), titanium alloy OT-4 (3.5Al–1.5Mg) and aluminium alloy AMg3 (Al–3Mg) were used to evaluate technological capabilities of the plasmatron in the microplasma welding mode.

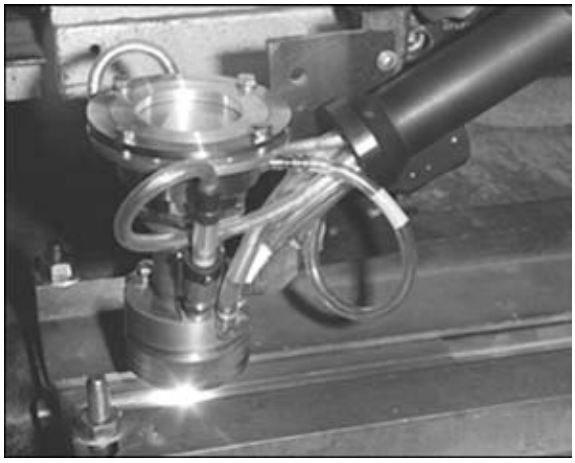

Figure 2. Microplasma welding at straight polarity using the integrated plasmatron

The samples welded were mounted on a fixed welding table (using a copper backing), and the plasmatron was fixed on the bracket of a welding tractor and moved during welding operations (Figure 2). The technological experiments conducted included penetration of the samples and welding of butt joints. The plasma gas, shielding gas flow rate and the cooling water consumption were 0.6, 8.0, 1.5 l/min, respectively.

It was established that welded joints with full penetration of samples of stainless steel and titanium alloy, 1.0–1.5 mm thick, could be produced by microplasma welding with the SP arc using the plasmatron developed. In that case the welding parameters were as follows: I = 43–52 A, U = 29–25 V and welding speed v_w = 0.24–0.40 m/min. Width of the welds thus produced was no more than 3.5 mm. No marked undercuts or sags of the welds were seen, and the welds produced at a distance to a sample equal to 2 mm looked better.

The experiments conducted revealed the insufficiency of shielding of the weld pool surface, which resulted in a marked oxidation of the welds. As an increase in the shielding gas flow rate failed to provide an improvement of the shielding quality, certain modifications were made on the plasmatron: diameter of the exit orifice of the shielding nozzle was increased and a fluoroplastic gas-distribution ring was made and installed into this nozzle. Although these measures provided some improvement of the quality of shielding of the welding zone, that was obviously insufficient (further optimisation of the weld shielding system is required).

Unfortunately, the attempts made at the first stage of the test to determine capabilities of the plasmatron in operation under conditions of the alternating-polarity current pulses failed because of unstable functioning of the available power unit.

Technological experiments. Technological experiments on utilisation of the integrated plasmatron for welding in the arc, laser and hybrid modes were conducted at BIAS in Germany. A standard power unit for arc and plasma welding of the MESSER TIG

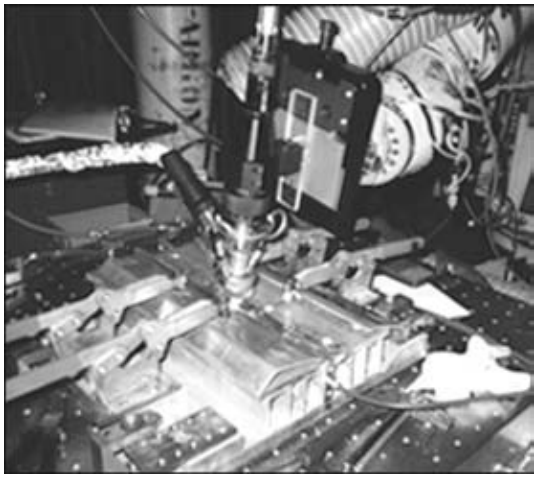

Figure 3. Integrated plasmatron with the laser focusing system connected to it

450 AC/DC-P model with a smooth regulation of the electric current from 5 to 450 A, including the plasma and shielding gas feed and control system and the closed loop of fluid cooling of the plasmatron with its switching-on interlocking, was used as a power supply. The power supply provided a stable ignition of the pilot arc both between one of the electrodes and the plasmatron nozzle and between the two electrodes. In addition, this power supply was equipped with an oscillator to ignite the main arc by breaking down the arc gap, which allowed the AC and DC main arc to be ignited further on without the use of the pilot arc.

Robot-manipulator of the KUKA Company was used to move the plasmatron during welding. The control system of the robot made it possible to program all the parameters of the welding process, which, in addition to advantages, also had certain drawbacks, as it did not allow adjustment of the process parameters during welding. In all the experiments the welding speed was set at a level of 0.25 m/min, which, firstly, is a mean value of the speed of manual welding operations, and, secondly, a limited power of the plasmatron did not allow operation at higher speed values. The distance from the exit section of the copper plasma-shaping nozzle to a sample was set to be equal to 2.0–2.5 mm, and diameter of the plasmatron nozzle channel was selected to be equal to 2.5 mm. Samples of the same materials and thicknesses, as those used for the tests conducted at the PWI, were employed for the above technological experiments.

Microplasma welding. SP microplasma welding of samples of the above stainless steel and titanium alloy was carried out to determine technological capabilities of the plasmatron in the arc mode operation. Six butt joints of samples 1.0–1.5 mm thick were welded at different combinations of the arc current I = 40–51 A, and penetration of four samples 2–3 mm thick was performed for subsequent comparison of the depth and width of penetration in microplasma welding with the corresponding parameters of the welds produced by laser and hybrid welding.

Samples of aluminium alloy were welded by the AC microplasma arc using alternating-polarity pulses with a frequency of 125 Hz. Duration of the SP and RP pulses was 65 and 35 %, respectively. Welding was performed at arc currents of 25–35 A. It should be noted that at a microplasma arc current of 25 A the sample 3 mm thick was just cleaned without a marked penetration. Welding of butt joints also provided a good cleaning of the surface, but no quality welds with full penetration were produced even at their thickness of 1 mm and an arc current of 35 A.

Laser welding. Upon completion of experiments in the arc mode, the plasmatron was connected to the focusing system RSY-FM-D160Z HP/2 (Figure 3) and then, via a flexible light guide, to the pulsed periodic-wave diode-pumped laser RS D4 044 (Rofin-Sinar Company) with a maximum power of 4.4 kW. Position of focus of the laser beam was adjusted (focal spot size 0.8–1.0 mm) relative to the sample surface at a distance from the plasmatron exit section equal to h = 2 mm.

The experiments started with welding and penetration of samples of stainless steel and titanium alloy. Prior to welding of aluminium samples, to prevent ingress of a reflected radiation into the optical system of the laser, the plasmatron with the focusing system installed on it was turned to a angle of 8° to a vertical line (see Figure 3). This provided correction of position of focus of the laser beam with respect to the sample surface. Ten samples of the above materials 1.5–3.0 mm thick were treated at a laser power of 500–1500 W. As a result, full penetration of the stainless steel samples 2 mm thick was achieved at a laser power of 1 kW. For the titanium and aluminium alloy samples 3 mm thick the penetration depth was 1.2 mm at a laser power of 0.5 kW (OT-4) and 0.8 mm at a laser power of 1.5 kW (AMg3). In the case of welding butt joints on the aluminium alloy samples 1.5 mm thick, the attempts to achieve full penetration by increasing the laser power from 1.0 to 1.3 kW failed.

Hybrid welding. Prior to beginning of the welding experiments in the combined mode, the plasmatron with the connected focusing system was electrically insulated from the robot. The switching on trials revealed problems with the cooling system of the 4.4 kW RS D4 044 laser. Therefore, the continuous-wave laser RS CW 020 with a power of 2 kW, the beam of which was focused on a workpiece into a spot 0.6 mm in size, was connected to the plasmatron.

Penetration in the hybrid mode (laser + AC microplasma arc) was performed on aluminium alloy samples 3 mm thick. At an arc current amplitude of 25 A and laser beam power of 1.0–1.5 kW the samples were penetrated to a depth of less than 1 mm, resulting in a strong blackening of the welds, although in the case of using only the AC microplasma arc this effect was not seen and a normal cleaning of the aluminium surface occurred. The plasmatron was disassembled (protective and plasma-shaping nozzles were re-

moved) and leakage of cooling water was detected in a soldered joint in the lower part of the plasmatron casing. It is likely that this leakage was a cause of deterioration of shielding of the welding zone. Despite this fact, penetration of two aluminium alloy samples 3 mm thick was performed in the hybrid welding mode (the plasmatron was disconnected from the cooling system during those experiments). The hybrid welding conditions were as follows: laser power was 1.2 kW and amplitude of the microplasma arc current pulses was 25 and 35 A, respectively.

Experimental results. The developed integrated plasmatron for microplasma, laser and hybrid welding allows butt joints with full penetration of the stainless steel and titanium alloy samples up to 1.5 mm thick to be produced in operation in the DCSP arc mode at an arc current of 40–50 A and welding speed of 0.25 m/min.

Power of the plasmatron in welding aluminium alloy using alternating-polarity pulses (current amplitude 25 A) allows no more than cleaning of the surfaces of samples 3 mm thick, without visible traces of melting (Figure 4, *a*). The attempts to produce butt joints in aluminium samples 1 mm thick showed that the above power was also insufficient for making the welds with full penetration. Therefore, power of the plasmatron should be increased (maximum value of the arc current should be increased at least to 50 A) for operation at the alternating-polarity pulses.

The experiments with laser welding showed that at the selected welding speed values the butt welded joints could be produced on the stainless steel and titanium samples 1.5 mm thick at a laser power of 750–800 W. At this point we have to note some instability of the process, which results in formation of regions on the weld surface differing in appearance, although the welding process parameters were unchanged.

The attempts to provide full penetration in making butt joints on aluminium alloy samples 1.5 mm thick by increasing the laser power to 1.3 kW failed. Most probably, the laser power required to do it should be not less than 1.5 kW. In addition, in laser welding of aluminium the oxide film is not cleaned from the surface during welding, which results in an insufficiently high quality of the welds.

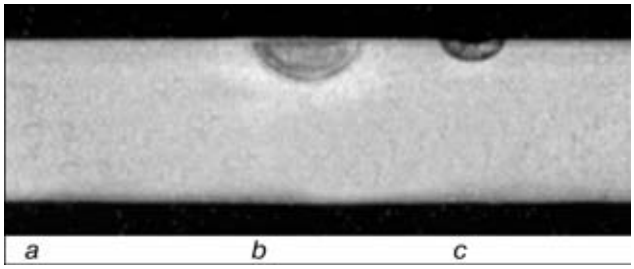

Figure 4. Macrosection of a sample of aluminium alloy AMg3 3.0 mm thick with penetration by microplasma (*a*), hybrid (*b*) and laser (*c*) welding (welding speed 0.25 m/min) using the alternating-polarity arc (current amplitude 25 A, frequency 125 Hz, plasma gas (Ar) flow rate 0.5 l/min) and YAG laser (radiation power 1.2 kW, focal spot size 0.6 mm)

Penetration of samples of different materials, 2–3 mm thick, at the same speed (0.25 m/min) was performed for comparative evaluation of different welding methods (microplasma, laser and hybrid welding). In particular, in the mode of SP microplasma welding and an arc current of 50 A the penetration depth was 0.6 mm for stainless steel and 2 mm for titanium alloy (the weld width was 2.8 and 5.5 mm, respectively). In the laser welding mode at a laser power of 1 kW and at the same welding speed a full penetration of the stainless steel sample 2 mm thick was achieved, while at a laser power of 0.5 kW the penetration depth was 0.8 mm for stainless steel and 1.2 mm for titanium alloy (at the weld width of 1.4 and 2.5 mm, respectively).

No visible melting was seen in penetration of aluminium alloy 3 mm thick by the AC microplasma arc (amplitude value of the current was 25 A) (see Figure 4, *a*), whereas with an increase in amplitude of the current pulses to 35 A the penetration depth was 0.7 mm, weld width was 4 mm and penetration area was 2 mm^2 (Figure 5, *a*). In laser penetration of the same sample at a speed of 0.25 m/min the penetration depth was 0.4 mm at a laser power of 1.2 kW (Figures 4, *c* and 5, *b*).

The combined use of the 1.2 kW laser beam and the AC microplasma arc (current amplitude 25 A) the depth of penetration of a sample 3 mm thick at a welding speed of 0.25 m/min is 0.8 mm, weld width is 2 mm and penetration depth is 1.1 mm^2 (see Figure 4, *b*), whereas in the case of laser welding (at the same beam power and welding speed) they were 0.4 mm, 1.2 mm and 0.35 mm^2, respectively (see Figure 4, *c*), and in the case of microplasma welding

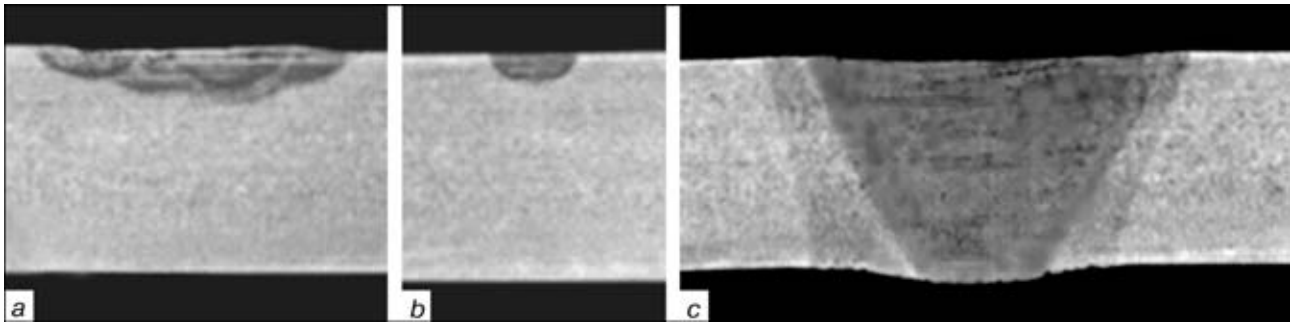

Figure 5. Macrosection of a sample of aluminium alloy AMg3 3.0 mm thick with penetration by microplasma (*a*), laser (*b*) and hybrid (*c*) welding using the alternating-polarity arc (current 35 A) and YAG laser (radiation power 1.2 kW)

using the 25 A arc there was no penetration at all (see Figure 4, *a*).

Results of using the 35 A microplasma arc and laser beam of the same power (1.2 kW) in the hybrid process turned out to be even more interesting. In particular, full penetration was achieved on the AMg3 sample 3 mm thick with a weld width of 4.9 mm and cross section area of 10.6 mm^2 (see Figure 5, *c*). While comparing the data obtained with the results of penetration of a sample in laser and microplasma welding performed separately (compare Figure 5, *a–c*), it can be noticed that the penetration area in hybrid welding of aluminium alloy is more than 4 times in excess of the sum of the corresponding areas in laser and microplasma welding performed separately. This is indicative of a substantial increase in the efficiency of utilisation of energy of the heat sources when they are combined in the hybrid process.

Unfortunately, for the above reasons only one penetration sample was made in this mode. Therefore, the results obtained require additional confirmation, for which it is necessary to make a plasmatron which would allow welding in the mode of alternating-polarity pulses at a current of 50 A and higher.

CONCLUSION

Preliminary studies of technological capabilities of the integrated plasmatron for microplasma, laser and laser-microplasma welding allow a conclusion of the high potential of hybrid welding of aluminium alloys using the laser beam and the microplasma arc burning in a mode of alternating-polarity pulses of the electric current. On the one hand, this combination enables cleaning of the aluminium surface during welding, which cannot be achieved in purely laser welding, and, therefore, improvement of quality of the produced welded joints. On the other hand, the combined use of the two heat sources allows a substantial increase in the efficiency of utilisation of energy of each of them, which makes hybrid welding very attractive for application, e.g. repair under conditions of space flying vehicles.

We believe it would be very appropriate to continue the original investigations for development of a higher-power integrated plasmatron, designed for current of up to 100 A for operation in the mode of alternating-polarity pulses, and intended for the use in combination with the 1.5–2.0 kW diode laser, for experimental and theoretical investigations of the process of hybrid welding of thin and medium sections of aluminium alloys, as well as in-depth investigation of technological capabilities of this process.

1. Steen, W.M., Eboo, M. (1979) Arc augmented laser welding. *Metal Construction*, **7**, 332–335.
2. Steen, W.M. (1980) Arc augmented laser processing of materials. *J. Appl. Phys.*, **11**, 5636–5641.
3. Diebold, T.P., Albright, C.E. (1984) «Laser-GTA» welding of aluminium alloy 5052. *Welding J.*, **6**, 18–24.
4. Matsuda, J., Utsumi, A., Katsumura, M. et al. (1988) TIG or MIG arc augmented laser welding of thick mild steel plate. *Joining and Materials*, **1**, 31–34.
5. Gorny, S.G., Lopota, V.A., Redozubov, V.D. et al. (1989) Peculiarities of heating of metal in laser-arc welding. *Avtomatich. Svarka*, **1**, 73–74.
6. Walduck, R.P., Biffin, J. (1994) Plasma arc augmented laser welding. *Welding & Metal Fabrication*, **4**, 172–176.
7. Walduck, R.P. *Enhanced laser beam welding*. Pat. 5866870 USA, Int. Cl. B 23 K 10/00, 26/00. Publ. 02.02.99.
8. Paton, B.E. (1995) Upgrading welding methods — one of the ways of improving quality and cost effectiveness of welded structures. *Avtomatich. Svarka*, **11**, 3–11.
9. Dykhno, I.S., Krivtsun, I.V., Ignatchenko, G.N. *Combined laser and plasma arc welding torch*. Pat. 5700989 USA, Int. Cl. B 23 K 26/00, 10/00. Publ. 21.12.97.
10. Som, A.I., Krivtsun, I.V. (2000) Laser + plasma: search for new possibilities in surfacing. *The Paton Welding J.*, **12**, 34–39.
11. Gvozdetsky, V.S., Krivtsun, I.V., Chizhenko, M.I. et al. (1995) Laser-arc discharge: Theory and application. *Welding and Surfacing Rev.*,Vol. 3, Part 3.3. Harwood A.P.
12. Krivtsun, I.V., Chizhenko, M.I. (1997) Principles of design of laser-arc plasmatrons. *Avtomatich. Svarka*, **1**, 16–23.

PROBLEMS IN APPLICATION OF NEW STEELS OF INCREASED AND HIGH STRENGTH IN WELDED STRUCTURES

V.I. KIRIAN and **L.M. MIKHODUJ**
The E.O. Paton Electric Welding Institute, NASU, Kyiv, Ukraine

Peculiar features of formation of structure and properties of welded joints of sparsely-alloyed structural steels of the new generation are described. The importance of a careful approach to the selection of materials and processes of their welding to prevent the susceptibility of weld metal and HAZ to brittle fractures. Principal problems of analysing a delayed fracture of welded joints of these steels are considered.

Key words: *sparse alloying, structural steels, welding consumables, cold resistance of metal, fitness-for-purpose, cold resistance of HAZ, delayed fracture, lamellar fracture, research program*

Rational use of low-alloyed steels of increased and high strength in welded structures can decrease effectively the metal content of machines, mechanisms and engineering works. The range of strength characteristics of these materials is wide enough. Minimum their yield strength is usually 400–450 MPa. Upper levels of strength characteristics of these steels depend on purpose and special features of service of structures. Thus, for example, in construction of bridges in the USA and Japan [1, 2] steels with 600–800 MPa yield strength are used. Metal with higher strength characteristics ($\sigma_{0.2}$ = 800–1000 MPa) is used at present in Germany and Sweden for road machinery [3–5]. It is planned in the near future to use steels with 1100 MPa yield strength in construction works [6] and in manufacture of crane equipment (Figure 1).

In most cases these are steels of the new generation. They contain up to 0.12 % carbon, limited amounts of manganese, molybdenum, niobium, titanium, boron, and can be alloyed additionally with nickel, chromium and other elements (up to 3–4 % amount in total). To attain the required complex of properties both thermal and thermomechanical treatment (controllable rolling, etc.) is used.

Table 1 gives the chemical composition and mechanical properties of some grades of steels of the new generation with 440–900 MPa yield strength [5, 8–14], designed for manufacture of welded structures.

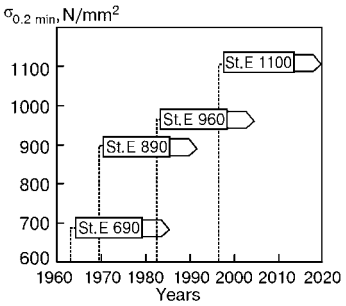

Figure 1. Strength characteristics of fine-grained structural steels used in welded structures of mobile cranes [7]

Among them, steels 09G2SYuch and 09KhG2SYuch (DNAOP 0.00-1.07–94, RD 22-16–96, SNiP 2.05.03–84) are used in domestic production.

The undoubted advantage of structural steels of the new generation is their higher cold resistance (Figure 2) and sparse alloying as compared with materials known earlier. At the same time these steels, due to the latter, represent a specific group of materials, which can provide premises during their technological processing for the reduction of resistance of welded structures to a delayed and brittle fracture.

Therefore, the aim of the present work was to analyse the effect of peculiarities of selection of methods and conditions of welding on formation of properties determining the technological and service strength of welded joints made from steels of increased and high strength of the new generation.

Cold resistance of steels and their welded joints. New compositions and technologies of manufacture have opened up the wide opportunities for achievement of high characteristics not only of strength, but also cold resistance of structural steels. As a result, the great difference in minimum guaranteed level of requirements to the impact strength of rolled metal was observed (KCV = 27–200 J/cm^2) (Table 1). These values of the impact strength are far from optimum, from the one hand, coming from the conditions of prevention of initiation of a brittle fracture and economic aspects of general-purpose welded metal structures, and, from the other hand, they make the problem of providing cold resistance of metal of welded joints at the level of base metal (BM) almost impossible in many cases. In this connection, the establishment of minimum guaranteed values of impact strength KCV depending on the temperature condi-

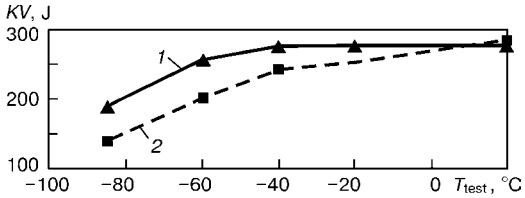

Figure 2. Impact energy of steel S460ML of 40 mm thickness at different test temperatures. Specimens were cut along (*1*) and transverse (*2*) rolling direction [9]

Table 1. Chemical composition and mechanical properties of steels of increased and high strength of the new generation [5, 8–14]

Steel grade	*Elements, wt.%*									
	C	*Si*	*Mn*	*Cr*	*Ni*	*Mo*	*Cu*	*Al*	*Ti*	*Nb*
AS-50	0.08	0.27	1.37	–	–	–	0.01	0.054	0.007	0.03
06G2BD	0.04–0.08	0.20–0.50	1.30–1.60	< 0.20	< 0.035	0.05–0.08	0.15–0.30	0.02–0.05	0.02	0.03–0.05
09G2SYuch	0.08–0.11	0.30–0.60	1.90–2.20	–	–	–	0.30–0.60	0.04–0.07	–	–
S460ML	0.115	0.37	1.55	0.04	0.03	0.002	–	0.031	–	–
09KhG2SYuch	0.08–0.11	0.30–0.60	1.90–2.20	1.00–1.30	–	–	–	0.04–0.70	–	–
HSLA-80	0.05	0.37	0.48	0.68	1.02	0.22	1.26	0.015	0.004	< 0.03
10G2FB	0.10	0.40–0.60	1.60–1.80	–	0.30–0.60	–	–	–	0.02–0.06	0.03–0.08
09KhGNFB	0.10	0.40–0.60	1.60–1.80	0.70–0.80	0.70–0.90	0.20	–	–	0.02–0.06	0.03–0.08
15G2MFYuTRA	0.12–0.18	0.17–0.40	1.40–1.80	–	–	0.01–0.08	–	0.02–0.09	0.02–0.06	–
Alform 700 MC	0.08	–	1.35	–	–	–	–	0.03	0.18	0.06
Bissalloy 80	0.17	0.40	1.15	0.85	–	–	–	–	–	–
8CHT80 OP	0.11	0.27	0.86	0.54	0.88	0.44	0.24	–	–	–
NK-HITEN-780B	0.12	0.25	0.92	0.44	1.04	0.32	0.21	–	–	–
09KhG2NMFB	0.10	0.40–0.60	1.60–1.80	0.60–0.80	0.70–0.90	0.20	–	–	0.02–0.06	0.03–0.08
15G2KhNMFYu-TRA	0.12–0.18	0.17–0.40	1.40–1.80	0.30–0.60	0.30–0.60	0.10–0.25	–	0.02–0.09	0.02–0.06	–
8ANT80	0.13	0.24	0.75	0.55	0.94	0.40	0.25	–	–	–
St. E 890	0.16	0.45	1.00	0.80	2.00	0.50	–	–	–	–
WELDOX-900	0.15	0.22	1.40	0.25	–	0.50	–	–	–	–
DQ-125	0.11	0.10	0.79	0.52	1.46	0.52	0.03	0.05	0.01	< 0.03

Table 1 (cont.)

Steel grade	*Elements, wt.%*					*Other elements*	P_{cm}	C_{eq} *IIW*	*Mechanical properties*		
	N_2	*V*	*B*	*S*	*P*				$\sigma_{0.2}$, *MPa*	T_{test}, °C	KCV, J/cm^2
AS-50	0.002	0.003	0.001	0.001	0.008	W, Sn, Zr	0.16	0.32	440	–50	> 40
06G2BD	< 0.012	0.04–0.07	–	< 0.01	< 0.02	–	0.13–0.20	0.33–0.43	440	–70	> 50
09G2SYuch	–	–	–	< 0.015	< 0.02	Ce, Ca	0.20–0.27	0.41–0.51	450	–70	> 30
S460ML	0.005	0.05	–	0.003	0.014	–	0.21	0.39	460	–20	> 31
09KhG2SYuch	–	–	–	< 0.01	< 0.02	Ce, Ca	0.23–0.30	0.59–0.73	550	–70	> 30
HSLA-80	0.01	0.005	0.002	0.002	0.004	W, Sn, Zr	0.22	0.46	572	–50	> 59
10G2FB	–	0.08	–	< 0.01	< 0.02	Ca, Zr, REM	0.20–0.22	0.40–0.46	590	–50	> 40
09KhGNFB	–	0.08	–	< 0.01	< 0.02	Ca, Zr, REM	0.24–0.27	0.60–0.68	685	–50	> 40
15G2MFYuTRA	–	0.08	0.001–0.005	< 0.01	< 0.02	Ca, Zr, REM	0.20–0.32	0.37–0.51	685	–40	> 30
Alform 700 MC	–	0.02	0.002	0.002	0.006	–	0.17	0.31	700	–20	> 40
Bissalloy 80	–	–	0.002	< 0.01	< 0.02	–	0.29	0.59	750	–20	> 60
8CHT80 OP	–	0.05	0.0016	0.004	0.013	–	0.25	0.53	751	–35	196
NK-HITEN-780B	–	–	0.001	0.002	0.008	–	0.25	0.51	768	–40	200
09KhG2NMFB	–	0.08	–	< 0.01	< 0.02	Ca, Zr, REM	0.27–0.32	0.59–0.68	785	–50	> 40
15G2KhNMFYu-TRA	–	0.16	0.001–0.005	< 0.01	< 0.02	Ca, Zr, REM	0.22–0.38	0.48–0.72	785	–40	> 30
8ANT80	–	0.05	0.002	0.01	0.013	–	0.26	0.53	834	–35	147
St. E 890	–	0.10	–	< 0.02	< 0.025	–	0.30	0.74	890	–60	> 27
WELDOX-900	–	–	0.002	< 0.01	< 0.03	–	0.30	0.53	900	–40	> 40
DQ-125	0.002	0.07	0.001	0.001	0.003	W, Sn, Zr	0.25	0.56	903	–50	> 40

tions of their service is rather important for the steels of the new generation of different classes designed for general-purpose welded metal structures. Such attempt was made for steels of 12–20 mm thickness with a yield strength $\sigma_{0.2}$ = 590–690 MPa (KCV = = 35 J/cm^2 at minimum service temperature) [15].

To provide cold resistance of welded joints of general-purpose metal structures, the minimum guaranteed level of requirements to impact strength KCV of BM is basic. In case of critical metal structures the requirements to the fracture toughness of welded joints is determined in accordance with a «fitness-for-purpose» conception, based on use of approaches and criteria of fracture mechanics.

Effect of thermal cycles of welding on strength and cold resistance of HAZ metal. Under the action of thermal cycles of welding (TCW) in HAZ the significant changes in BM properties occur, which can influence greatly the serviceability of welded joints. In this respect, the reduction in characteristics of strength and fracture toughness is most hazardous.

In all structural steels, which are subjected to polymorphous $\alpha \rightarrow \gamma \rightarrow \alpha$ transformations in welding, the following typical regions are usually observed [16, 17]: fusion (transition from HAZ metal to weld metal); overheating (temperature interval above 1050–1150 °C, when the intensive growth of primary grains occurs depending on the composition of steels); heating to temperatures above point A_3 (polymorphous transformations occur completely in metal); heating in interval of temperatures A_1–A_3 (zones with partial polymorphous transformation); heating below temperatures A_1. Width of these areas is changed (except the fusion region) and depends greatly on methods and parameters of welding (Table 2)

As a rule, the initial structure of steel is stable only up to transformation point A_1. At higher temperatures (in A_1–A_3 interval) the gradual changes in eutectoid are occurred, thus transforming into austenite. The final result of these processes is defined to a great extent by the composition and initial structure of BM. In case if it is ferritic-pearlitic or sorbitic, then the non-homogeneous structure with insufficient ductility and toughness may occur as a result of a short stay of metal within the interval of A_1–A_3 temperatures in HAZ. In welding of improved steels this difference in structure and properties of HAZ metal can be decreased significantly.

The structure of HAZ regions heated to temperatures above point A_1 is austenitic, not depending on the composition and methods of production of steels. Therefore, the form of thermal cycle or cooling rate have a decisive effect on their secondary structure and properties. At a delayed cooling (typical of the electroslag welding, and in some cases also of arc welding) the ferritic-pearlitic structures with a Widmannstaetten structures can occur in this zone. In HAZ region, being under the action of temperatures above 1050–1150 °C, $\alpha \rightarrow \gamma$ transformation at similar conditions can be accompanied also by an intensive growth of grains. The excessive cooling will promote the appearance of undesirable quenched structures in these zones.

Table 2. Effect of welding methods on width of HAZ regions [16]

Method of welding	*Width of HAZ regions, mm*		
	Above A_1	*Above* A_3	*Overheating zone*
Manual arc	3–8	0.3–1.0	0.1–0.3
Shielded-gas	3–8	0.3–1.0	0.1–0.3
Submerged-arc	3–15	0.3–2.0	0.1–0.5

Mixture of ferrite, bainite (including lower), martensite and residual austenite is most often formed in the near-weld metal [16].

Thus, HAZ structures of structural steels of the new generation can be quite different. However, the study of near-weld metal, and also regions of HAZ metal, characterized by an increased susceptibility to the growth of primary grains is seemed to be most important. For this purpose, a complex analysis of peculiarities of proceeding of structural transformations and formation of properties of metal of a local region of welded joints is required. Metallographic examinations in this case envisage the use of well-known methodological procedures (construction of diagrams of continuous decay of austenite, fractography, methods of optical or electron microscopy, etc.). As the length of this region is small (≈ 0.1–0.5 mm), the use of only standard mechanical tests of samples, manufactured from real welded joints, is not examplary.

Analysis of a possible reduction in characteristics of strength and embrittlement of HAZ metal should be realized preferably using samples-simulators, produced in accoradnce with welding thermal cycles in units of type «Thermorestor-W», «Gleeble» or IMET, which enable simulation of the thermodeformational processes of welding [16] and also in the equipment developed at the PWI [18, 19]. Large enough workpieces are subjected to the effect of thermal cycle of welding, that makes it possible to manufacture specimens from them for tensile tests and impact bent tests in accordance with GOST 6996–66 and GOST 9454–78.

Depending on the results of investigation of effect of cooling rate the structural steels are usually considered as sensitive and non- or low-sensitive to the changes in strength of the near-weld zone metal. To provide the performance of the welded joint as a single unit, the maximum strength (or hardness) of HAZ metal should not exceed the similar values of BM by more than 20–30 %. The more strict requirement are specified to the decrease in strength of welded joints. In this case the conditions of welding are selected so that to provide the design strength of the welded joint metal with a removed reinforcement at the BM level. Moreover, the admissible decrease in strength of a local region of HAZ is defined by a degree of the developing contact strengthening depending on the size of HAZ region and mechanical properties of BM [20]. Factor of HAZ metal weakening can be, probably, most dangerous for the sparsely-alloyed steels of the new generation of Mn–Si–V and Mn–Si–Nb alloying systems. This danger is little probable for the high-strength steels with $\sigma_{0.2} \geq$ 550–650 MPa, containing even a limited amount of alloying elements (nickel, chrome, molybdenum and so on). The selection of such welding conditions for them at which the

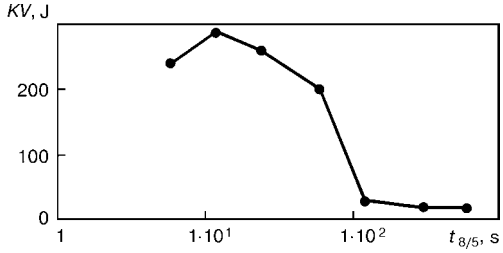

Figure 3. Dependence of impact energy at +20 °C of simulated specimens of HAZ of steel S460ML on time of cooling $t_{8/5}$ in the interval 800–500 °C [9]

excessive increase in strength (hardness) of metal of this region of the welded joint does not occur can be more actual.

The impact strength of HAZ metal of structural steels is usually decreased [21, 22]. This regularity is also preserved for steels of the new generation. Investigations of J. Brozda and M. Zeman prove about the significant decrease in toughness of HAZ metal of steel S460ML within the temperature range +20–−40 °C as compared with that of BM depending on the welding conditions (Figure 3).

Many investigations were devoted to the study of dependencies between the chemical composition of steels, time of HAZ metal cooling, technology of welding and level of impact strength of the near-weld zone metal. However, the equations, given in [16] do not take into consideration the effect of dispersion or dislocation strengthening, especially dispersion strengthening with carbides or carbonitrides formed at interface surfaces, which influence unfavourably the level of impact strength. These precipitations are carbides of niobium and partially vanadium in microalloyed steels. If unfavourable effect of niobium can be manifested even at 0.03–0.04 % in steels, microalloyed with niobium, then in steels, containing vanadium the same effect of vanadium carbide precipitations is observed only at the content of vanadium above 0.10 %. Limiting contents of the mentioned elements, at which they influence negatively on the cold resistance of HAZ metal can change depending on the composition of steels. The experience of welding main pipelines from microalloyed steels of controllable rolling prove the importance of the above-mentioned problem. As regards to the mentioned steels the region of welded joint with a decreased toughness was named as a local brittle zone (LBZ) and studied comprehensively [23]. This was stipulated by the fact that it is not always possible to prevent LBZ when traditional methods of welding are used. Therefore, at present the problem of LBZ admissibility is considered with respect to definite types of welded joints (for example, butt double-sided joint with LBZ location at angle to the acting tensile stresses) [24]. In addition, the method of evaluation of «fitness-for-purpose» of welded joints with LBZ and standards of requirements to fracture toughness are specified.

Thus, it is rational that the study of effect of TCW on change of HAZ cold resistance of new materials using simulation specimens was added to tests of real welded joints with use of approaches and criteria of fracture mechanics. Notches in specimens should be made so that they intersected completely HAZ and revealed its weakest regions.

Indirect evaluation of steels susceptibility to a delayed fracture. The main method of its realization is the calculated determination of carbon equivalent C_{eq}. Many variants of expressions C_{eq} [17] were suggested, differing by coefficients of alloying elements. Most of them was based on heat treatment practice as a parameter characterizing the hardenability of steels or critical rate of cooling. As all the researches used groups of steels, differing in composition, then the different coefficients were obtained at alloying elements, reflecting their effect on hardenability. Unfortunately, all the expressions C_{eq}, as a rule, are recommended without indication for which steel compositions they were obtained. At the same time, at complex alloying the effect of elements can be mutually intensified [16, 25]. The variant of carbon equivalent, calculated in accordance with an approach recommended by IIW is used often for the preliminary evaluation of weldability of structural steels, %:

$$C_{eq} = C + \frac{Mn}{6} + \frac{Cr + Mo + V}{5} + \frac{Ni + Cu}{15}.$$

It is assumed to consider that steels with $C_{eq} >$ > 0.45 % are usually susceptible to cracking. In parallel with C_{eq}, the different parametric equations find application for the preliminary evaluation of weldability of steels. Among them, the equation of Ito–Beshio [26] is most widely spread, %:

$$P_{cm} = C + \frac{Mn + Cu + Cr}{20} + \frac{Si}{30} + \frac{Ni}{60} + \frac{Mo}{15} + \frac{V}{10} + 5B.$$

Numerous investigations showed that the structural steels are sensitive to formation of cracks in those cases when $P_{cm} > 0.27$–0.28 %. One of the criteria indicating the possible embrittlement due to structural transformations is also hardness HV of HAZ metal. And though the relation of these characteristics (P_{cm}, C_{eq}, HV) is not adequate, the level of hardness to HV 350 in most of structural steels proves that they are not susceptible to the cold crack formation [16, 17, 25].

Taking into account the above-mentioned, the indirect evaluation of susceptibility of structural steels of the new generation to a delayed fracture was made. Characteristics C_{eq} and P_{cm} were criteria, as it was quite difficult to determine the effect of cooling rates on hardness of HAZ metal for all the steels given in Table 1.

The results obtained prove about the insufficient coincidence of an indirect evaluation of weldability of steels with the results of use of these two characteristics (about 50–60 %). It should be noted that all the known parameters were developed in principle as far back as the 1960–1970s on the basis of investigations of steels of quite another generation. As a rule, they did not contain microalloying elements and rare-earth metals (REM), and the content of inclusions of harmful elements (sulphur and phosphorous) was too high in metal.

It seems very difficult to realize the preliminary evaluation of weldability of new steels using the mentioned characteristics. It becomes more difficult by

the circumstance that there is no adequate information until now about the effect of separate elements on resistance of welded joints to a delayed cooling. Thus, for example, there is an opinion in [27–29] about the increase in probability of crack initiation in HAZ of alloyed steels at decrease of sulphur content to 0.001 %. Authors of works [30–32] came to the opposite opinion: change in sulphur content in low-alloyed steels from 0.001 to 0.02 % influences negligibly their susceptibility to the crack formation. In work [33] the cause of discrepancy in opinions of different authors concerning this problem is explained by the effect of composition of steels and type of non-metallic inclusions (NMI) on the formation of structure and properties of HAZ of steels of an increased purity. The effect of other elements (REM and microalloying), existing in steels of the new generation on a delayed cooling, is little studied.

It is rational to add the indirect evaluation of susceptibility to a delayed fracture of these materials with investigations using well-known technological samples (implant or Tekken). Such approaches make it possible to obtain evaluation of resistance of welded joints of new steels to cold crack formation as compared with that of well-studied structural materials.

Resistance of steels to lamellar fracture. Anisotropy of ductility and toughness is typical of sheet rolled metal of structural steels. It is expressed in a remarkable decrease in values of these properties in transition from longitudinal direction to transverse and in an abrupt their decrease in the direction of thickness (direction Z) [16, 34, 35]. The latter is associated usually with the presence of NMI in steel. Moreover, their composition, shape, sizes, nature of distribution, susceptibility to deforming, strength of adhesion with matrix, etc. are of importance. In steels of a controllable rolling, with a negligible content of NMI, the crystallographic texture and weakening of subgrain boundaries are decisive. The low ductility and toughness in combination with forces occurring in the direction Z in zones of metal structures with T- and fillet welded joints serve the main cause of formation of lamellar cracks.

The lamellar fractures of welded joints are associated most often with the presence of sulphide inclusions in steels, which are capable to be deformed and, therefore, they are elongated and flattened during rolling. The new generation of steels is subjected in most cases to different refining treatments and contains a limited content of sulphur. The role of sulphide inclusions in lamellar fracture of such rolled stock is decreased.

When analysing the lamellar fracture it is, probably, rational to concentrate also attention to the role of nitride inclusions having, as a rule, an acicular shape, in this process. The structural steels of the new generation contain in most cases nitrogen and nitride-forming elements (aluminium, boron, vanadium, niobium, chromium, titanium, zirconium, etc.). The process of steel production can promote itself the formation of nitride inclusions, as they are formed in cooling or heat treatment of metal [36].

In some cases the process of welding can effect negatively on the metal resistance to a lamellar fracture. Thus, in the zones of a high concentration of thermoplastic welding deformations, the decrease in adhesion of NMI with matrix metal, formation of large clusters of deformations and deformational ageing of metal are possible. The increased concentration of diffusive hydrogen, and also composition of BM can occur to be an essential factor in this case. Consequently, to prevent the formation of lamellar cracks in the zone of welded joints it is necessary to use, except selection of BM with high characteristics of properties in direction Z, the technological measures (preliminary facing of edges before welding, rational selection of sequence of welds layout and technology of welding [37, 38] and others).

To evaluate the susceptibility of steels to the formation of lamellar cracks the reduction in area ψ_Z of smooth specimens with an axis in Z direction are widely used. The procedure of preparation of standard specimens and their testing is available in GOST 28870–90. As to the requirements to ψ_Z, then in accordance with technical specifications, for example, to thin-sheet rolled metal from a low-alloyed steel for bridge construction, its values should be provided at the level of > 20 % that is optimum from the point of view of prevention of formation of lamellar cracks in welding of metal structures. As regards to the steels of the new generation and to provide the safe service of welded joints it is necessary to evaluate the properties of metal in the direction Z together with determination of ψ_Z using approaches and criteria of fracture mechanics. In this case, the requirements to the fracture toughness should be specified coming from the «fitness-for-purpose» conception.

Peculiarities of selection of materials and processes of welding. Metallurgical and technological processes of welding structural steels are usually selected so that to provide the producing of weld metals of optimum chemical composition (for each level of strength of materials) with a limited content of sulphur, phosphorous and NMI. This is defined in each concrete case by the selection of filler materials, edge preparation of welded joints, methods and conditions of welding. As a result, the transition of alloying and impurity elements from BM into the deposited metal predetermines its structure and properties. The share of BM in welds can change within the wide enough ranges ($\approx$ 15–70 %) for the main processes of arc welding.

In this connection the steels of the new generation can provide another action on structure and properties of weld metals than the well-studied structural materials used at present. This is, first of all, can be expressed in the fact that in welding steels with $\sigma \approx$ $\approx$ 400–550 MPa the transition of alloying elements (nickel, chromium, molybdenum, etc.) into weld metal will not take place, and in welding of steels of a higher strength (with $\sigma_{0.2} \geq 600$ MPa) it will be much lower. Therefore, the use of traditional materials for welding steels of appropriate categories of strength, can lead to the deterioration of service properties of the deposited metal. This problem can be, probably, overcome at the expense of development of sparsely-alloyed welding materials of the new generation [39]

Table 3. Impact strength of welds in arc welding of steels with different content of Σ Al, V, Nb

Method of welding	*Σ Al, V, Nb in steel, %*	*KCV, J/cm², at T, °C*			T_{BT1}, °C	*Peculiarities of welding joints*
		+20	*−40*	*−70*		
Manual electric arc	0.07	71–78	40–44	33–38	−70	Joints were welded using traditional technological processes
	0.18	70–77	35–40	30–32	−50	The same
	0.27	65–74	31–37	23–28	−40	»
		69–76	35–40	28–33	−55	Joints were welded by changing conditions and technology of welding
Shielded-gas mechanized	0.09	75–105	45–65	35–50	−70	Joints were welded using traditional technological processes
	0.18	67–95	45–60	30–37	−70	The same
	0.27	65–95	35–52	25–32	−50	»
		75–95	48–53	27–37	−65	Joints were welded by changing conditions and technology of welding
Automatic submerged-arc	0.07	75–79	47–52	35–42	−70	Joints were welded using traditional technological processes
	0.17	61–64	25–35	16–23	−30	The same
	0.27	60–62	22–33	15–19	−20	»
		71–88	54–73	32–42	−70	Joints were welded by changing conditions and technology of welding

Note. Results of testing 4–5 specimens are given.

or an allowance for conditions of formation of properties of weld metals of different types of joints [40]. The use of more alloyed welding materials for this purpose is hardly promising from the economic point of view. According to the opinion of some researchers [41, 42] the weld metal of alloyed steels with $\sigma_{0.2} \geq$ ≥ 600 MPa is more susceptible to the formation of cold cracks, than steel.

However, in welding of microalloyed steels the transition of niobium, vanadium, aluminium, and also their nitrides, carbonitrides and REM into the deposited metal takes place. This can contribute to the increase of NMI in it and influence negatively both the impact strength and also temperature of weld metal transition into a brittle state [43, 44]. The composition of these inclusions and their amount depend on many factors and are the subject of special investigations. Thus, as regards to welding the large-diameter pipes the data of [45] prove that it is necessary to limit the total content of carbide- and nitride-forming elements in steels. Therefore, it is necessary to evaluate the possibilities of use of basic processes of arc welding for manufacture of welded structures from domestic high-strength microalloyed steels. To conduct these investigations, all of them were divided conditionally into three groups depending on the total content of aluminium, vanadium and niobium [46–48]:

- steels with Σ Al, V, Nb < 0.15 % (13KhGMRB and 12GN3MFAYuDR grades with Σ Al, V, Nb ≈ ≈ 0.07–0.09 %);
- steels with Σ Al, V, Nb = 0.15–0.20 % (12GN2MFAYu and 14KhG2SAFD grades with Σ AL, V, Nb = 0.17–0.18 %);
- steels with Σ Al, V, Nb ≥ 0.20 % (14KhGN2MDAFR grade with Σ Al, V, Nb = = 0.27 %).

Butt joints with V-shaped edge preparation, made by manual electric arc welding (Q_w = 10–12 kJ/cm), and also by mechanized welding in mixture Ar + CO_2 (Q_w = 18–19 kJ/cm) and automatic SAW (Q_w = = 25–27 kJ/cm) using the traditional materials and approaches were prepared from separate representatives of each group of 20 mm thick steels. During present investigations the impact strength of weld metal and its transition from tough to quasi-brittle state T_{BT1} were evaluated. Results of investigations are given in Table 3.

As follows from the Table, the highest toughness of weld metal was reached at Σ Al, V, Nb < 0.15 % in steels. With increase in amount of these elements and decrease in test temperature the impact strength of metal of all the welds is decreased. This is clearly expressed when the welds made by the automatic SAW on steels with Σ Al, V, Nb > 0.15 % are tested. In this case the temperature T_{BT1} is shifted to the region of the higher temperatures by 40–50 °C that is due to a higher share of BM in the formation of these welds (≈ 40–45 %).

The investigations carried out prove that the problems of increase of cold resistance of weld metal of microalloyed high-strength steels can be solved by improvement of welding processes, which is directed to the reduction of BM share in weld metals. In the investigations described this was easily attained in manual electric arc and mechanized shielded-gas welding of steels with Σ Al, V, Nb = 0.07–0.27 %. The automatic SAW of these steels is rational at Σ Al, V, Nb < 0.15 %, as in the rest cases this is connected with a significant complication of technological processes and decrease in their productivity.

Thus, specific approaches to the selection of filler materials and realization of main processes of arc welding can be required in separate cases for the new generation of structural steels. To take the decisions

about the necessity of conductance of these works, the preliminary investigations are, probably, rational by using the known earlier materials and technological solutions.

CONCLUSION

Investigations and analysis of peculiarities of formation of structure and properties of welded joints of sparsely-alloyed structural steels of the new generation demonstrated the need in a careful approach to the selection of materials and processes of their welding due to a possible increase in susceptibility of metal of welds and HAZ to brittle fractures. «Program of investigations of weldability of new low-alloyed steels of increased and high strength with more than 400 MPa yield strength, designed for use in critical welded structures» has been created, in which the evaluation of service properties of BM, effect of thermal cycles of welding on service properties of HAZ metal, susceptibility of new structural steels to the crack formation (hot, cold, lamellar) in welded joints, peculiar features of formation of service properties of weld metals are envisaged using the advanced methods.

The information obtained for all these trends of investigations and assurance of an appropriate level of service properties of BM and metal of welded joints will be a good base for the creation of efficient and reliable welded structures of steels of the new generation.

1. Fischer, J.W., Dexter, R.I. (1994) High-performance steel for America's bridges. *Welding J.*, **1**, 35–43.
2. Tani, S., Kaneko, V., Ishiguro, M. et al. (1996) Recently developed structure steel for use in civil engineering and constructions. *NKK Techn. Rev.*, **74**, 17–25.
3. Dieter, U., Belmeyer, H. (1986) Erfahrungen mit dem Verarbeiten des hochfesten wasservergüteten Baustahls St. E 890. *Schweißen und Schneiden*, **9**, 430–436.
4. Gerster, P., Hauser, J. (1988) Erfahrungen mit der Anwendung hochfester wasservergüteten Feinkornbaustähle beim Bau von Teleskop-Autokränen. *DVS-Ber.*, **112**, 61–67.
5. Fredin, E.H., Ahlton, B., Hoglund, T. et al. (1995) Fabrication a mobile bridge for the Swedish army. *Welding Rev. Int.*, **3**, 121–122.
6. Herold, E.H., Zinke, M., Zwickert, H. et al. (1999) Neues in der Schweißtechnik 1998. *Schweißen und Schneiden*, **5**, 266–288.
7. Dreves, E.-J., Angle, B., Kruze, I. (1999) High-strength steels — the present and the future. *Chyorn. Metally*, **10**, 48–55.
8. Lundin, C.D., Gill, T.P.S., Qino, C.Y.P. et al. (1990) Weldability of low-carbon micro-alloyed steels for marine structures. *WRS Bull.*, **359**, 1–100.
9. Brozda, J., Zeman, M. (2000) Weldability evaluation of a modern TMCP steel by using simulation techniques. *Acta Metallurgica*, **1**, 103–111.
10. Stolyarov, V.I., Nikitin, V.N., Efron, L.I. et al. (1993) State-of-the-art and prospectives of development of technology and composition of high-strength weldable steels with yield point of 700 N/mm^2. *Stal*, **6**, 61–67.
11. von Rauch, R., Eigelsberger, M., Linder, W. et al. (1994) Herstellung und Verarbeitungseigenschaften eines thermomechanisch gewalzten Warmbreitbandes mit 700 N/mm^2 Mindeststreckgrenze. *Schweißtechnik*, **6**, 82–87.
12. Campbell, J.B. (1985) Welding of high-strength and wear-resistant quenched and tempered steels. *Australian Welding*, **3**, 35–40.
13. Hoiser, A., Nis, X., Ruusila, Yu. et al. (1988) Fracture behavior of welded joints from high-strength structural steels. *Chyorn. Metally*, **4**, 20–29.
14. von Mayerhofer, M., Aigmuller, G., Geyer, D. et al. (1993) Hochfeste schweißbare Baustähle. *Schweißtechnik*, **11**, 3–11.
15. Kirian, V., Mikhoduj, L.I. (1993) Fracture toughness of alloyed bainitic-martensitic steels and their welded joints. *Avtomatich. Svarka*, **12**, 3–7.
16. Hrivnak, I. (1984) *Weldability of steels*. Moscow: Mashinostroyeniye.
17. Hrivnak, I. (1989) *Teoria zvaritelnosti kovov a zliatin*. Bratislava: VSAV.
18. Sidoruk, V.A., Dudko, D.A., Gorbenko, N.V. et al. (1985) Simulation of welding thermal cycle in heat-affected zone during electroslag welding with a modulated current. *Avtomatich. Svarka*, **7**, 12–15.
19. Kasatkin, B.S., Strizhius, G.N., Tsaryuk, A.K. et al. (1990) Simulation of HAZ structure and cold cracks in welding of medium-alloyed steel. *Ibid.*, **2**, 1–5.
20. Shron, R.Z., Bakshi, O.A. (1962) About problem of evaluation of strength of welded joints with a soft layer. *Svarochn. Proizvodstvo*, **9**, 11–14.
21. Hanner, N.E. The influence of niobium on the microstructure and mechanical properties of submerged-arc weld metals for CMn steels. *IIW Doc. II-612–72*.
22. Hanner, N.E., Jonson-Holtquist, B.M. (1974) Influence of vanadium of the HAZ properties of mild steel. *Metal Sci.*, **8**, 224–234.
23. Toyoda, M. Fracture toughness evaluation of steel welds. Part 1. *IIW Doc. X-1191–89*.
24. Kirian, V.I., Semyonov, S.E. (1995) Evaluation of fitness-for-purpose of welded joints of main pipelines from microalloyed steels. *Avtomatich. Svarka*, **3**, 4–9.
25. Makarov, E.L. (1981) *Cold cracks in welding of alloyed steels*. Moscow: Mashinostroyeniye.
26. Ito, Y., Beshio, K. Weldability formula of high strength steels. *IIW Doc. IX-576–68*.
27. Hirai, Y., Minakami, S., Tsuboi, J. Effect of sulphur on hydrogen-assisted HAZ cracking in Al-killed steel plates. *IIW Doc. IX-1160–80*.
28. Hart, P.H.M. The influence of steel cleanless HAZ hydrogen cracking: The present position. *IIW Doc. IX-1308–84*.
29. Mikhoduj, L.I., Movchan, M.B., Poznyakov, V.D. et al. (1990) Properties of extrapure high-strength steel 12GN2MFAYu. *Problemy Spets. Elektrometallurgii*, **1**, 99–106.
30. Serio, N., Saito, T., Miyasaka, H. (1981) Effect of sulphur and nitrogen on cold cracking. *Monthly Rep. NSC*, Apr., 9–10.
31. Yurioka, N., Ohshita, S., Saito, T. (1981) Effect of sulphur on cold cracking. *Ibid.*, Aug., 33–34.
32. Chrysler, K., Shubert, J., Dal, V. et al. (1995) Cold cracking resistance of high-strength structural steels with ultra low content of sulphur. *Chyorn. Metally*, **2**, 58–63.
33. Okumura, M., Kasuya, T., Yurioka, N. et al. (1988) Effect of cleanness on its weldability. *Quart. J. JWS*, **6**, 144–150.
34. Gladshtein, L.I., Litvinenko, D.A., Onuchin, L.G. (1983) *Structure of austenite and properties of hot rolled steel*. Moscow: Metallurgiya.
35. Novikov, V.I., Girenko, V.S., Bernadsky, A.V. (1985) Anisotropy of properties of rolled metal and performance of welded structures (Review). *Avtomatich. Svarka*, **12**, 13–19.
36. Yavojsky, V.I., Rubenchik, Yu.I., Okenko, A.P. (1980) *Nonmetallics and properties of steel*. Moscow: Metallurgiya.
37. Gladshtein, L.I., Rivanenok, T.N. (1995) Evaluation of fracture susceptibility in simulated thermal and deformational cycles of welding. *Zavodskaya Laboratoriya*, **7**, 37–43.
38. Kasatkin, B.S., Musiyachenko, V.F., Mikhoduj, L.I. (1977) Technology of welding of structures from 14Kh2GMR steel in erection of highway bridge span. *Avtomatich. Svarka*, **5**, 37–39.
39. Mikhoduj, L.I., Vasiliev, V.G., Poznyakov, V.D. et al. (1996) Kinetics of austenite transformation of sparsely-alloyed weld metal with yield point of 600–800 MPa. *Ibid.*, **11**, 3–10.
40. Asnis, A.E., Ivashchenko, G.A. (1985) *Increase in strength of welded structures*. Kyiv: Naukova Dumka.
41. Uwer, D., Dibelmeyer, H. (1986) Erfahrungen mit dem Verarbeiten des hochfesten wasservergüteten Baustahls St. E 890. *Schweißen und Schneiden*, **9**, 430–436.
42. Hart, H.M. (1986) Resistance to hydrogen cracking in steel weld metal. *Welding J.*, **1**, 14–22.
43. Dolby, R.E. Review of work on the influence of Nb on the microstructure and toughness of ferritic weld metal. *IIW Doc. IX-1175–80*.
44. Dolby, R.E. Review of work on the influence of vanadium on microstructure and toughness of ferritic weld metal. *IIW Doc. IX-1213–81*.
45. Mandelberg, S.L., Bogachek, Yu.S., Kovalevsky, V.A. et al. (1986) Increase in impact toughness of weld metal of large-diameter tubes from microalloyed steels. *Avtomatich. Svarka*, **1**, 36–40.
46. Gladstein, L.I., Litvinenko, D.A. (1972) *High-strength building steel*. Moscow: Metallurgiya.
47. Nikitin, V.N. (1977) High-strength low-alloyed steels for manufacturing of motor-car, excavator and mining engineering. *Stal*, **11**, 1044–1047.
48. Melnikov, N.P., Gladshtein, L.I., Bobylyova, L.A. (1987) 12GN2MFAYu high-strength steel of increased cold-resistance in welded structures. *Avtomatich. Svarka*, **2**, 50–54.

Tribute to the memory of Viktor N. Zemzin

ROLE OF MATHEMATICAL MODELLING IN SOLVING PROBLEMS OF WELDING DISSIMILAR STEELS (REVIEW)

V.I. MAKHNENKO and **G.Yu. SAPRYKINA**
The E.O. Paton Electric Welding Institute, NASU, Kyiv, Ukraine

Considered are the main aspects of problems associated with fusion welding of steels of the austenitic and ferritic-pearlitic grades. Analysis of calculations and ways of solving the problems for each of the above grades are based on studies published lately. The role of mathematical modelling in solving the above problems is shown.

Key words: *fusion welding (surfacing), dissimilar steels, penetration (fusion) zone, phase composition, chemical heterogeneity, welding stresses and strains, hot and cold cracks*

The known book by Prof. V.N. Zemzin [1], in which the author formulated main problems of welding dissimilar steels, was published 35 years ago. Most problems covered by the book are still topical, which is proved by a number of recent publications [2–5, etc.]. It follows from them that despite the substantially increased level of knowledge on the main problems of welding dissimilar steels and methods for their solving, a great deal is yet based on purely qualitative estimates and empirical methods that require a large scope of experimental work to be done to find rational design and technology solutions. The latter is attributable to the complexity of physical processes occurring in local volumes of the fusion zone between dissimilar metals and to a large number of influencing factors. Kinetics of these processes is difficult to quantitatively estimate by experimental methods. In addition, a large number of influencing factors, associated with differences in physical and chemical properties of materials involved in joining, hampers the use of traditional methods for quantitative estimation of the extent of their influence on the required quality of a welded joint.

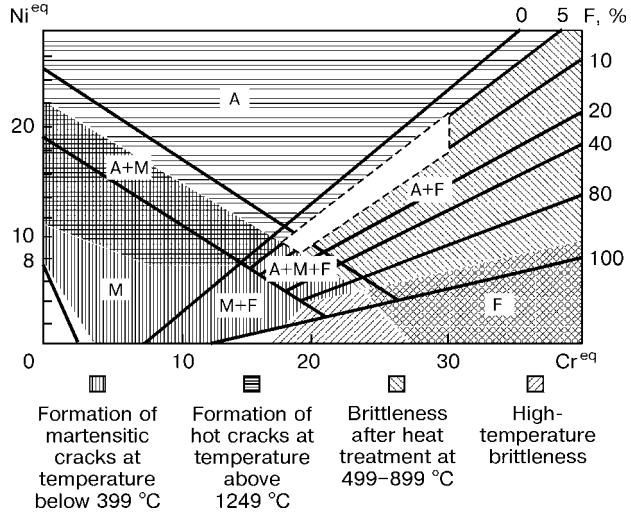

Figure 1. Schaeffler diagram: A — austenite; M — martensite; F — ferrite

The above-said stipulates an increased interest in the use of mathematical modelling methods, based on rapidly increasing capabilities of computer facilities, along with the use of traditional experimental methods of investigations. As an example, we can mention a number of studies [5–10, etc.] where mathematical modelling yields positive results in solving specific problems. The authors of this review made it their aim not so much to note what has been already achieved in this area, as to show potentialities of mathematical modelling for solving characteristic problems of welding dissimilar steels by an example of the most common combination of ferritic-pearlitic plus austenitic steel. Then, proceeding from [1], the authors consider seven areas closely connected with selection of rational design or technology solutions to provide fusion welded joints in the above steels.

Heating of a workpiece, sizes of the penetration zone and its mean chemical composition. These problems are of a key importance not only for welding dissimilar metals, although for the latter they have certain peculiarities associated with different thermal-physical properties (for example, thermal conductivity of each of the steels welded may differ by a factor of 3, and melting point — almost by 100 °C). This exerts a marked effect on distribution of heat from the welding source and sizes of the penetration zone, which determines its mean chemical composition, as well as microstructure and properties. Also, chemical composition strongly affects susceptibility of metal of the penetration zone to hot and cold cracking. Figure 1 shows the Schaeffler diagram which represents the microstructural state of alloyed Cr–Ni steel depending upon the values of equivalents of chromium, Cr^{eq}, and nickel, Ni^{eq}, respectively. The diagram also shows regions of a structural state of

the steel in accordance with the content of austenising and ferritising elements, differing in susceptibility to formation of cold (martensitic) cracks at a temperature below 400 °C, hot cracks at a temperature above 1250 °C, embrittlement in heat treatment within a range of 500–900 °C and high-temperature brittleness [11]. Such diagrams allow an important estimation of metal of the penetration zone, provided that chemical composition of the zone is known, which serves as a sufficiently strong impetus to development of appropriate methods for prediction of this composition, depending upon the content of input materials, as well as welding conditions and parameters. In this case the following relationship is used:

$$X = \sum_i X_i D_i, \qquad (1)$$

where X is the mean content of an element in the penetration zone produced by a given pass, %; X_i is the content of this element in the i-th region of the penetration zone (Figure 2); and D_i is the share of the i-th region in the penetration zone. Values of D_i are traditionally determined experimentally, which is very labour-consuming for generating the corresponding base of values depending upon different technology and design factors.

The first calculation approaches to description of peculiarities of thermal processes occurring in welding dissimilar materials were developed approximately 35 years ago. They relate to analytical solutions for single-pass welding of parts of dissimilar materials [12, 13]. Solutions derived within the framework of the theory accepted at that time [14] allow prediction of temperature fields at a certain distance from the weld pool. However, it is very difficult to obtain sufficiently reliable values of D_i on their basis.

Progress in computer facilities and numerical methods has substantially widened capabilities of modelling of penetration of a material welded, depending upon welding conditions and parameters [15]. In this case differences in properties of elements being welded involve no substantial difficulties.

Mathematical models based on the theory of thermal conductivity, provided that thermal-physical characteristics of a material depend upon the temperature and, in a number of cases, additionally upon the microstructural state [13], are used to obtain adequate calculation data on size of the penetration zone. Increased heat transfer and latent heat of melting (solidification) in the liquidus–solidus temperature range in a liquid portion of the weld pool are allowed for in terms of the effective thermal conductivity coefficient. An important parameter of the model is distribution of thermal power of the heat source. For the case of welding with a filler metal, the thermal power introduced by the filler can be determined with a certain extent of approximation as follows:

$$q_f = \frac{\alpha_d I_w}{3600}(T_f c + q_l), \qquad (2)$$

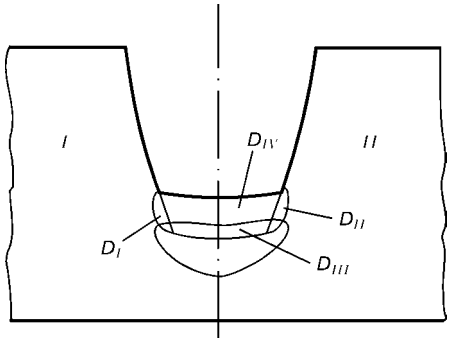

Figure 2. Diagram for determination of mean chemical composition of metal of the penetration zone in welding dissimilar materials I and II, depending upon penetration volume D_I, D_{II}, D_{III} and D_{IV} of the solidifying weld pool

where α_d is the deposition efficiency; I_w is the welding current; T_f is the temperature of the filler metal used; c is its mass heat capacity; and q_l is the latent melting heat.

The rest of the thermal power of the welding arc is distributed following the normal law with a centre at the point of an instantaneous position of the arc axis [6, etc.]. Algorithms of a numerical solution of these problems within the framework of both three- and two-dimensional models have been verified at a sufficient confidence level. Therefore, there is no need to dwell on this fact now.

Primary solidification, peculiarities of local chemical heterogeneity and microstructure near the fusion boundaries. In the last years the special consideration has been given to the microstructural state and properties of a material near the fusion boundary between dissimilar materials [2–5, etc.]. Supposedly, these factors in many cases have a fundamental effect on strength characteristics of a welded joint (brittle fracture resistance, behaviour at variable temperatures, etc.).

As known from practice, a local zone differing in chemistry and microstructure from the base and weld metals is formed near the fusion line in welding dissimilar metals. Processes which determine structure and properties of the penetration zone can be conditionally subdivided into two groups [1]. The first group includes the processes of solidification of dissimilar materials, determining primary microstructure of the fusion zone and, in many cases, also the final microstructure of this zone; and the second group includes processes related to diffusion phenomena occurring in the solidified metal, formation of carbides during cooling and subsequent heating of both technology (multilayer welding, heat treatment) and service origin.

Results of numerous studies [1] show that under the fusion welding conditions the centres of solidification of the weld pool are the fused grains of the base metal, with the solidifying phase atoms adjoining these grains (Figure 3). The rate of this solidification depends upon the welding parameters, thus determining the size, shape and rate of displacement of isotherm T_L (liquidus temperature) for a mean composition of the weld pool. In this case, because of dif-

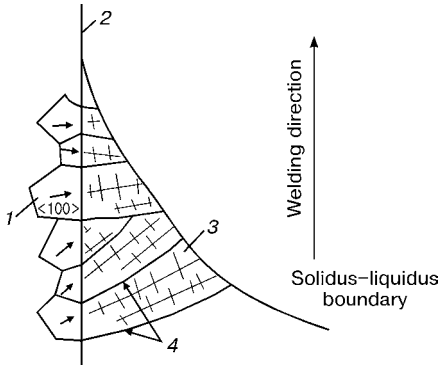

Figure 3. Diagram of solidification of the weld pool near the base metal melting boundary [3]: *1* — base metal; *2* — melting boundary; *3* — weld pool; *4* — boundary of solidifying grains

ferring solubility of alloying elements of the penetration zone in liquid and solid phases, chemical composition along the axes of growing crystals changes to a substantial degree.

An alloy with a low carbon content, i.e. having a microstructure of a low-alloyed δ-ferrite, first solidifies near the fusion line, despite the mean substantially alloyed composition of the penetration zone. As a crystal increases in size, the degree of alloying and carbon content approach the mean composition of metal of the penetration zone, i.e. low-alloyed austenite starts solidifying at a certain time moment, and then follows alloyed austenite, the composition of which corresponds to the mean chemical composition of the penetration zone metal. The zone of alloyed austenite may retain its microstructure up to complete cooling, whereas the rest of microstructures of the zone undergo changes associated with allotropic iron transformations (Figure 4).

It is the opinion of a number of specialists [4] that this circumstance is a cause of formation of the so-called parallel boundary (see Figure 4), the presence of which is seen in some macrosections (Figure 5). As follows from [4], this boundary formed during primary solidification is a location of the substantial concentration of various impurities diffusing to the boundaries of the penetration zone regions at high temperatures and precipitating in non-austenitic steel during the austenitic transformation process at the above boundaries. This is the cause of frequent intercrystalline brittle fractures which take place directly at the parallel boundary (Figure 6).

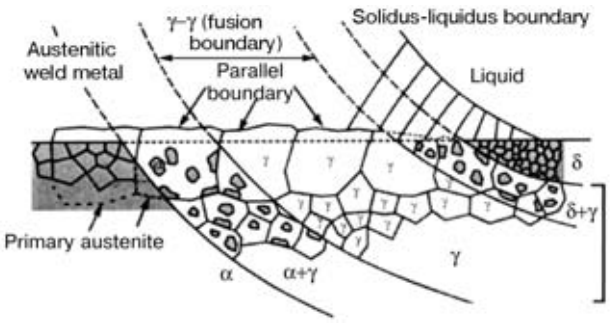

Figure 4. Kinetics of microstructural changes in dissimilar metals of the weld in the zone located near the fusion boundary (base metal — low-alloy carbon steel)

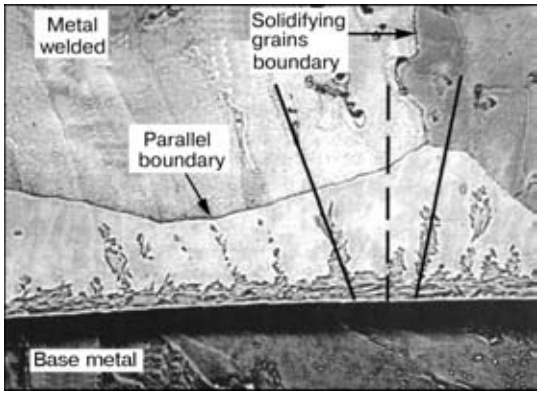

Figure 5. Growth of dendrites in a direction to the parallel boundary [4]

In the national literature [10], it is noted in description of peculiarities of structure of the penetration zone that it has distortions in boundary grains and the fusion boundary proper. Besides, the lower the safety factor for austenisation of the weld metal, the higher the degree of differences in structures of individual regions of the penetration zone.

Naturally, defects of the type of the «parallel boundary» are just a type of a large group of defects formed during solidification of a welded joint between dissimilar steels [1]. Their formation is greatly affected by chemical composition of the penetration zone metal and base materials, solidification rate, etc. Finding the corresponding quantitative relationships between initial parameters and kinetics of the solidification processes occurring near the fusion zone by using experimental data on final microstructures (see Figure 5) or chemical heterogeneity of metal (Figure 7) as reference points is a topical problem of mathematical modelling.

It should be noted that a number of studies that appeared in the last years contain mathematical description of heat transfer processes which occur in the molten weld pool [16, 17]. References to earlier studies can be found in the review article [15]. However, almost no studies dedicated to mathematical description of peculiarities of primary solidification of the weld pool are available. No new ingenious research has been known in this area so far, except for the

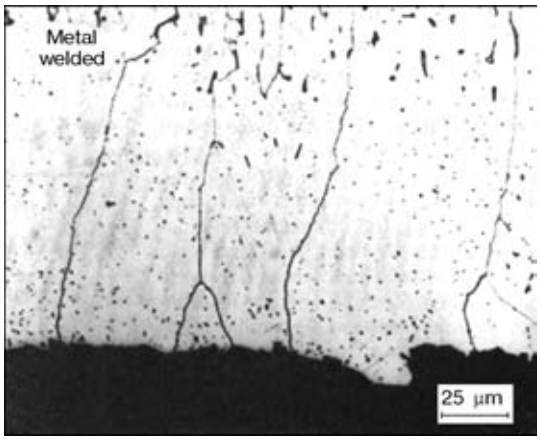

Figure 6. Vertical section of a crack located in the deposited part along the parallel boundary [4]

studies by B.A. Movchan [18], G.L. Petrov [9], Yu.A. Sterenbogen [19] and N.N. Prokhorov [20]. Meanwhile, in the last years a substantial interest is expressed in mathematical modelling of the processes of primary solidification and formation of various defects related to chemical heterogeneity in the field of such related technologies as electroslag and vacuum-arc remelting [21]. Of special note are the approaches based on the theory of chaos employed for description of the characteristic stages of these processes [22], where the use of a determinate approach of mathematical physics is of low efficiency.

Formation of carbides. Carbon is one of the elements which have a considerable effect on formation of carbides in steel alloys, which may be both in the form of chemical solid solutions and in the form of chemical compounds. Steels are more characterised by the presence of iron carbide Fe_3C, i.e. cementite. However, in addition to iron, modern steels contain also other metals of the transition group, which are situated to the left from iron in the periodic table [23]. Therefore, in addition to Fe_3C, a number of other similar carbides with metal properties may be formed in steels. For the combination of steels under consideration, these may be carbides of titanium, vanadium, niobium, chromium, molybdenum, tungsten, etc.

Activity of carbide formation and stability of carbides in alloyed steels grow in a reverse order with respect to the above listed elements [24]. However, carbides of the above elements do not exist in the pure form in steels. Carbides of all alloying elements contain iron in their solution. If a steel contains a number of carbide-forming elements, the solution will also contain these elements.

As the above carbide-forming elements are dissolved in α- and γ-iron, and the amount of carbon in alloyed steels is limited, a large amount of the alloying carbide-forming elements, such as chromium, is contained in iron solution, which leads to certain properties of the alloy, i.e. corrosion resistance. At a chromium content of less than 12 wt.%, the iron solution will have a much lower corrosion resistance. Therefore, local formation of chromium carbides along the austenite grain boundaries may lead to intercrystalline corrosion. To illustrate, Figure 8 shows macrosection of such a defect, i.e. cracks initiated in the weld root at the fusion boundary in the near-weld zone of a circumferential welded joint in the 10Kh18N10T (C — 0.1; Cr — 18.0; Ni — 10.0; Ti — 0.6 wt.%) steel piping with nominal diameter D_n 300 (Chronobyl Nuclear Power Station).

Development of this defect near the fusion zone of Ti-stabilised austenitic steel is favoured by the process of sensitisation of this zone under the effect of thermal cycle of multilayer welding [25]. Carbides formed in this process play a very important role.

Ternary constitutional diagram Fe–C–Cr at 12 and 20 % Cr (Figure 9) gives an idea of the temperatures of formation of chromium carbides. It can be seen

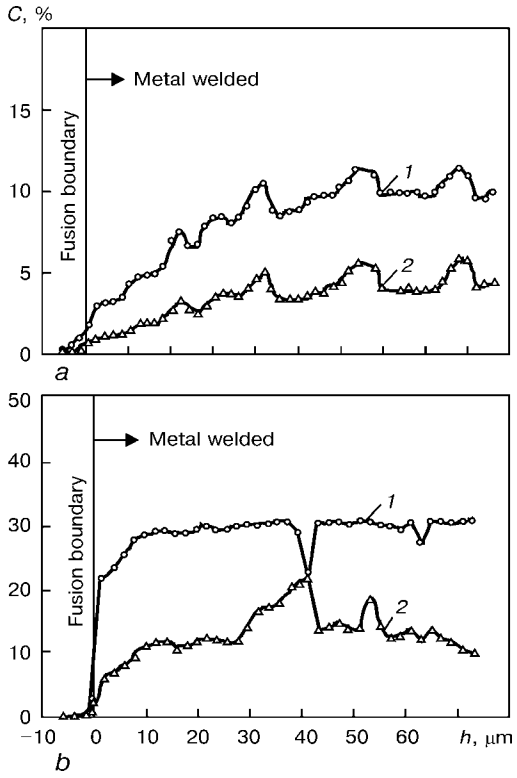

Figure 7. Dependence of the content of nickel (*1*) and copper (*2*) in the penetration zone of the 2.25Cr–1Mo steel welded joint produced by using austenitic filler metal upon the mass fraction of carbon in base metal at 80 % Ni (*a*) and 46 % C (*b*) [4]: *h* — distance from the fusion boundary; *C* — nickel and carbon contents

from the Figure that at C < 0.15 % chromium carbides are formed in steels at temperatures below 900 °C, when carbon is in solid solution of iron or in the form of Fe_3C. Before the beginning of the $\gamma \rightarrow \alpha$ transformation, chromium carbides are formed due to substitution for iron atoms in cementite, and then due to precipitating carbon. As a result, equilibrium cooling conditions lead to formation of a microstructure of Cr-alloyed ferrite and carbides of the type of $(Cr, Fe)_4C$ at a substantial mass fraction (20 %) of chromium and $(Cr, Fe)_4C + (Cr, Fe)_7C_3$ at 12 % Cr.

In the case of the third carbide-forming element (in addition to iron and chromium) the character of the process changes but slightly, providing that in the periodic table this element is situated to the right from chromium, e.g. manganese. Then the chromium

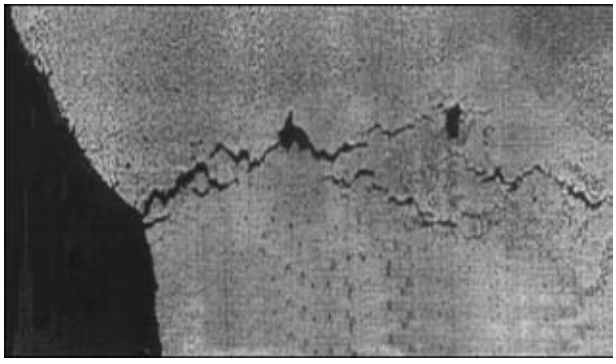

Figure 8. Intercrystalline corrosion in section of the circumferential welded joint in the 10Kh18N10T steel piping with nominal diameter D_n 300

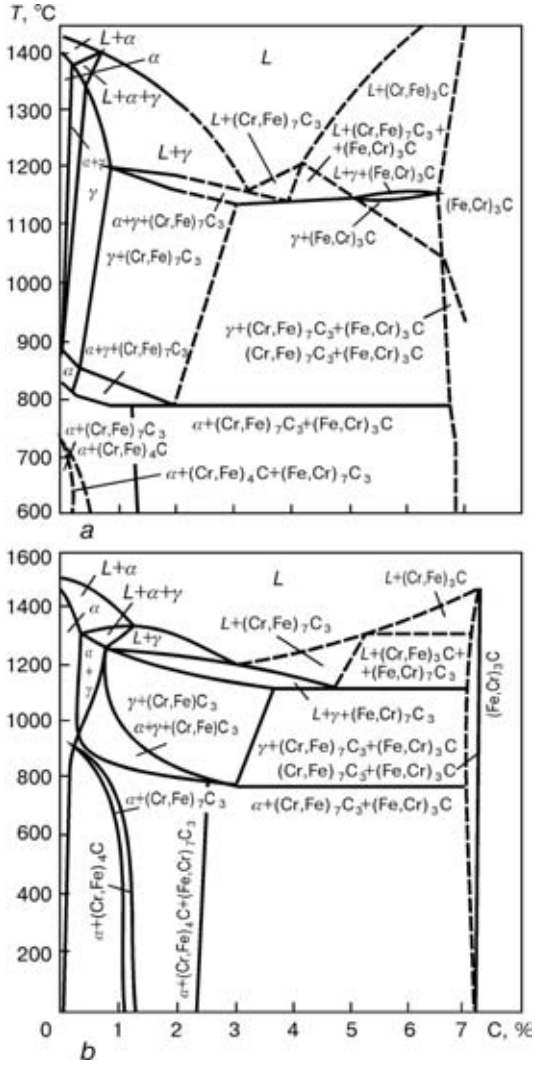

Figure 9. Ternary constitutional diagram Fe–C–Cr (Cr = const) at 12 % (*a*) and 20 % (*b*) Cr: *L* — liquidus zone

carbide solution will also contain manganese, in addition to iron, i.e. carbides of the type of (Cr, Mn, Fe)$_4$C and (Cr, Mn, Fe)$_7$C$_3$, etc. will be formed.

If the carbide-forming element is to the left from chromium in the periodic table, e.g. titanium, titanium carbides containing chromium, iron, etc. in the solution will be formed.

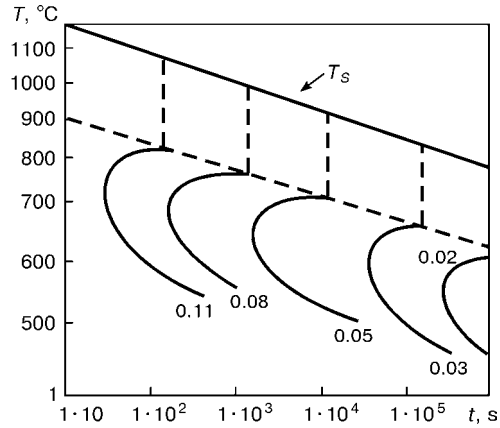

Figure 10. Temperature-time diagram of formation of carbides $M_{23}C_6$ in steel 18Cr–9Ni with a differing mass fraction of carbon, %: T_S — solidus temperature

A marked impact on the process of formation of carbides might be exerted by alloying non-carbide-forming elements, such as nickel, which have a substantial effect on the $\gamma \rightarrow \alpha$ transformations. All this hampers mathematical description of the process of formation of carbides in the alloyed material of the penetration zone of steels considered.

Of the highest interest in this area is the use of the specific alloy temperature-time diagrams (of the type shown in Figure 10) for steel 18Cr–9Ni [9]. It can be seen from this diagram that at C < 0.02 % almost no carbides are formed, as carbon required for this purpose can be obtained primarily from tertiary cementite, and this is not enough for the carbide formation process to start.

The possibility of formation of carbide ridges in the solidifying metal enriched with carbon near the penetration boundaries depends to a considerable degree upon the mass fraction of carbon. At a higher content of the latter the process of formation of chromium carbides becomes more intensive.

Therefore, at least two areas are worthy of notice in consideration of the issue of formation of carbides during the process of welding dissimilar steels of the above combination: the first is associated with depletion of grain boundaries of the base metal, i.e. austenitic steel, near the fusion boundaries in chromium, and the second is associated with formation of carbide ridges within the penetration zone near the fusion boundaries.

Microstructure and properties. Microstructure and properties of metal in the penetration zones and HAZ in welding of dissimilar steels under consideration are determined by chemistry of these zones and corresponding thermal cycles. Mathematical description of microstructural changes occurring in welding was tried in a number of studies [26–33, etc.]. One of the simplest approaches is based on an assumption that at the stage of heating a change in the initial microstructural state takes place only at high (above A_3) temperatures, e.g. at $T_* = 850$–900 °C for steels. However, in this case no allowance is made for microstructural changes occurring at lower heating temperatures, i.e. in the absence of the $\alpha \rightarrow \gamma$ transformations.

Accordingly, the range of $T_{\max}(x, y, z) \geq T_*$ determines the zone where phase transformations at the stages of heating and cooling may lead to changes in a relative content of the j-th microstructure in unit mass V_j of the metal being in a certain state (at a certain time moment).

Mathematically, for a simple cycle heating–cooling this assumption can be formulated as follows:

$$\begin{gathered} \text{in zone where } T_{\max} < T_*,\ dV_j \equiv 0; \\ \text{in zone where } T_{\max} > T_* \\ \text{at } T > T_*,\ \ V_a = 1.0,\ V_j \equiv 0, \text{ if } j \neq a \end{gathered} \qquad (3)$$

(here j corresponds to: a — austenite, m — martensite, f — ferrite, p — pearlite, etc.);

Table 1. Calculated dependencies for Cr^{eq} and Ni^{eq}

Source	Cr^{eq}, %	Ni^{eq}, %
Sheaffler	Cr + Mo + 1.5Si + 0.5Nb	Ni + 30C + 0.5Mo
DeLong	Cr + Mo + 1.5Si + 0.5Nb	Ni + 30(C + N) + 0.5Mo
Hammer and Svenson	Cr + 1.3 Mo + 1.5Si + 2Nb + 3Ti	Ni + 22C + 14.2N + 1.31Mn + Cu
WRC-1992	Cr + Mo + 0.7Nb	Ni + 35C + 20N + 0.25Cu

$$\text{at } T \le T_* \text{ and } \frac{\partial T}{\partial t} > 0,\ dV_j \equiv 0;$$

$$\text{at } T \le T_* \text{ and } \frac{\partial T}{\partial t} < 0,\ V_j = V_j(T).$$

Here the kind of function $V_j(T)$ is determined by a corresponding diagram of transformation of austenite for steel of a given chemistry under conditions of continuous cooling, or using equivalent calculation dependencies (parametrical equations) [26, 28, 30, 32, 33, etc.].

The second way, despite its approximated character, is very convenient for realisation.

Studies [7, 8] suggest that for estimation of the kinetics of variations in V_j in the weld zone this kinetics should be expressed in terms of the function of cooling rate $\Delta t_{8/5}$ and temperature T, i.e.

$$V_j(T) = V_j^{\max}(\Delta t_{8/5})\, f_j(T), \qquad (4)$$

where

$$f_j(T) = 0 \text{ at } T > T_{st}^j - T \text{ or } T < T_{st}^j;$$

$$f_j(T) = 1 - \exp\left[a_j \frac{T_{st}^j - T}{T_{st}^j - T_e^j}\right] \text{ at } T_{st}^j > T > T_e^j.$$

Here T_{st}^j and T_e^j are the temperatures of start and end of transformation of austenite into the j-th microstructure ($j \neq a$), respectively; $V_j^{\max}(\Delta t_{8/5})$ is the final quantity of the j-th microstructure under the said cooling conditions for steel of a corresponding chemistry; and a_j is the coefficient equal approximately to 3.

Values of T_{st}^j and T_e^j are selected from the corresponding time-temperature transformation (TTT) diagrams for a given steel grade. As these values are hardly sensitive to small variations in chemistry and cooling rate at a temperature below 800 °C, their selection involves no special difficulties [29]. Some attempts were made to construct parametric dependencies [33] for these values; however, special care should be taken for using them.

It is most convenient to determine the $V_j^{\max}$ values for the penetration zone of dissimilar steels on the basis of the Schaeffler diagram (see Figure 1) or its more perfect versions (DeLong, WRC-1992, etc.). In this case the main microstructural components are austenite, ferrite and martensite. The input data for their estimation are the values of Cr^{eq} and Ni^{eq}, for which the appropriate dependencies are suggested (Table 1). Kinetics of variations in the $V_j(T)$ value can be calculated from (4). For this we assume that $T_{st}^f \approx T_{cryst}$, where T_{cryst} is the crystallisation temperature of the alloy (Figure 11), $T_e^f \approx T_{st}^m$. According to [31], the following dependence can be used for T_{st}^m at $0.03 < C < 0.35$ %:

$$T_{st}^m = 454 - 210C + \frac{4.2}{C} - A\cdot Ni - 16.8Cr^{eq} - 10.5Mn,$$

where $A = 21$ at $Ni > 5$ %; $A = 1.6Ni + \frac{65}{Ni}$ at $1.4 < Ni < 5$ %.

The value of T_e^m for such steels is approximately equal to $T_{st}^m = 126$ °C [31].

Various parametric equations [28, 30] can be used to obtain data on $V_j^{\max}$ for the near-weld zone on the side of ferritic steel sensitive to $\Delta t_{8/5}$. Thus, study [30] suggests the following dependence:

$$V_j^{\max} = \frac{1}{2}\left[1 + \text{erf}\,\frac{\ln(\Delta t_{8/5}/\Delta t_j^{50})}{\sqrt{2}\,\ln s_j}\right], \qquad (5)$$

where $j = m, f, fp$; $V_b^{\max} = 1 - V_m^{\max} - V_{fp}^{\max}$; $V_p^{\max} = V_{fp}^{\max} - V_f^{\max}$.

Here b is bainite; $\Delta t_{8/5}$ is the time of cooling of a material in the temperature range of 800–500 °C; and Δt_m^{50}, Δt_{fp}^{50}, Δt_f^{50}, s_m, s_f, s_{fp} are the model parameters. Δt_j^{50} corresponds to time $\Delta t_{8/5}$ at which $V_j^{\max} = 0.5$. Respectively, if Δt_j^{85} is time $\Delta t_{8/5}$ at which

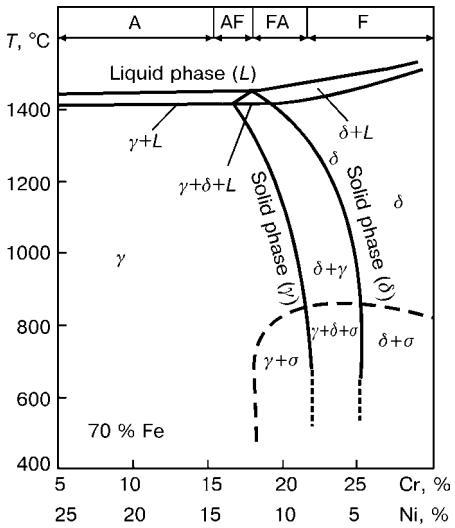

Figure 11. Constitutional diagram of alloy Fe–Cr–Ni (solidifying structures): A — austenite; AF — primary austenite; FA — primary ferrite; F — ferrite

$V_j^{max} = 0.85$, then $s_j = \Delta t_j^{50}/\Delta t_j^{85}$. The Δt_j^{50} and Δt_j^{85} values can be determined from the corresponding TTT diagrams.

Study [30] suggests, on the basis of statistical investigation of different groups of steels, dependencies relating these parameters to chemistry of steel; for example, for steel with the following chemical composition, %: C ≤ 0.3; Mn ≤ 2.0; Si ≤ 0.8; Cr ≤ ≤ 2.0; Mo ≤ 1.0; Ni ≤ 2.0; V ≤ 0.3; Ti ≤ 0.06; Al ≤ ≤ 0.06; Nb ≤ 0.1; W ≤ 0.5; Cu ≤ 0.5:

$$\begin{aligned}
\ln\Delta t_m^{50} &= -2.1 + 15.5C + 0.96Mn + 0.84Si + 0.66Cr + \\
&+ 0.74Mo + 0.55Ni + 0.3V + 4.0Al + 0.5W + 0.8Cu - \\
&- 0.25Nb - 13.5C^2 - 0.55Si^2; \\
-\ln s_m &= 0.56 - 0.41C + 0.1Mn + 0.14Cr - 0.3Mo + \\
&+ 2.7Ti + 0.5Cu - 1.1Nb + 1.7C{\cdot}Mo; \\
\ln\Delta t_{fp}^{50} &= 0.34 + 5.2C + 1.3Mn + 0.53Si + 0.33Cr + \\
&+ 2.9Mo + 0.36Ni + 1.5V + 1.0Cu - \\
&- 6.0C{\cdot}V - 5.1C^2 + 0.5Si^2; \qquad (6) \\
\ln s_{fp} &= 0.91 - 0.9C + 0.09Mn + 0.08Cr + 0.34Mo + \\
&+ 0.15Ni + 0.85V + 2.2Ti + 0.43W; \\
\ln\Delta t_f^{50} &= 0.66 + 10.0C + 1.3Mn - 0.48Si + 1.3Cr + \\
&+ 1.5Mo + 1.2Ni - 1.4W + 3.5C{\cdot}Mo - 5.9C^2; \\
\ln s_f &= 1.23 + 0.17Mn - 0.37Si + 0.3Cr - 0.5Mo + \\
&+ 0.31Ni + 0.09Nb - 0.43W - 0.3Cu.
\end{aligned}$$

The data on chemistry and microstructure of an alloy allow certain qualitative and quantitative estimations of service properties of the material.

An example of the qualitative estimation is shown in Figure 1. However, a number of quantitative characteristics of physical and mechanical properties of the alloy can be synthesised to a certain degree from the V_j values, the corresponding properties of the j-th microstructure being known, i.e.

$$X = \sum_{j=a,\,m,\,f,\,p} X_j V_j, \qquad (7)$$

where X is the desired characteristic (thermal conductivity, heat capacity, temperature elongation coefficient, yield strength, etc.), to which the additivity rule applies.

There is a number of studies where this approach is used to advantage [7, 8, 26, etc.].

Stresses and strains in welding dissimilar steels. Heterogeneity of properties of the weld and near-weld zone metal in welding dissimilar steels has a certain effect both on the kinetics of welding stresses (strains) and on the distribution of residual stresses, which is noted in studies [1, 4, 5, etc.].

Locality of variations in properties and, accordingly, high gradients of variations in stresses (strains) involve extra difficulties in employment of experimental methods for evaluation of the actual picture of distribution of residual stresses.

Stresses (strains) in welding depend upon sizes and shapes of parts joined and upon local phenomena occurring in microstructural changes in the weld and penetration zone. This circumstance leads to an additional increase in the number of the affecting parameters, which causes a special interest in application of the calculation methods both for evaluation of residual stresses and for description of the kinetics of variations in stresses (strains) at different stages of formation of a welded joint. The state-of-the-art numerical methods for calculation of stresses and strains during welding [34, 35, etc.] enable this problem to be successfully solved, providing that the adequate allowance is made for the kinetics of variations in volumetric factors and mechanical properties of a material during welding heating and cooling, resulting from the above microstructural variations. It is shown in studies [7, 8] that the free elongation function $\varphi(T)$ in heating–cooling, allowing for microstructural changes, can be calculated from the following dependence:

$$\varphi(T) = \frac{\sum_j V_j(T)\gamma_j(T) - \sum_j V_j(T_0)\gamma_j(T_0)}{3\sum_j V_j(T_0)\gamma_j(T_0)}, \qquad (8)$$

where T_0 is the initial temperature with respect to which the $\varphi(T)$ function is determined; $\gamma_j(T)$ is the volume of one gram of a material in the given j-th microstructural state at temperature T.

An idea of the values of $\gamma_j(T)$ can be obtained from the following data taken from [36], cm^3/g:

$$\begin{aligned}
\gamma_a(T) &= 0.12282 + 8.36{\cdot}10^{-6}(T + 273) + 2.15{\cdot}10^{-3}C; \\
\gamma_m(T) &= 0.12708 + 4.448{\cdot}10^{-6}(T + 273) + 2.79{\cdot}10^{-3}C; \\
\gamma_f(T) &\approx \gamma_b(T) \approx \gamma_p(T) = 0.12708 + 5.528{\cdot}10^{-6}(T + 273).
\end{aligned}$$

Yield strength of materials welded is an important characteristic for calculation of stresses (strains) in welding. Variations in the microstructural state have a substantial effect on this value. This is confirmed by the data shown in Figure 12 concerning variations in yield strength of different characteristic microstructures of steel A508 of the following composition, %: C — 0.162; Mn — 1.35; Si — 0.296; Cr — 0.196; Ni — 0.7; Mo — 0.504; Nb — 0.006; Al — 0.017.

They are indicative of the fact that differences in deformation resistance of some structural components are substantial. Using these data, it is possible to synthesise with a sufficient accuracy the values of $\sigma_y(T)$ with a differing combination of $V_j(T)$ from

$$\sigma_y(T) = \sum_j \sigma_y^j(T)\, V_j(T). \qquad (9)$$

To confirm, Figure 12 shows curve *3* plotted according to (9) using experimental data.

It should be noted that the values of $\sigma_y^j(T)$ retain an approximately constant dependence upon the temperature for the $\sigma_y^j(T)/\sigma_y^j(20\ ^\circ C)$ ratio within a sufficiently wide range of compositions of steels, which substantially facilitates the search for the required information in the case of absence of the data (of the

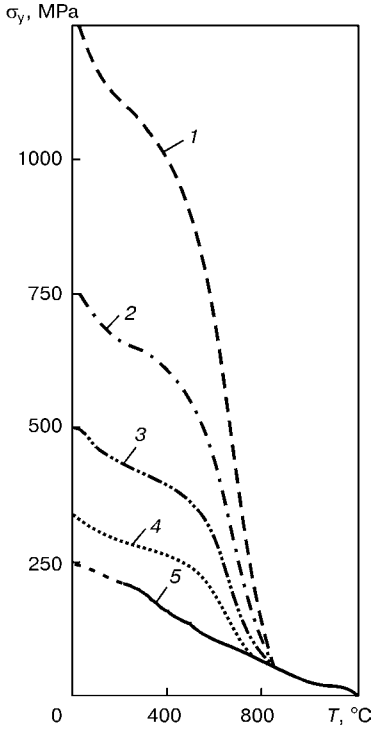

Figure 12. Dependence of yield strength σ_y upon temperature and microstructural state: *1* — $V_m = 1.0$; *2* — $V_b = 1.0$; *3* — $V_b = 0.4$, $V_f = 0.6$ (experiment); *4* — $V_f = 1.0$; *5* — $V_a = 1.0$

type of those given in Figure 12) for a specific chemistry of steel.

As far as the $\sigma_y^j(20\ ^\circ C)$ values are concerned, different approximated regression dependencies can be used in the case of absence of experimental data. Thus, according to the data of [26], for increased and high strength steels ($C \le 0.3$; $Mn \le 2.0$; $Si \le 0.8$; $Cr \le 2.0$; $Mo \le 1.0$; $Ni \le 2.0$; $V \le 0.3$; $Ti \le 0.06$; $Al \le 0.06$; $Nb \le 0.1$; $W \le 0.5$; $Cu \le 0.5$) the following dependencies can be used, MPa:

$$\begin{aligned} \sigma_y^m(20\ ^\circ C) &\cong 662 + 2150C + 500Mo; \\ \sigma_y^b(20\ ^\circ C) &\cong 500 + 400C - 120C^2 + \\ &+ 150V + 300Mo; \\ \sigma_y^{fp}(20\ ^\circ C) &\cong 187 + 92C = 47Mn + 90V. \end{aligned} \qquad (10)$$

As characteristics of elasticity (Young modulus, Poisson's ratio) hardly depend upon the phase composition of structural steels, allowance for microstructural variations causes no problems with selection of their values in the calculation of welding stresses and strains due to a very wide variation in chemistry and microstructure of metal of the penetration zone in welding of the dissimilar steels considered. It should

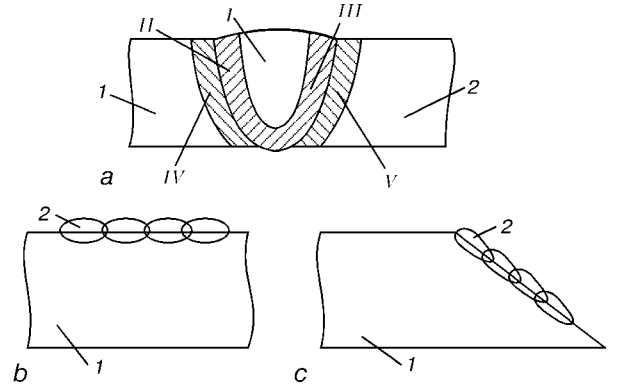

Figure 13. Schematics of welded joints in austenitic and ferritic steels in one-pass welding (*a*) and surfacing (*b, c*): *I* — weld zone of a mean composition; *II* and *III* — diffusion zone near the boundary with ferritic and austenitic steels, respectively; *IV* and *V* — HAZ in ferritic and austenitic steels, respectively; *1, 2* — ferritic and austenitic steels, respectively

be noted that varying the chemistry and microstructure of the penetration zone metal may have some effect on a temperature field through the thermal conductivity coefficient, the values of which may change depending upon the said parameters.

Table 2 gives data on $\lambda(T)$ for austenite of low-carbon austenitic steels and ferrite (pearlite) of low-carbon low-alloyed and Cr- (≈ 17 %) and Ni- (≈ 4 %) alloyed steels. It can be seen that thermal conductivity of ferrite $\lambda_f(T)$ can substantially change depending upon the chromium content.

As noted above, for the calculation of welding stresses (strains), in the case of welding dissimilar steels, the important factors are geometry and size of a part welded. Here it is necessary to distinguish the processes of welding proper for joining parts of dissimilar steels from the processes of depositing one material onto the other, i.e. the processes of deposition of a covering layer to impart certain functional properties to the parts (Figure 13).

In addition, it is important to note that in the cases considered the use can be made of multipass welding [37] and multilayer cladding [38].

Risk of formation of hot and cold cracks. The most characteristic defects in welding steels of the grade under consideration are those of the type of hot cracks formed primarily in the penetration zone, although there are cases where cold cracks may be formed in the near-weld zone of ferritic steel, or even in the penetration zone (see Figure 1).

The main cause of formation of hot cracks is a decrease in the ability of a material to deform at high temperatures in the so-called brittle temperature

Table 2. Dependence of thermal conductivity $\lambda(T)$ of different grades of steels upon the temperature, W/(m·°C)

Material	*Temperature, °C*										
	0	*100*	*200*	*300*	*400*	*500*	*600*	*700*	*800*	*900*	*1000*
Austenite	14.644	15.899	17.991	19.247	20.247	21.757	24.268	25.105	26.778	27.615	28.033
Alloyed ferrite	16.736	18.828	19.247	20.921	21.757	23.013	23.849	–	23.849	–	–
Unalloyed ferrite	62.762	57.322	51.138	46.025	41.841	41.004	35.983	31.799	–	–	–

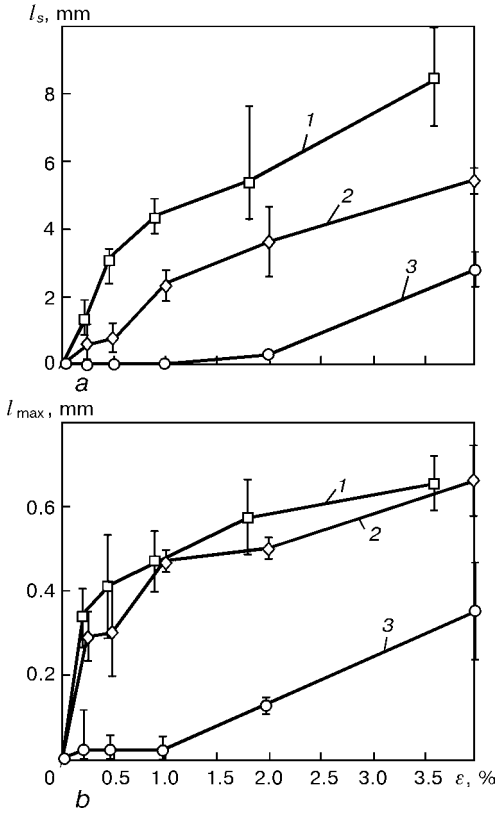

Figure 14. Effect of strain rate ε in Varestraint test on total length l_s of hot cracks (*a*) and maximum length l_{max} of one crack (*b*) in different alloys [39]: *1* — 316LN; *2* — D9; *3* — 316L

range (BTR). Tensile strains may form during welding in the penetration zone and the adjoining regions of the base metal. If a material cannot resist these strains, this leads to discontinuities, i.e. hot cracks. The ability of the material to resist deformation in BTR is usually determined experimentally. Among many methods used for this purpose the most popular one is the Varestraint test. Figure 14 shows an example of evaluation of resistance of the penetration zone of Cr–Ni alloys to formation of hot cracks using this method [39]. Chemistry of metal of the studied penetration zones produced by the method of argon-arc welding without a filler is given in Table 3.

By assigning a permissible total length of hot cracks (e.g. 1 mm), based on Figure 14, *a*, it is possible to obtain the value of critical strain ε^c_{xx} for transverse cracks in the penetration zone within the following ranges: 316LN — ε^c_{xx} = 0.2, D9 — ε^c_{xx} = 0.5 and 316L — ε^c_{xx} = 2.6 %. By assigning the permissible maximum length of a transverse crack (e.g. 0.1 mm), we will obtain, proceeding from Figure 14, *b*: for 316LN — ε^c_{xx} = 0.15, for D9 — ε^c_{xx} = 0.2 and for 316L — $\varepsilon^c_{xx} \cong$ 1.7 %.

It should be noted that the ε^c_{xx} values obtained in this way fail to fully characterise the history of deformation of a specific region in BTR, as they do not allow for welding strains which precede bending loading in the Varestraint test [39]. Because the values of true ε^c_{xx} are very small, the error in this case cannot be substantial.

In this connection, of note is the method of adjustment of the ε^c_{xx} values for transverse and longitudinal cracks obtained by the Varestraint test by an appropriate estimation of plastic strains accumulated in BTR prior to application of external load.

It can be seen from Figure 14 that chemistry of austenitic steel has a considerable effect on critical values of strains in BTR.

As proved by results of numerous studies [11, 20], resistance of austenitic and austenitic-ferritic steels to formation of solidification and segregation cracks greatly depends upon their microstructural state in BTR.

It can be seen from Figure 11 that in primary solidification the steel structure contains γ-austenite and δ-ferrite, in addition to the liquid phase *L*.

There is a number of theories which relate the probability of formation of solidification (as well as segregation) cracks to the indicated types of solidification modes for Cr–Ni stainless steels of the austenitic grades.

Main principles of these theories are based on the following considerations [10]: impurities of the type of sulphur and phosphorus have a higher solubility in ferrite, compared with austenite, which leads to decrease in their concentration at the grain boundaries, as well as the probability of hot cracking; molten metal containing δ-ferrite has a narrower solidification range; ferrite has a lower temperature elongation coefficient than austenite, which leads to lower shrinkage deformations for ferrite, compared with austenite, cooling conditions being identical; δ-ferrite has less favourable energy conditions for formation of low-melting point films with impurities of the type of sulphur, phosphorus and others in the solidification temperature range, compared with austenite, which leads to much easier conditions for formation of such films at the grain boundaries in the fully austenitic metal of the penetration zone; two-phase microstructural state of the penetration zone leads to formation

Table 3. Chemistry of metal of the penetration zones investigated by the Varestraint test method, %

Steel grade	*C*	*Ni*	*Cr*	*Mo*	*Mn*	*Si*	*P*	*S*	*N*
316L	0.029	11.9	17.0	2.25	1.8	0.7	0.035	0.012	0.036
316LN	0.03	11.15	16.8	2.06	1.45	0.53	0.031	0.001	0.073
D9*	0.052	15.06	15.05	2.25	1.5	0.5	0.011	0.002	0.066

*Steel contains 0.33 % Ti, in addition to the elements indicated.

of much stronger obstacles for propagation of cracks, compared with one-phase austenite.

The above considerations are proved by experimental studies. Thus, Figure 15 shows dependence [11] of susceptibility of Cr–Ni alloys to hot cracking upon the solidification modes. It follows from the Figure that the most favourable mode is FA, where the $\kappa_w = Cr^{eq}/Ni^{eq}$ ratio based on the WRC-1992 diagram (see Table 1) is within the following limits:

$$1.47 < \kappa_w < 2.00. \qquad (11)$$

Inequality (11) can be regarded as a metallurgical prerequisite for a low risk of formation of hot cracks in the penetration zone with a composition similar to that of Cr–Ni steels. This prerequisite corresponds to some mean deformation conditions which are determined by the test procedure (Varestraint test). However, as follows from Figure 14, the risk of hot cracking may depend to a substantial degree upon the specific values of strains in the BTR zone, which are characteristic of a given technology. This issue has been already widely discussed in literature [8, 11, 20, etc.].

Within the framework of the deformation theories of strength of materials and operational experience [8, 20], the deformation criterion of risk Γ_{ii} of formation of cracks with i normal to its plane can be developed, providing that the active plastic strain D_{ii} in the BTR zone, accumulated in cooling of a material, is known:

$$D_{ii} = \sum_i \Delta\varepsilon_{ii}^p \text{ at } \Delta\varepsilon_{ii}^p > 0; \quad \frac{\partial T}{\partial t} < 0; \quad \sigma_{ii} > 0; \quad T_1 < T < T_2, \qquad (12)$$

where T_1 and T_2 are the BTR limits.

It follows from expression (12) that in finding D_{ii} in BTR only the active plastic strains determined by the $\sigma_{ii} > 0$ are summed up.

If the critical values of ε_{ii}^c are known, then relationship

$$\tilde{D}_{ii} = \frac{D_{ii}}{\varepsilon_{ii}^c} \qquad (13)$$

can provide a quantitative characterisation of the risk of formation of cracks, Γ_{ii}, at a given point of the penetration zone, if the material, according to (11), has a sufficient sensitivity to such defects.

Unfortunately, the information available so far on the ε_{ii}^c values of alloys of different chemistries is scanty. Therefore, like in study [8], we suggest that condition (11) should be considered sufficient for a case of absence of hot cracks in the penetration zone of dissimilar steels studied; and where condition (11) is not met, condition (13) should be used to compare different variants in terms of the risk of formation of such defects.

As follows from Figure 1, cold cracks can be formed in the penetration zone of dissimilar steels of

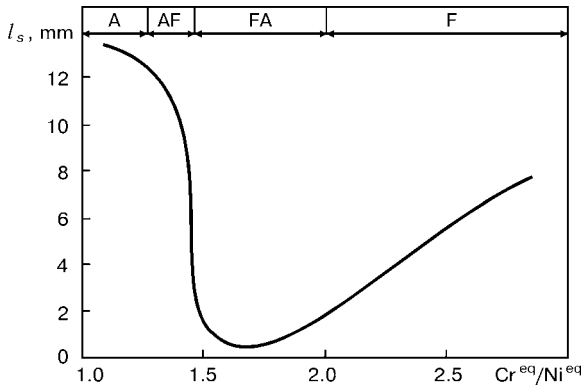

Figure 15. Dependence of susceptibility to hot cracking (based on the Varestraint test) upon Cr^{eq}/Ni^{eq}

the grade under consideration only in the case if this zone has a martensitic structure, which imposes substantial limitations on variants of compositions of the steels susceptible to formation of such defects. Nevertheless, we must reckon the probability of formation of cold cracks in the penetration zone.

Ferritic steels are characterised by a higher risk of formation of cold cracks in the near-weld zone. The vast arsenal of methods, including the calculation ones [8, 15, 20, 32], intended for prevention of cold cracking, can be applied for this zone. Therefore, there is no need to consider this issue in this article.

The following condition [8] can serve as a real criterion of elimination of cold cracking of the penetration zone:

$$V_m = 0 \text{ or } \sigma_{ii} < 0, \qquad (14)$$

i.e. there is no martensite in microstructure at any point of this zone, or in the presence of martensite the principal stresses are not tensile.

Behaviour under service conditions. Joints in dissimilar steels under consideration have certain peculiarities of behaviour under service conditions, especially if these conditions involve increased temperatures or thermal cycling, which is characteristic of certain structures used in power generation, chemical engineering, etc. [1]. Here the decisive role is often played by thermal stresses induced by differences in physical properties of steels joined, such as temperature elongation characterised by the temperature elon-

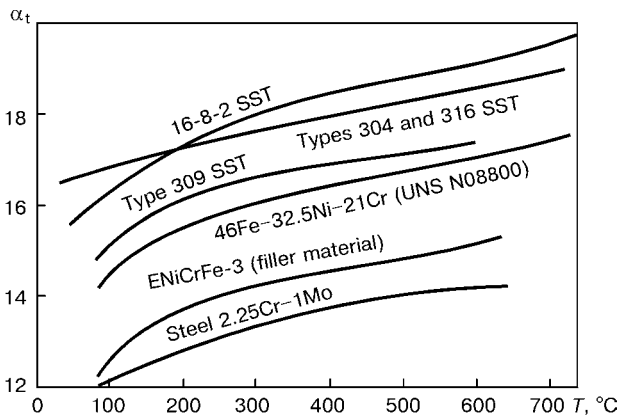

Figure 16. Variation in the temperature elongation coefficient $\alpha_t(T)$ with temperature for different alloys [10]

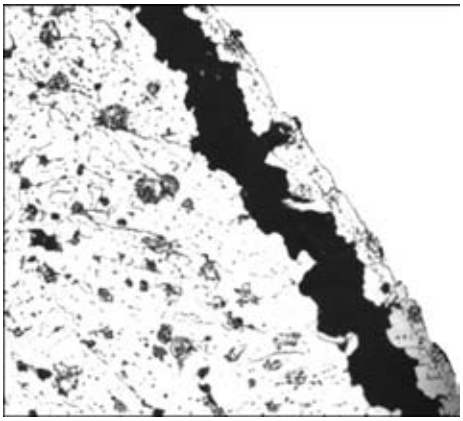

Figure 17. Typical appearance of a crack formed along the welded joint between austenitic stainless steel (deposited metal — *to the left*) and ferritic steel (base metal — *to the right*)

gation coefficient α_t. In this connection, of high importance is the issue of producing a weld (penetration zone) of a required composition, which would provide a more or less smooth transition between the joined dissimilar steels in terms of the α_t values.

As an example, Figure 16 shows data from [11] on the $\alpha_t(T)$ values of austenitic steels of the types of 304 (or 316) and Cr–Mo steel 2.25Cr–1Mo, this combination being characteristic of the power generation objects.

It is seen that in a temperature range of 100–700 °C the difference between the values of temperature elongation coefficients of austenite and ferrite will amount approximately to $6 \cdot 10^{-6}$ 1/deg:

$$\Delta\alpha_t(T) = \alpha_t^a(T) - \alpha_t^f(T) \approx 6 \cdot 10^{-6} \text{ 1/deg}.$$

Hence, every 100 °C of a uniform variation in temperature may cause variation in stresses in the joining zone amounting to 80–100 MPa, i.e. at a working temperature of about 500–550 °C due to differences in properties of materials welded, peaks of stresses may be of substantial values. Under such conditions, inelastic strains [1] are formed both due to instantaneous plasticity and due to creep. It is characteristic that tensile stresses and strains in heating are dominant near the fusion boundary in ferritic steel, and compressive ones are dominant in austenitic steels, respectively. To a certain extent, this circumstance results in the fact that among various kinds of service fractures of the joints under consideration, operating at increased temperatures and especially in thermal cycling, the cracks are dominant near the fusion boundary of a ferritic material [8, 11] (Figure 17).

Figure 16 shows values of $\alpha_t(T)$ for different filler materials used for welding of the considered dissimilar steels to form the above transition layer. As shown by the results of experimental studies, this can provide a substantial extension of service life of a welded joint. The data on a relative service life of butt welded joints (Figure 16) in austenitic steel of the type of 304 and Cr–Mo steel 2.25Cr–1Mo are a convincing proof of the above-said. For example, the relative

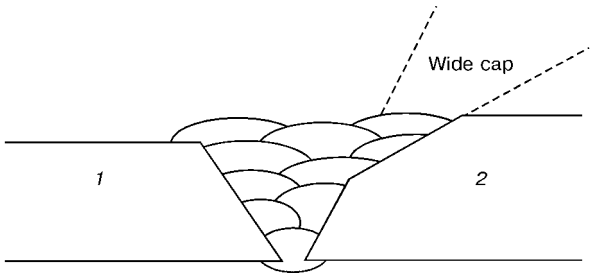

Figure 18. Wide cap groove of a joint between dissimilar steels: *1* — stainless steel; *2* — Cr–Mo steel

service life of a butt welded joint in steels 304 and 2.25Cr–1Mo, depending upon the filler material used, varies as follows: in the case of use of the E309 filler metal the relative service life is 1.0, with the ENiCrFe-1 filler metal it is 4.6, and with the ENiCrFe-2 and ENiCrFe-3 filler metals the relative service life is 5.1 and 5.1–5.6, respectively.

A change in the groove shape, i.e. the so-called wide cap (Figure 18), for edge preparation of ferritic steel also leads to an extension of life due to a more favourable stressed state formed in thermal cycling.

For the above combination of materials welded the use of the wide cap groove and ENiCrFe-1 filler metal, instead of E309, increases life by a factor of 7.7 [11], which enables the life of the considered joints in thermal cycling to be extended by varying design and technology parameters.

Mathematical modelling of the stress-strain state of the joints under consideration during thermal cycling, depending upon the groove shape and chemistry of a filler metal, can be very helpful in search for rational solutions.

CONCLUSIONS

Upon considering seven areas associated with the problem of selection of optimal design-technology conditions for welding (surfacing) of joints in dissimilar steels, we can distinguish a number of problems which can be solved in the most rational way by using the methods of mathematical modelling with a limited scope of experiments. To use this way to solve the posed problems, it is necessary to develop the appropriate algorithms and software. It should be noted that the processes of primary solidification and carbide formation during welding, as well as degradation of properties in service thermal cycling, are least studied in terms of mathematical description.

Therefore, the main purpose in handling the tasks posed will be development of a computer system capable of solving the following problems in an integrated way: heating and formation of the penetration zone; determination of chemistry of the weld pool; evaluation of primary solidification defects; quantitative estimation of the kinetics of structural changes in the weld and near-weld zone, stresses and strains, as well as risk of formation of hot and cold cracks; and prediction of behaviour of a welded joint under different service conditions.

1. Zemzin, V.N. (1966) *Welded joints in dissimilar steels*. Moscow-Leningrad: Mashinostroyeniye.
2. Murugan, N., Parmar, R.S. (1997) Effect of welding conditions on microstructure and properties of type 310 stainless steel submerged-arc cladding. *Welding J.*, **5**, 210–220.
3. Nelson, T.W., Lippold, J.C., Mills, M.J. (1999) Nature and evolution of the fusion boundary in ferritic-austenitic dissimilar weld metals. Part 1, Nucleation and growth. *Ibid.*, **10**, 329–337.
4. Nelson, T.W., Lippold, J.C., Mills, M.J. (2000) Nature and evolution of the fusion boundary in ferritic-austenitic dissimilar weld metals. Part 2, On-cooling transformations. *Ibid.*, **10**, 267–277.
5. Nho, S.-H., Ann, H.-S., Ong, C.-W. (1992) Derivation of theoretical residual stress and stress intensity factors in dissimilar weld metal of nuclear vessel. In: *Proc. of Int. Conf. on Trends in Welding Research*, Gatlinburg.
6. Taliat, B., Zacharia, T., Wang, X.-L. et al. (1998) Numerical analysis of residual stress distribution in tubes with spiral weld cladding. *Welding J.*, **8**, 328–335.
7. Makhnenko, V.I., Velikoivanenko, E.A., Rozynka, G.F. et al. (1999) Choice of rational sizes of mock-up of welded assemblies in development of welding technology. *Avtomatich. Svarka*, **7**, 3–-14.
8. Makhnenko, V.I., Velikoivanenko, E.A., Rozynka, G.F. et al. (1999) Computer modelling of welding processes as the means for prediction of defects in welded joints. *Ibid.*, **12**, 10–19.
9. Petrov, G.L. (1963) *Heterogeneity of welded joint metal*. Leningrad: Sudpromgiz.
10. Sterenbogen, Yu.A. (1971) *Study of the process of chemical heterogeneity formation in welds and near-weld zone*. Syn. of Thesis for Dr. of Sci. Degree. Kyiv: PWI.
11. (1998) *Welding Handbook*. Part 2, Materials and applications. Miami: AWS.
12. Makhnenko, V.I. (1967) Calculation of thermal processes in welding of dissimilar plates. *Fizika i Khimiya Obrab. Materialov*, **6**, 1–5.
13. Rykalin, N.N., Uglov, A.A. (1965) Temperature field in dissimilar materials in butt welding with surface heat source. *Ibid.*, **5**, 3–10.
14. Rykalin, N.N. (1951) *Calculation of thermal processes in welding*. Moscow: Mashgiz.
15. Makhnenko, V.I. (1998) Computer modelling of welding processes. In: *Modern Materials Science for the 21st Century*. Kyiv: Naukova Dumka.
16. Kim, S.D., Na, S.I. (1992) Effect of weld pool deformation on weld penetration in stationary gas tungsten arc welding. *Welding J.*, **5**, 179–193.
17. Ohrig, S., Lugt, H.J. (1999) Numerical simulation of time-dependent 3-D GMA weld pool due to a moving arc. *Ibid.*, **12**, 417–424.
18. Movchan, B.A. (1956) Diffusion processes and chemical compositions of fusion zone in welds. *Avtomatich. Svarka*, **6**, 3–9.
19. Sterenbogen, Yu.A., Demchenko, V.F., Abdulakh, V.M. (1977) Study of the process of chemical heterogeneity formation in weld metal solidification. *Ibid.*, **2**, 5–8.
20. Prokhorov, N.N. (1976) *Physical processes taking place in welds during welding*. Moscow: Metallurgiya.
21. Bertram, L.A., Schunk, P.R., Kempka, S.N. et al. (1998) The macroscale simulation of remelting processes. *J. Metals*, **3**, 18–20.
22. Mastac, L., Sundarraj, S. (1998) The stochastic modelling of solidification structures in alloy 718 remelted ingots. *Ibid.*, **3**, 30–35.
23. Kryzhanovsky, R.E., Shtern, Z.Yu. (1977). *Thermophysical properties of nonmetallic materials (carbides)*. Leningrad: Energiya.
24. Gulyaev, A.P. (1966) *Physical metallurgy*. Moscow: Metallurgiya.
25. Karzov, G.P., Margolin, B.Z., Markov, V.G. et al. (1998) Nature of damage of KPPTs downtake pipelines of RBMK reactors and means for their elimination. In: *Proc. of 5th Int. Conf. on Materials Science Problems in Design, Manufacture and Service of Nuclear Power Plant Equipment*, St.-Petersburg.
26. Kasatkin, O.G. (1990) *Mathematical modelling of relationships composition-properties of welded joints and development of the calculation-experiment system for optimisation of principal factors of low-alloy steel welding*. Syn. of Thesis for Dr. of Sci. Degree. Kyiv: PWI.
27. Ueda, J., Murakawa, H., Luo Ju. (1995) A computational model of phase transformation for welding processes. *Transact. of JWRI*, **1**, 95–100.
28. Jon, I.C., Salminen, A.S., Sun, Z. (1966) Process diagrams for laser beam welding of carbon manganese steels. *Welding J.*, **7**, 225–232.
29. Seyffarth, P. (1982) *Groβer Atlas Schweiβ-ZTU-Schaubieder*. Düsseldorf: DVS-Verlag.
30. Seyffarth, P., Kassatkin, O. (1982) Calculation of structural transformation in welding process. *IIW Doc. IX*.
31. Beres, L. (1998) Processed modification to Schaeffler's diagram for chrome equivalents and carbon for more accurate prediction of martensite content. *Welding J.*, **7**, 273–276.
32. Hrivnyak, I., Makhnenko, V.I. (1983) Application of computational methods for study of steel weldability. In: *Proc. of 2nd CMEA Symp. on Application of Mathematical Methods for Study of Weldability*, Sozopol, Sept. 3–5. Sofia: V.I. Lenin VMEI.
33. Bruzda, E., Zeman, M. (1983) Statistical analysis of austenite anisothermal decomposition diagrams for a selected group of steels performed at the Welding Institute. *Ibid.*
34. Makhnenko, V.I. (1976) *Computational methods of study of welding stresses and strains*. Kyiv: Naukova Dumka.
35. Ueda, J., Murakawa, H., Nakano, K. et al. (1995) Establishment of computation welding mechanics. *Transact. of JWRI*, **2**, 73–85.
36. Yuriev, S.F. (1950) *Specific volume of phase in martensitic transformation of austenite*. Moscow: Metallurgizdat.
37. Makhnenko, V.I., Velikoivanenko, E.A., Makhnenko, O.V. et al. (1999) Study of influence of phase transformations on residual stresses in welding of tube circular joints. *Avtomatich. Svarka*, **12**, 10–19.
38. Makhnenko, V.I., Velikoivanenko, E.A., Kravtsov, T.G. et al. (2001) Numerical studies of thermomechanical processes in surfacing of shafts of ship mechanisms. *The Paton Welding J.*, **1**, 2–10.
39. Shaukar, V., Gill, N.P.S., Marnan, S.L. et al. (1998) Evaluation of hot cracking in nitrogen-bearing and fully austenitic stainless steel weldments. *Welding J.*, **5**, 193–201.

EXPERIMENTAL INVESTIGATIONS OF FIELDS OF RESIDUAL STRESSES IN WELDED AND ROLLED I-BEAMS

A.I. GOLODNOV[1] and **M.Yu. KHVORTOVA**[2]
[1]The E.O. Paton Electric Welding Institute, NASU, Kyiv, Ukraine
[2]Donbass State Academy of Civil Engineering and Architecture, Lugansk, Ukraine

Stress-strain state of I-beams was determined using experimental data. Method of preliminary stress inducing to I-beams by a local thermal effect allowing increase in load-carrying capacity of compressed I-beam columns and improvement in structure of steel in the HAZ zones forming in fabrication of welded I-beams was suggested.

Key words: *I-beam, local thermal effects, residual stresses*

Technological processes of fabrication of welded and rolled I-beams with a use of rolling, flame cutting and welding are a cause of occurrence of high internal residual stresses, which can influence greatly the further structure operation under the load. Thus, the internal stresses in rolled I-beams caused by a non-homogeneous plastic deformation during rolling in stand and non-uniform temperature fields during rolling and cooling can reach $0.8\sigma_y$ (σ_y — steel yield strength). Using experimental investigations [1], it was found that the cooling conditions, in particular the difference in temperature between the coldest and hottest points of section after the rolling in the stand is the most significant factor among other factors influencing the distribution and level of residual stresses in the I-beam section.

In welded I-beams the residual stresses can reach the level of the steel yield strength in the zones of girth welds [2, 3]. Moreover, both in as-delivered welded and rolled I-beams the diagrams of internal stresses have a common origin: a compressed web, as well as flange, being under tension in a central part and with compressed free ends. Stresses in compressed edges of flanges, subjected to the action of a compressive service load, reach the yield strength earlier than in other elements of the section, thus decreasing the moment of inertia of the section due to far distance of zones of plastic deformation from the symmetry axes.

To create the favourable distribution of residual stresses in the sections of I-beam columns operating for compression under the service load, a method of high-temperature preliminary stress inducing by heating edges of the girth to about 950 °C was suggested. The appearance of zones of residual tensile stresses at the edges of girths promotes the later transition of edges into a plastic state and leads to increase in a load-carrying capacity of the column.

During testing the technological procedure, different schemes of a preliminary stress generation were suggested [4]. Here, such technological parameters were varying as temperature and sequence of heating, power source capacity, rate of heating and cooling, sizes of HAZ. The preliminary stress was realized both in the laboratory (at the Chair of Engineering Structures of Donbass Mining-Metallurgical Institute) and shop conditions (at the I.V. Babushkin DZMK, investigations were headed by I.I. Nabokov). In the latter case the preliminary stress was generated in a specially-designed bench by a simultaneous heating of flange edges to 850–900 °C with a displacement of torches along the all length of the specimen and cooling of heated areas with a compressed air.

During preparation of the program of experimental investigations the following tasks were set:

- to determine the internal stressed state of as-delivered rolled H-beams of K-type;
- to establish natural residual stresses in welded I-beams fabricated at the I.V. Babushkin DZMK using an accepted technological scheme of assembly and welding of I-beams in the production line;
- to determine the internal stress-strain state of welded and rolled I-beams, being preliminary subjected to stress using local thermal effects (LTE), by heating I-beam flange edges up to temperature of about 950 °C;
- to develop the technological scheme of prestressing by LTE depending on the section shape and sizes of the specimens.

Welded specimens-beams (further beams) of series SL and ST and hot-rolled I-beams 35K1 with parallel sides of flanges of series SP were used. All the specimens were manufactured at the I.V. Babuskin DZMK in 1981. The length of specimens was 1400 mm. Specimens of series ST were subjected preliminary to stresses in shop conditions by a local heating of edges with a next cooling with a compressed air, while the series SL were designed and fabricated as analog of the prestressed specimens, but without subjecting to the preliminary stress.

Before the tests the specimens of metal were examined to define their physical-mechanical properties.

At the first stage of investigations the internal stress-strain state of as-delivered experimental beams was determined. The residual strains and stresses were determined using a destructive method.

The specimens of series SL and SP were preliminary subjected to stresses in the laboratory conditions by a local thermal heating of edges with a next cooling in air. Taking into account that the sizes of specimens were close to full-scale specimens, then an individual scheme of preliminary stressing by LTE was accepted for each specimen.

The preliminary stress was induced in the following sequence:

- geometric parameters of the specimen were measured and areas for next preheating were marked, then the holders were welded to determine the absolute deformations in a middle section of the specimen;
- the specimen was mounted on a bench and instruments were installed, the initial data were measured;
- the preliminary stress was induced to one of the edges; after cooling the intermediate results were taken;
- the preliminary stress was induced to another edge of the flange to record the final results after cooling.

In the course of testing the deflections in six points of the specimen and absolute displacements in the middle section were determined. For each specimen the individual scheme of preliminary stress inducing by LTE was taken. Residual strains and stresses in beam flanges were determined using a destructive method.

In the process of the experiment the initial stress-strain state of the sections of beams was determined. Some results of investigations are given in Figure 1.

A conclusion was made on the basis of analysis of used schemes of preliminary stresses (sequence of edge heating) that the preliminary stressing by LTE should be realized by a symmetrical heating of areas of girths using the heat sources of a similar capacity to prevent the non-uniform deforming. The comparative analysis of schemes of the preliminary stress inducing was based on the evaluation of the following parameters:

- level of residual stresses in the section of I-beams;

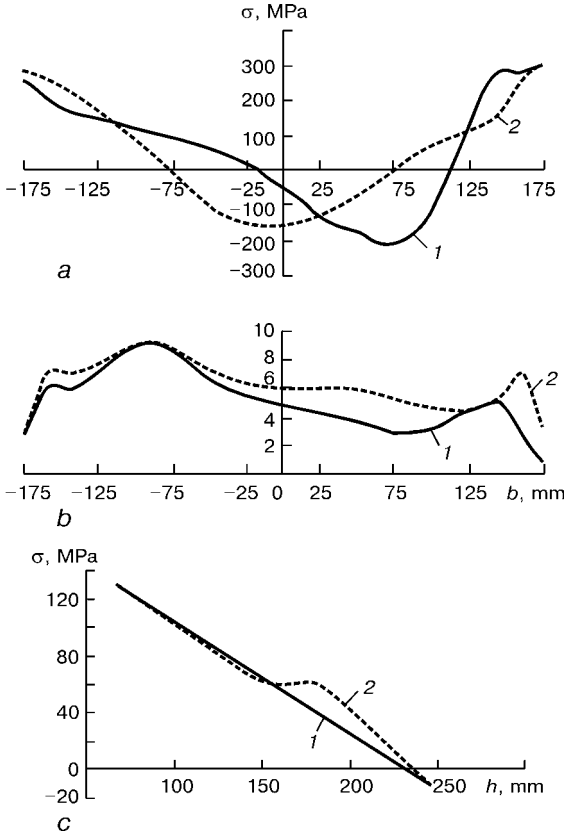

Figure 1. Results of determination of residual internal stresses in sections of I-beams in a heated flange stresses (*a*), in flange without preliminary stress inducing (*b*) and in web (*c*): *1* — specimen SP 20/1; *2* — specimen SP 20/2 (*b* — flange width; *h* — web height)

- shape of diagram of distribution of residual stresses in a transverse section;
- structural changes in steel as a result of heating.

The level and shape of the diagram of distribution of residual stresses in the sections of I-beams were determined using a destructive method [5]. Conclusion was made that the preliminary stress by LTE should be induced using symmetrical heat sources of a similar capacity (due to a non-uniform distribution of residual stresses and non-uniform deforming), i.e. to perform only in the shop conditions at a strict control of parameters of heating and cooling.

It was stated on the basis of the metallographic analysis of changing the structure of steel of the speci-

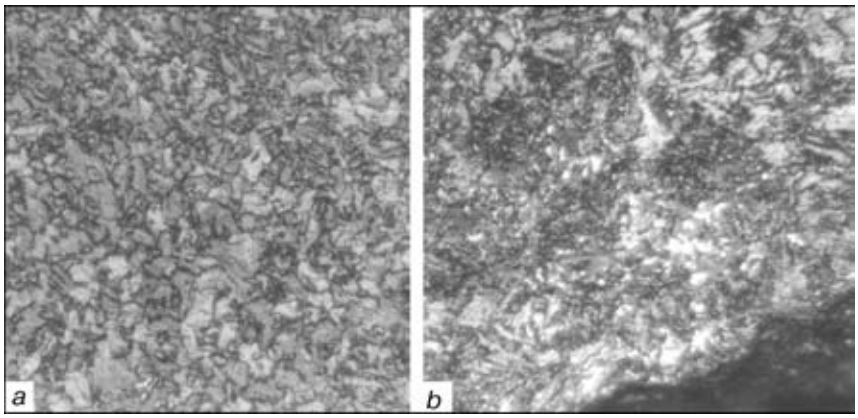

Figure 2. Microstructure St.3 in a normalized state (*a*) and in fusion zone during thermal cutting (*b*) (×400) (reduced by 2/3)

mens examined that at preliminary stress inducing by LTE the heating temperature should be by 40–50 °C higher than the temperature of point A_{c_3} with a next cooling in air. It is the temperature of heating at which the normalizing of hypoeutectoid steels is occurred, to which the structural steels also belong.

In normalizing the low-carbon steels the same processes are proceeding, that in annealing, i.e. refining of grains (Figure 2, *a*). In addition, due to a more rapid cooling than in annealing, the pearlite becomes more dispersed as a result of a high overcooling, and its amount becomes larger as the precipitation of ferrite or cementite with a formation of a quasi-eutectoid is partially suppressed. The characteristics of mechanical properties are occurred to be higher than those in a delayed cooling (annealing).

Thus, at LTE on the edges of beam flanges with a small overheating above the temperature of polymorphous transformation a secondary diffusion-free crystallization (recrystallization) in a solid state is occurred in the metal of edges of the girths. This causes the changes in a crystal structure of the metal due to appearance and growth of new grains.

In fabrication of welded I-beams the defibring of sheets by a thermal cutting is occurred that leads to the formation of the metal structure with a clearly expressed zone of overheating at the edges of flanges (Figure 2, *b*), which is typical of the coarse-grained structure of Widmanstaetten type. Metal of this zone is characterized by low values of mechanical properties. At a preliminary stress inducing by LTE of zones of this structures a fine-grained structure is formed anew as a result of an additional heating (see Figure 2, *a*).

Thus, the application of the preliminary stress inducing by LTE for metal structures makes it possible not only to create the diagrams of residual stresses, which influence positively on the structure operation under the load, but also to improve significantly the steel structure by refining grains of the parent metal and elimination of HAZ which are formed due to temperature effects in fabrication of metal structures.

1. Nyashin, Yu.I. (1980) Investigation of methods of reduction of residual stresses in hot-rolled shape sections. *Izv. Vuzov, Chyorn. Metallurgiya*, **10**, 25–27.
2. Shelestenko, L.P. (1954) Effect of natural residual stresses on a total stability of compressed welded H-shaped elements. *Zheleznodorozhn. Stroitelstvo*, **2**, 22–24.
3. Lui, Kh., Massone, Ch. (1962) Effect of welding residual stresses on critical load caused by longitudinal bending of I-beams. In: *Proc. of 13th IIW Congress*, Liege, July 13–19, 1960. Moscow: Mashgiz.
4. Zhdanova, I.V., Khvortova, M.Yu., Golodnov, A.I. (1998) Experimental determination of deflection of metallic beams with fields of initial stresses. In: *Transact. of Alchevsk DGMI*, Issue 7. Alchevsk: DGMI.
5. Khvortova, M.Yu. (1998) Determination of initial stresses in sections of I-beams after local thermal action. *Ibid*.

FLUX-CORED WIRES of FeCrB+Al and FeCr+Al+C SYSTEMS for ELECTRIC ARC METALLIZING

V.I. POKHMURSKY, M.M. STUDENT, V.M. DOVGUNYK and **I.I. SIDORAK**
G.V. Karpenko Physico-Mechanical Institute, NASU, Lviv, Ukraine

The electric arc metallizing can be effectively used for restoration of worn-out surfaces of machine parts at relatively small expenses. The use of flux-cored or composite wires widens significantly the application of this technological process. However, the need appears here in optimizing composition of electrode wires and improvement of system of their spraying.

Key words: *electric metal spray-gun, electric arc metallizing, flux-cored wire, thermal coating, wear, wear-resistance, phase transformations*

To increase the quality of coating formation in electric arc metallizing, we have developed the new spray heads for metal spray-guns (MSG) [1, 2] and flux-cored wires (FCW) and also performed the comparative tribologic examination of the coatings produced.

Metal coatings were formed from 1.8 mm diameter FCW of an optimized chemical composition of two systems: FeCrB+Al and FeCr+Al+C. Ferrochrome-boron FKhB-2 and Al–Mg powder PAM-40 and, respectively, ferrochrome FKh-800, iron powder PShO, Al–Mg powder PAM-40 and crucible graphite GT-1 were used as charge materials. The external sheath was manufactured from 0.4 mm thick rimmed steel 08 (C — 0.1; Si — 0.03; Mn — 0.35–0.65 wt.%; Fe — balance). Coefficient of wire filling was about 20 %. The coatings were formed by a base MSG M-17 with a modified system of electrode material spraying that provided the formation of fine-grained coatings of a low porosity (≈ 10 %).

Metallizing conditions were as follows: arc current 150 A, arc voltage 34 V, compressed air pressure 0.6 MPa, distance from arc to sample 100 mm. The coatings were deposited on samples of «disc» type made from steel 45 (C — 0.45 wt.%; Fe — balance) (*HRC* 28–30) and subjected to grinding to the 1 mm

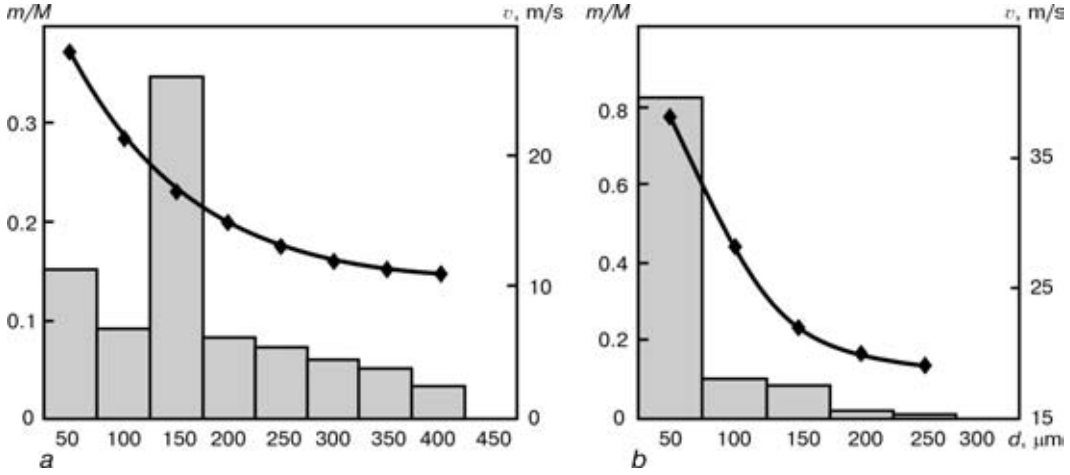

Figure 1. Dependence of relative amount of molten metal particles and rate of their fight v (◆) on the size of particles d (m — mass share of particles of a proper fraction; M — mass share of all the particles at central nozzle (*a*) and differential (*b*) diagram of spraying)

working thickness R_a = 0.63. Mating samples were made from bronze BrS.30 and high-tin alloy AMO.

Tribologic properties of the obtained coatings were studied in friction equipment SMTs-2 using scheme «disc–block» at a boundary slipping friction, and also in motor oil (M14V2) with an abrasive addition (a quartz sand of dispersity up to 40 μm) at contact pressure 5 MPa. Path of friction was 20 km.

The phase composition of coatings in initial state, its changes in near-surface layers after grinding and friction were examined in Dron-3 diffractometer (CuK_α, U = 32 kV, I = 13 mA) with a 0.05° scanning pitch at 1, 3, 5, 10° angles of inclination of sample to emission and next computer processing by program CSD [3].

Systems of spraying of flux-cored wires. They are based on differential and closed diagrams of formation of a metal-air flow. In realization of the differential diagram of spraying there are no differences between the conditions of melting wires, used as anode or cathode. The metal-air flow has an ellipsoid structure in its section at ratio of axes 1:3–5 at 100 mm distance from the arc (Figure 1).

The differential diagram of formation of the metal-air flow was used in MSG, manufactured by GMP «Gasothermic» at G.V. Karpenko Physico-Mechanical Institute of the NAS of Ukraine. The design feature of the spray head of such spray-gun is that the electrode wire and air are fed through the same channels. In addition, the conditions of effective cooling of current conductors and spray-gun head are created, thus providing the formation of concentrated gas external (plasma) and internal (for nozzle cooling) flows. The use of a ring-shaped profiled nozzle increases the rate of the air flow, creates a high dynamic pressure in the zone of arc burning that provides the intensive dispersion of the molten metal. Due to this, the adhesion and cohesion characteristics of the coating are increased. At such diagram of FCW spraying the largest size of the particles of molten metal is 150 μm. MSG with this diagram of spraying provides the formation of quality restoration and wear-resistant coatings from FCW with a refractory charge.

The closed diagram promotes the producing finer fractions of particles (< 50 μm) characterizing the high rate of flight. This diagram of spraying is used in formation of the fine-dispersed coating of a small thickness (50–200 μm) produced by using FCW (charge with refractory components).

Flux-cored wires of FeCrB+Al systems. As is known, the amorphous boron, boron carbide and ferrochromeboron can be used as a B-containing component in manufacture of FCW. However, we used a ferrochromeboron of FKhB-2 grade, as the amorphous boron is expensive and a boron carbide provides an intensive wear of grooves in wire manufacture.

At the same time the coatings produced from FCW with a charge only from ferrochromeboron are characterized by a high porosity as the powder has no time to be completely melted. The complete melting of a comparatively refractory B-containing core can be realized in adding components forming eutectics with it or the aluminium powder in amounts providing the proceeding of alumothermic reaction. Addition of other elements to the charge forming eutectics with a ferrochromeboron or ready eutectic mixtures, leads to a significant decrease in a cohesion strength of the coating.

It was established by us that only the aluminium powder promotes the producing coatings with high mechanical characteristics, increases, in particular, the rupture strength of the coating from 180 to 230 MPa. From the relationship, given in Figure 2, it is possible to judge about the effect of aluminium content in the FCW charge. Increase in aluminium concentration in the charge up to 30 % promotes the increase in the coating hardness. This is stipulated by decrease in porosity of the coating with a simultaneous increase in its structural homogeneity. The further increase in the aluminium content in the FCW charge composition leads to the decrease in hardness. A monotonous increase in cohesion and adhesion is observed in the whole range of changing the aluminium concentration. The positive effect of aluminium on the strength properties of coatings can be explained by the presence of a refractory oxide film Al_2O_3 produc-

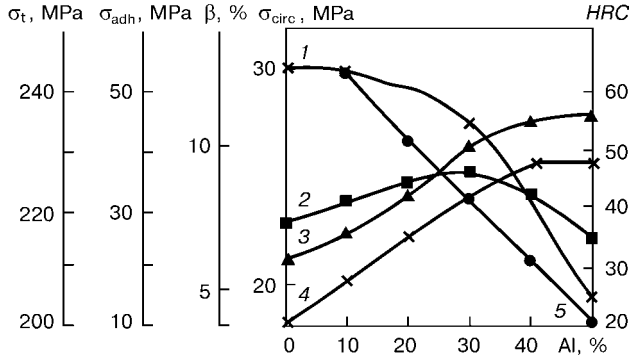

Figure 2. Effect of aluminium content in charge of FCW (FeCrB+Al) on physical-mechanical characteristics of 1 mm thick coatings: *1* — maximum circumferential stresses in coating σ_{circ}; *2* — hardness *HRC*; *3* — adhesion strength of coating with substrate σ_{adh}; *4* — rupture strength of coating σ_t; *5* — porosity β

ing plastic grains of pure aluminium in the coating. This contributes to the relaxation of tensile stresses in the process of the coating formation and subsequent cooling and also prevents the crack formation. The coatings are rather heterogeneous, which is proved by a large scattering of values of microhardness, from 4000 to 10000 MPa. Maximum porosity is not more than 10 %.

It was established that the boron content in the coating is proportional to that in ferrochromeboron and can be increased by increasing the FCW diameter. Here, the coefficient of wire filling will be also increased. However, it can be noted, that in use of large-diameter FCW the coating hardness is increased simultaneously with decrease in its adhesion to the substrate. Therefore, in restoration of heavy-duty parts it is necessary to use FCW of diameter to 2 mm.

The level of air pressure also greatly influences the distribution of stresses in the coatings. With its increase from 0.2 to 0.7 MPa the size of particles of FCW melt is decreased that provides in turn the decrease in size of pores in the coating from 400 to 50 μm (Figure 3).

Flux-cored wires of FeCr+Al+C systems. The base of charge in manufacture of FCW of system FeCr+Al+C is high-carbon ferrochrome of FKh-850 grade. To attain the complete melting of the charge due to proceeding of exothermal reaction, similar to

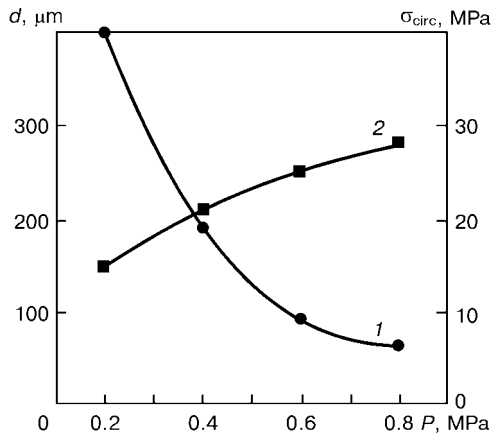

Figure 3. Effect of air pressure *P* on diameter of pores in coating *d* (*1*) and value of maximum circumferential stresses σ_{circ} (*2*)

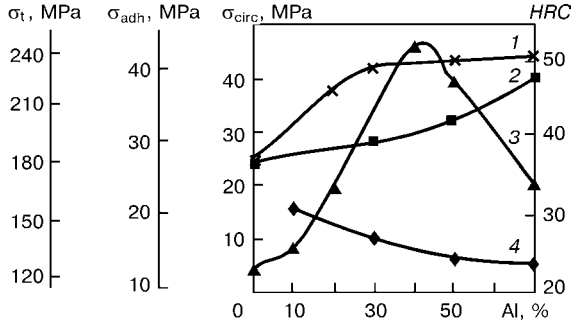

Figure 4. Effect of aluminium content in charge FCW (FeCr+Al+C) on physical-mechanical characteristics of 1 mm thick coating: *1* — rupture strength of coating σ_t; *2* — adhesion strength of coating with substrate σ_{adh}; *3* — maximum circumferential stresses in coating σ_{circ}; *4* — hardness *HRC*

previous FCW, the aluminium powder was added to the charge. At its content to 10 % the coatings possess maximum hardness (*HRC* 30) and retain the low level of maximum circumferential stresses (to 10 MPa). The increase in concentration leads to the decrease in coating hardness and increase in stresses reaching their maximum values (46 MPa at 40 % Al). Further, their decrease to 20 MPa at 70 % Al is observed. Adhesion of coatings is increased in the whole range of changing the aluminium concentrations.

It was established that at low concentrations of aluminium in FCW charge the γ-Fe→α-Fe occurs in the process of coating cooling. At appropriate amount of carbon in the coating (≈ 1 %), the high hardness and low residual tensile stresses are typical of the coatings because of austenite transformation into martensite. The increase in aluminium amount in the coating stabilizes α-Fe and narrows the region γ-Fe that prevents the feasibility of proceeding transformation (FeCr+Al+C). This leads to the increase in tensile stresses and decrease in the coating hardness.

Thus, in formation of coatings using FCW with a charge on FeCr+Al+C base two concentration (by aluminium content) regions are most important from the practical point of view (Figure 4) [4]. At aluminium content to 10 % the coatings are characterized by a high hardness and low level of residual tensile stresses and can be used as wear-resistant. Above 50 % the coating hardness does not exceed *HRC* 26, the level of tensile stresses is ≈ 20 MPa, and the adhesion strength is ≈ 40 MPa. In this connection, they are recommended for use as restoration coatings for appropriate surfaces of heavy-duty machine parts.

Tribologic properties of coatings. It was established by the comparative tests of coatings from solid and FCW in the conditions of boundary slipping friction that the best tribologic properties are typical of coatings produced by using FCW with a charge (FeCrB+Al) and (FeCr+Al+C) [5, 6].

Metallographic examinations of the coatings showed that they have a lamellar structure typical for the given class of coatings (Figure 5).

The phase composition of coatings from FCW on FeCrB+Al base in initial state is a mechanical mixture consisting of an oversaturated solid solution on α-Fe

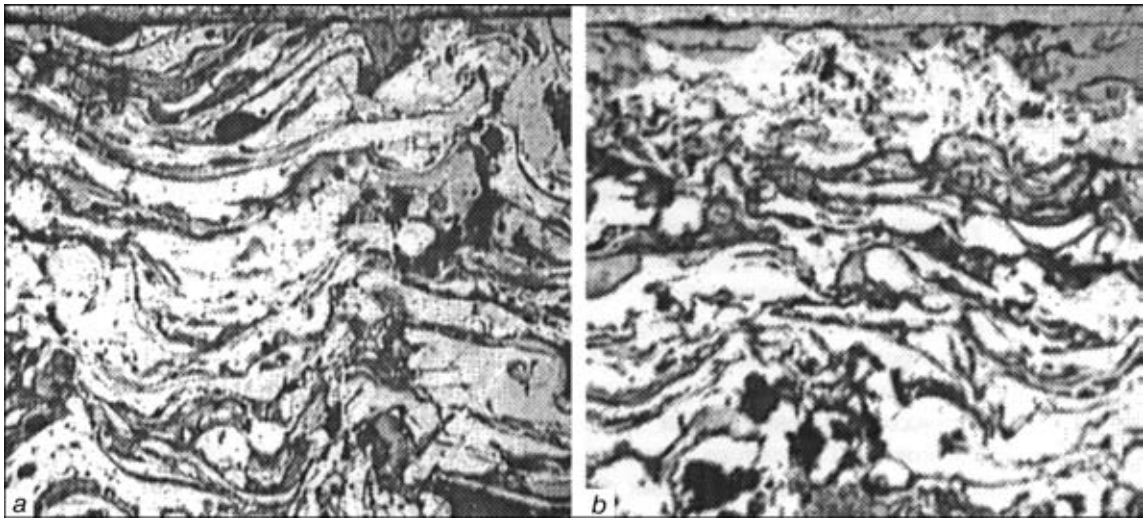

Figure 5. Microstructure of coatings made from FCW of systems FeCrB+Al (*a*) and FeCr+Al+C (*b*) (×250)

base, negligible amount of solid solution on γ-Fe base, chrome borides CrB, iron Fe_2B and FeB, and also nitride CrN and oxides of iron Fe_3O_4 and chrome Cr_2O_3 [7].

The phase composition of coatings from FCW on FeCr+Al+C base in initial state is a mechanical mixture consisting of a residual austenite, martensite, oxides of iron Fe_3O_4 and chrome Cr_2O_3, and also a negligible amount of nitrides of aluminium and chromium [4].

As a result of friction interaction the change in phase composition and simultaneous strengthening occur in the surface layers. Using an inclined X-ray filming it was stated that a negligible amount of γ'-phase ($(Fe, Al)_4N$ and $Fe_3(C_{0.2}B_{0.8})$) was revealed additionally in coatings produced from FCW of FeCrB+Al system even after grinding. In this case the microhardness of coating increases from 6500 to 8500 MPa owing to formation a structure in the surface layers consisting of a nitrogen martensite, dispersed γ'-phase and carboboride. The surface layers of coatings produced from FCW of FeCr+Al+C system consist of a mechanical mixture which already contains 90 % martensite, and also chromium carbides $Cr_{23}C_6$ and Cr_7C_3 and negligible amount of carbide of a cementite type $(Fe, Cr)_3C$. Thus, even in grinding the residual austenite is decomposed partially with a formation of special carbides. It becomes less alloyed and is subjected to a martensitic transformation in cooling. This contributes to strengthening of surface layer of coatings even after grinding. The phase composition of coatings is not practically changed in the process of a boundary friction. The averaged temperature of samples did not exceed 25–30 °C. The coating material wear was not observed in a preset path of friction of 20 km.

At the boundary friction with abrasive adding the averaged temperature of samples reached 120 °C (FeCrB+Al system) and 60 °C (FeCr+Al+C system). The increase in temperature in the zone of a real contact and plastic deformation leads to some change in the phase composition. The amount of carboboride $Fe_3(C_{0.2}B_{0.8})$ in the coating surface layer FeCrB+Al is increased while in the coating FeCr+Al+C the austenite amount is increased, carbides $Cr_{23}C_6$ and Cr_7C_3 were not observed. Only carbide of a cementite type and oxides of iron and chromium were revealed.

Thus, composition of charge of FCW, phase composition of coatings in initial state, its changes in surface layer during friction influence greatly the wear resistance.

The above-mentioned materials have been developed for the restoration, as a rule, of external surfaces of parts of «shaft» type operating in pair with slipping bearings made of a traditional materials. The FCW with a charge (FeCrB+Al) provides the highest complex of mechanical characteristics, it is mass produced and widely used in Ukraine and beyond it for the restoration of worn-out crankshaft pins, tractors, locomotive diesels, compressors, pumping stations. FCW with a charge (FeCr+Al+C) is also used for restoration of crankshaft pins of tractors and other equipment operating in less severe conditions.

1. Pokhmursky, V.I., Student, M.M., Pikh, V.S. et al. *Head for spray gun*. USSR author's certificate 1657230, Int. Cl. B 05 B 7/22. Publ. 23.06.91.
2. Vabishchevich, V.G., Prishlyak, A.M., Ostashevsky, N.D. et al. *Wire arc spray-gun*. USSR author's certificate 1484378, Int. Cl. B 05 B 7/22. Publ. 07.06.89.
3. Pokhmursky, V.I., Student, M.M., Dovgunyk, V.M. et al. (1999) Use of arc spraying with flux-cored wire of Fe–Cr–Al–C system for restoration of machine parts. *Mashinoznavstvo*, **1**, 13–18.
4. Student, M.M., Dovgunyk, V.M., Sydorak, I.Y. et al. (1999) Effect of friction on structural-phase transformations in near-surface layer of FeCr+Al+C thermal spray coatings. *Ibid.*, **5**, 113–116.
5. Pokhmursky, V.I., Shyrokov, V.V., Student, M.M. et al. (1997) Wear-resistant thermal coatings produced from flux-cored wires of Fe–Cr–Al–C system. *Problemy Trybologii*, **3**, 48–55.
6. Student, M.M. (1988) Burning of charge components of flux-cored wire during arc spraying of coatings. In: *Proc. of 4th Corrosion-98 Int. Conf.-Exhibition on Problems of Corrosion and Anticorrosive Protection of Materials*, Lviv, June 9–-11.
7. Student, M.M., Dovgunyk, V.M., Sydorak, I.Y. et al. (2000) Effect of friction of phase changes in near-surface layers of FeCrB+Al thermal spray coatings. *Fiz.-Khim. Mekhanika Materialiv*, **4**, 109–113.

The paper presented below describes just one example of multi-faceted engineering and development activity of V.E. Paton, related to designing equipment for mechanized and automatic welding. Together with a team of other developers, V.E. Paton was awarded the State Prize of Ukr. SSR in the field of science and technology for development and introduction into production of microplasma welding processes, equipment and technology for unique advanced engineering systems.

The past decades have confirmed the timeliness of the ideas and the high effectiveness of the original engineering solutions, incorporated by V.E. Paton and the team led by him, into development of a system of precision welding equipment.

Editorial

A SYSTEM FOR MECHANIZED MICROPLASMA WELDING OF HONEYCOMB ALUMINIUM METAL STRUCTURES

V.E. PATON, N.M. VOROPAJ and **V.S. GVOZDETSKY**
The E.O. Paton Electric Welding Institute, NASU, Kyiv, Ukraine

The paper deals with the design principles and features of all-purpose and specialised microplasma welding equipment. Examples of application of mechanised units in fabrication of unique open honeycomb metal structures of thin aluminium are given.

Key words: *microplasma welding, plasmatron, welding units, power source, open honeycomb metal structures, welding technology, weld quality*

The industry's need for high-quality joints of various metals and alloys of the thickness of several tens up to 1–2 mm led to development of microplasma welding. This is, essentially, a new method of precision processing of metallic and non-metallic materials by a constricted arc, that runs in a stable manner at low currents, that are practically unachievable in the conventional non-consumable and consumable electrode arc welding.

As far back as 1967 the E.O. Paton Electric Welding Institute suggested original methods of AC microplasma welding and equipment for its implementation [1, 2]. They are patented in England, Germany, Italy, France and Japan.

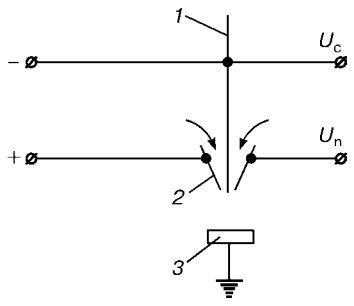

Figure 1. Schematic of the process of microplasma welding at current of different polarity (for designations see the text)

The essence of the microplasma process (Figure 1) consists in that in order to achieve the cathode breaking up of the oxide films on the metal being welded, voltage pulses positive relative to item *3* are fed to the nozzle of plasmatron *2* for powering the reverse polarity (RP) arc, and in the intervals between them voltage pulses, negative relative to the item, are fed to tungsten electrode *1*, generating a straight polarity (SP) plasma arc between the electrode and the item. A DC low-amperage pilot arc, generating the plasma plume, runs continuously between the tungsten electrode and the nozzle in the plasma gas flow. It results is a stable condition of the microplasma arc of different polarity current. Plasma gas (argon) comes to a circular gap between the tungsten electrode and the nozzle; shielding gas (as a rule, helium) — to the gap between the plasma gas and the protective nozzle.

This method turned out to be the most effective in welding aluminium and aluminium alloys 0.2–2.0 mm thick. It is exactly the method that allowed creation of unique items of thin commercial aluminium. The PWI developed a range of all-purpose and specialised units, fitted with the plasmatrons and power sources for mechanised microplasma welding of this type of metal structures. This paper is devoted to description of the principles and features of their design.

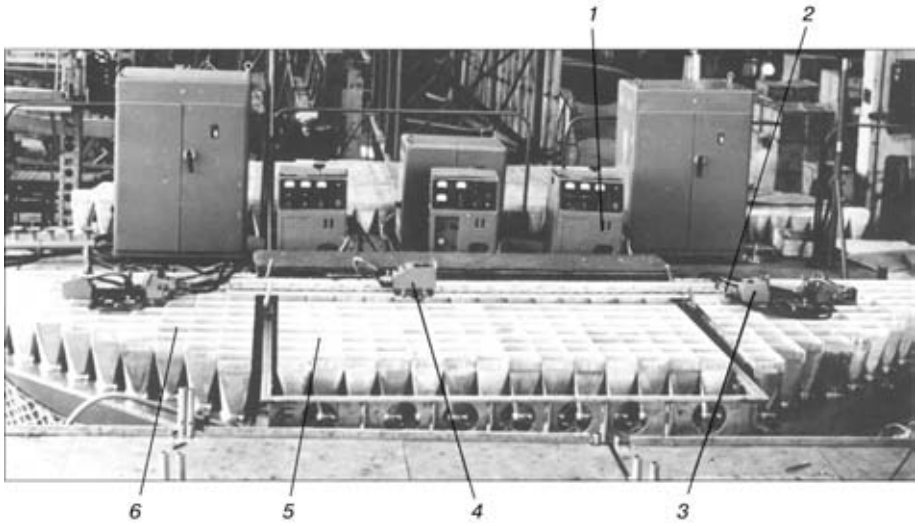

Figure 2. Welded sections of honeycomb metal structures: *1* — A-1281 power source; 2 — OB-213 plasmatron; *3* — A-1284B automatic machine; *4* — A-1284 automatic machine; *5* — inner section; *6* — peripheral section

An open honeycomb structure of array antennas is assembled of individual sections, consisting of a large number of abutted elements (horns), where the upper edges are 0.5–2.0 mm thick (Figure 2). Total length of welds on one item is more than 10,000 m. The edges of the aluminium horns should have a reliable electrical and mechanical contact over the entire perimeter to provide the required performance of the antenna. The tolerances specified for geometrical dimensions of edge welds of the antenna elements are very close. Horns are usually made in the form of a welded tetrahedral truncated pyramid, with an up to 10 mm thick aluminium flange butt welded to its smaller base. Considering the exceptionally high technical requirements to the quality of welded honeycomb antenna elements and a rather large scope of welding operations, performed both under the stationary shop conditions and in site, the design of the microplasma welding units should provide a number of new functional capabilities, namely:

- precise guiding of the electrode along the weld axis (deviation of not more than ±0.1 mm per the linear length of 1 m of the weld);
- minimal axial deviations of the arc from the set value (not more than ±0.1 mm);
- reliable operation of the plasmatron elements and other components at continuous welding for not less than 8 h;
- stable feed of the soft and stiff small-diameter filler wire (0.8–1.2 mm);
- absence of excess forces of inertia in the unit components, disturbing the uniformity of welding speed;
- minimal weight and overall dimensions of the unit;
- ability to readjust the equipment to perform welding operations in site.

The basic model for development of specialised welding equipment was the precision automatic machine A-1342 designed by the PWI Experimental Design-Technology Bureau, with OB-1213 plasmatron and A-1281 power source, that was used for development of A-1284 and A-1284B units for welding antenna sections (Figure 2) and A-1478 and A-1579 units for welding the longitudinal welds of horn billets and welding-on the flanges, respectively.

A-1342 automatic machine (Figure 3) is designed for mechanised microplasma welding of butt, fillet, edge and overlap joints of 0.2–2.0 mm thick metal. It consists of carriage *1*, filler wire feed mechanism *2*, plasmatron *3*, correction system *4*, control panel *5* and guide rail *6*. The carriage is fitted with four freely rotating runners with a vertical axis of rotation. Two runners are mounted directly on the carriage, and two others — on levers with spring loading. The carriage is driven by an electric motor, with a gear wheel mounted on its output shaft. The gear wheel is connected to the guide rail rack. Welding speed is smoothly adjustable in the range of 10–100 m/h. Deviations in the electrode guiding to the butt in the transverse and vertical directions do not exceed ±0.1 mm along the guide rail length of 1300 mm.

Filler wire is fed, using a special device that provides a stable and accurate guiding of the soft aluminium wire of 0.8–1.2 mm diameter. The wire feed rate is smoothly adjustable in the range of 5 to 150 m/h. The wire feeder incorporates a drive and a clamping element, made of an elastic belt put on two

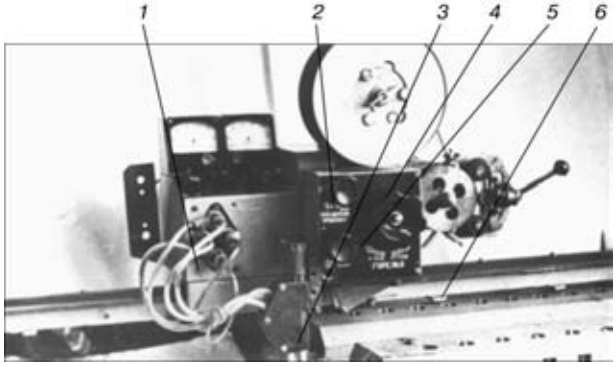

Figure 3. All-purpose automatic machine A-1342 for microplasma welding (for designations see the text)

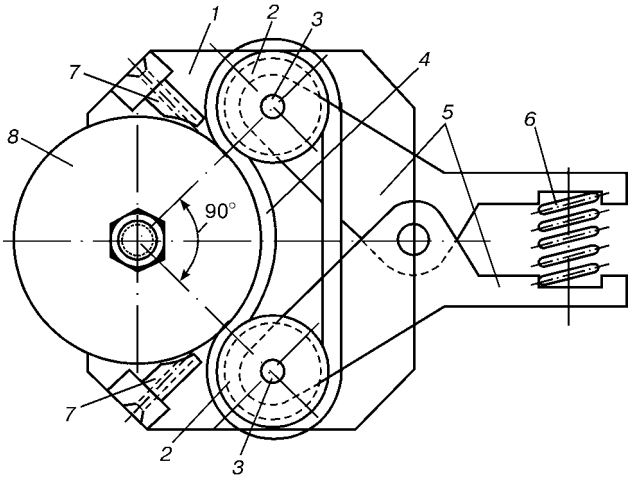

Figure 4. Filler wire feeder (for designations see the text)

rollers, loosely mounted on axles. To avoid deformation of the wire when a rigid feed roller is used, the belt is mounted on the rollers so that it is in engagement with the feed roller groove and encloses it along an arc of not more than 90°.

Wire feeder (Figure 4) consists of base *1*, levers *5* with spring *6*, two loose rollers *2* on axles *3*, elastic belt *4*, rigid shaped feed roller *8*. The base accommodates receiver bushings *7* for guiding the filler wire. The device operates as follows. Filler wire, uncoiled from the reel, is first passed through the receiver guide bushings, then is pressed down by the belt under the action of the spring and the levers. After the roller is set in rotation, the wire is fed to the welding zone under the impact of the forces of friction. The belt starts rotating simultaneously, as it is put on the rollers, loosely mounted on the axles. The described system provides rather high forces of pulling the filler wire, irrespective of its rigidity.

The block of correctors, on which the plasmatron is mounted, provides its transverse and vertical displacement simultaneously with the filler wire. Independent correction of the wire position in the horizontal and vertical planes is also envisaged. The lateral corrector is made in the form of a lever, fastened on two ball-bearings with a worm gear. The vertical corrector is a lead screw, driven by the nut of the gear that is driven by a screw-gear. The carriage body carries the control panel of the welding process monitoring and control. At operation in the automatic mode the automatic machine design envisages initial switching on and subsequent switching off of the plasma and shielding gas feed, and changing of the mode parameters by a preset program.

OB-1213 plasmatron was developed specifically to provide reliable operation of the equipment in the mode of welding extended welds. It differs from the earlier applied OB-1115 and OB-1160 plasmatrons by more intensive water cooling of the working elements and ability to perform welding at relatively high speeds (up to 50 m/h) and high currents (up to 100 A), respectively. In OB-1213 plasmatron the cathode, made of lanthanum-alloyed tungsten of 1.2–1.6 mm diameter, is aligned with the water-cooled molybdenum plasma-shaping nozzle. A collet spring-loaded device allows adjustment of the depth of electrode insertion inside the nozzle in the range of 1–10 mm. Geometrical shape of the nozzle inner channels provides a laminar outflow of the plasma and shielding gases. Plasmatron power is 3 kW, its outer diameter is 25 mm and height is 130 mm, hose length being up to 5 m at the weight of 350 g.

A-1281 machine (Figure 5) is used for supplying AC power to OB-1213 plasmatron with an adjustable amplitude of SP and RP pulses. It consists of a power transformer *TV*, thyristor blocks *VS1*, *VS2* and control panel *4*. Positive half-cycles of voltage come to nozzle *1* via *VS1*, and the negative half-cycles arrive at tungsten electrode *2* of the plasmatron via *VS2*. The current of the SP and RP arc is adjusted by choke *L*, connected into the transformer primary circuit or by moving the transformer secondary circuit. A pilot arc powered by DC source *3* is used for a stable excitation of the charge at the start of each half-period.

A-1284 automatic machine (Figure 6) is designed for microplasma welding of longitudinal and transverse edge welds of honeycomb structure sections. It consists of carriage *1*, plasmatron *2*, guide rail *3* of 10 m length and a system of pneumatic key clips *4* for horns *5* being welded. The carriage body design is the same as in A-1342 automatic machine. Wire feeder is absent in this case. For convenience of welding operations performance, the control panel is

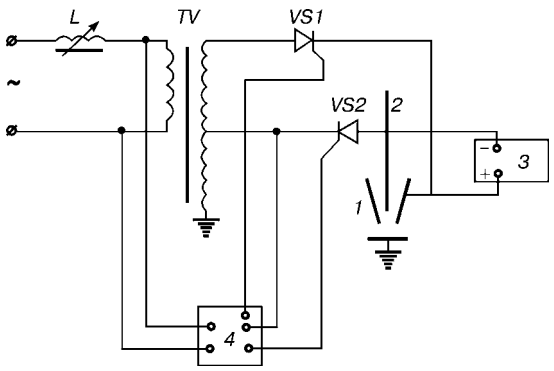

Figure 5. Block diagram of A-1281 machine (for designations see the text)

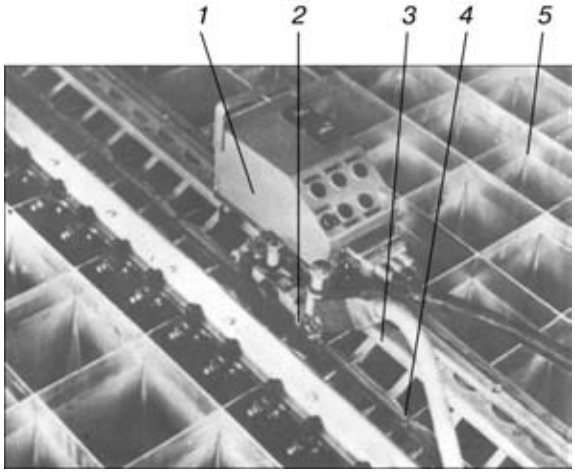

Figure 6. A-1284 automatic machine for welding longitudinal and transverse welds (for designations see the text)

mounted on a carriage. A-1284 automatic machine incorporates OB-1213 plasmatron and A-1281 power source.

A-1284B automatic machine (Figure 7) allows performance of welding of the honeycomb structure peripheral sections around a rectangular profile. It is made in the form of two self-propelled carriages *1* and *2*, providing displacement of OB-1213 type plasmatron *3* in two directions normal to each other around the closed perimeter of individual horn *4*. Use of this automatic machine is rational in site for preassembly of peripheral sections of a honeycomb array and during repeated repair operations. Control circuit diagram of A-1281 power source is adjusted to a preset cyclogram of the welding process.

A-1578 machine (Figure 8) is designed for mechanised microplasma welding of longitudinal butt welds on box-shaped elements. Given the appropriate re-adjustment the unit provides welding of horns of three types: from two rectilinear or curvilinear blanks or four trapezoidal blanks of 400–1000 mm height. The size of the horns opening is 100×100–500×500 mm at the dimensions of the flange part of 30×30–70×70 mm.

Machine specification

Thickness of metal being welded, mm	0.5–2.0
Welding speed, m/h	10–50
Plasmatron correction, mm	
transverse	±15
vertical	–50
Tungsten electrode diameter, mm	1.2–1.6
Filler wire diameter, mm	0.8–1.2

The machine comprises self-propelled carriage *1* (A-1342 automatic machine), plasmatron *2*, bed plate *3*, frame *4*, mandrel *5*, panel accommodating pneumatic equipment *6*, pneumatic cylinder *8*, control panel *9*, support *10* and power source *7*. The carriage is fitted with four runners with triangular grooves. Two runners are located directly on the carriage, and two others — on spring-loaded levers. Electric drive UT-11M is provided to move the carriage along the weld axis, its drive shaft carrying a gear wheel, that comes into engagement with the guide rail rack. A hand-wheel of vertical corrector is located in the upper part of the carriage body.

During welding the horn remains stationary, and the plasmatron moves along the butt with the speed of welding. Vertical displacement of the plasmatron in welding of horns of a curvilinear shape is provided by a copying system. The mandrel is used for product assembly before welding. Fastened to the mandrel is a technological backing of stainless steel with an oval groove. Frame *4* carries the mechanism of pneumatic key clamps.

A-1579 system is designed for mechanised microplasma welding of butt welds of individual elements of box-shaped items with rounded corners of a square or rectangular cross-section [3]. This is the case of manufacturing the elements of honeycomb structures

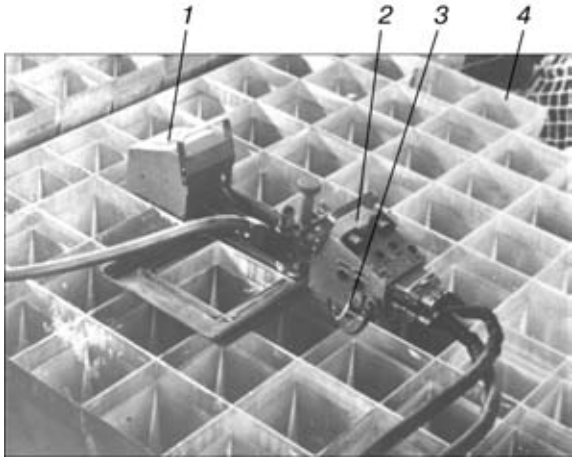

Figure 7. A-1284B automatic machine for making welds around a rectangular perimeter (for designations see the text)

of commercial pure aluminium 1 mm thick (flanges welding to the box).

To eliminate the forces of inertia, arising in rotation of this kind of items and the process fixture, the parts being welded and the fixture are not imparted any rotation in this unit, but are only displaced relative to the plasmatron along rectangular coordinates. At the moment, when the item displacement is finished, the plasmatron rotates by an angle, corresponding to the angle between the adjacent welds. This angle is equal to 90° for an item of a rectangular cross-section. To reduce the overall dimensions of the unit, the microplasma welding is performed by making a horizontal weld in the vertical plane.

Under the conditions of mass production of box-shaped welded items, application of the above unit

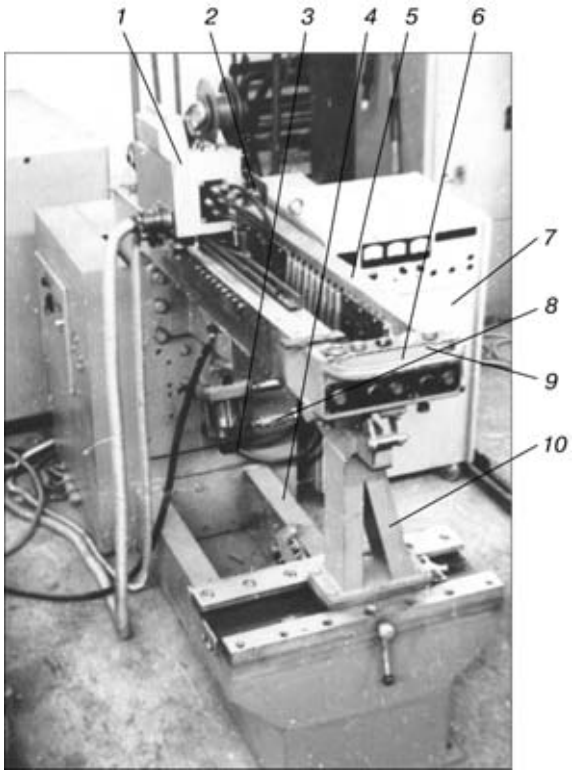

Figure 8. A-1578 machine for making longitudinal butt welds of box-shaped elements (for designations see the text)

allowed the efficiency of microplasma welding to be increased 2 to 3 times. Weld quality is essentially improved due to a precise guiding of the arc along the axis of a butt of a complex profile.

Based on the above design developments, mechanised microplasma welding has been successfully mastered in fabrication of various products of light metals and alloys in aircraft, radio engineering, mechanical engineering and other branches [4]. Technology and equipment for microplasma welding of aluminium cases of household electric water heaters of BAS-10/MCh-04 type of 10 l capacity have been developed [5]. The casing of this part is made of two extruded billets of Al–Mn alloy 1.5 mm thick. The billets are joined by microplasma welding of edge welds around the entire perimeter of the casing in a unit, similar to A-1579 machine. An example of application of mechanised microplasma welding for thin aluminium butt joints are blanks for sealing gaskets of chemical apparatuses [6, 7]. The thickness of the metal being welded in this case is 0.2 to 0.3 mm. Specialised U-549 unit has been developed for microplasma welding of this type of gaskets. Many years of experience of welded gasket operation demonstrate their reliability under the extreme conditions of high temperatures and dynamic loads.

Experience has also been accumulated of microplasma welding of aluminium cases of capacitors, protective casings and shells, as well as other critical items [4]. The basic design ideas, incorporated into the high-precision equipment, have become applied for development of equipment for mechanised welding of position butts of joints on aluminium and steel piping [8].

There is considerable potential for further widening of the areas and increasing the volumes of application of microplasma technology. Special attention should be given to development of the technology and equipment for microplasma welding of cost-effective sheet structures of alloyed steels, various non-ferrous, refractory and less-common metals and alloys, that can stand high temperatures, alternating loads and temperature gradients, having the high temperature and corrosion resistance and a number of other properties. Such structures have an important role for cosmonautics, aviation, nuclear engineering, chemical industry and other areas.

It is of interest to study the technological capabilities of microplasma, fed by high-frequency square-wave current pulses, when the rate of current rise is much higher, than the rate of ionisation front development in the radial direction. It has become necessary to unify the main components of microplasma welding equipment, namely power unit, ignition unit, current interrupter, mechanisms of displacement and filler wire feed, plasmatrons and gas equipment. Promising is the development of multi-station power sources, allowing equipment operation to be simplified in batch production. Combined multihead systems, consisting of three to four or more plasmatrons can be highly efficient, this being the key to an even more abrupt increase of microplasma welding speed. Such welding speeds should be used in fabrication of thin-walled pipes of a strip, honeycomb profiles of various cross-sections, in welding strips for continuous rolled stock. It is natural that an abrupt increase of welding speed is directly related to solving the problem of complete mechanisation, automation and robotisation of the microplasma welding process. The possible fields of application of microplasma welding equipment are certainly not limited by the examples given in the paper.

1. Paton, B.E., Dudko, D.A., Gvozdetsky, V.S. et al. *Plasma welding process*. USSR author's certificate 221477, Int. Cl. B 23 K. Publ. 18.04.68.
2. Paton, B.E., Dudko, D.A., Gvozdetsky, V.S. et al. *Power source for AC welding*. USSR author's certificate 234574, Int. Cl. B 23 K. Publ. 22.10.68.
3. Paton, V.E., Belfor, M.G., Voropaj, N.M. et al. *Unit for welding box-shaped items with rounded corners*. USSR author's certificate 498141, Int. Cl. B 23 K/37/04. Publ. 05.01.76.
4. (1979) *Microplasma welding*. Ed. by B.E. Paton. Kyiv: Naukova Dumka.
5. Voropaj, N.M., Patsovsky, Yu.V., Petrov, V.Yu. et al. (1976) Microplasma welding of casings of electric water heaters. *Avtomatich. Svarka*, **2**, 73–74.
6. Voropaj, N.M., Shcherbak, V.V., Grigoriev, A.A. (1971) Pulsed microplasma welding of thin aluminium gaskets. *Khimich. i Neftyan. Mashinostroyeniye*, **11**, 19.
7. Yarinich, L.M., Gvozdetsky, V.S., Ignatchenko, G.N. (1974) Microplasma welding of seal rings. *Avtomatich. Svarka*, **6**, 41–42.
8. Paton, V.E., Voropaj, N.M., Kushniruk, V.P. et al. (1975) Automatic welding of pipeline position joints. *Ibid.*, **11**, 36–38.

FEATURES OF PULSED-PLASMA ALLOYING OF THE SURFACE OF IRON-BASE ALLOYS

Yu.N. TYURIN, M.L. ZHADKEVICH, B.G. GUBENKO and **O.V. KOLISNICHENKO**
The E.O. Paton Electric Welding Institute, NASU, Kyiv, Ukraine

A technology of surface alloying, based on the use of high-speed pulsed-plasma jets and electric discharges has been studied. In this case, electric current of 3 to 5 kA is passed through the jet. Alloying material in the form of a rod or wire is fed into the plasma jet. The high speed of the metal-containing plasma jet and the interaction of its pulses with the electromagnetic field, provide mixing of the alloy with the partially-melted surface of the item. As a result, the studied coating has no pores or any clearly-defined boundary with the base.

Key words: *pulsed plasma, alloying, alloyed surface structure, alloying device*

Mechanical engineering deals with a number of products (stamping and cutting tools, hydraulic rods, valves, camshafts, etc.) where the surfaces should be protected from the impact of high contact and dynamic loads. Thermal processes under these conditions do not provide the required density and strength of the coating adhesion to the substrate, and surfacing does not always satisfy the service requirements, because of formation of thick layers and heating of the entire item.

New processes of surface alloying have been developed, using concentrated heat sources (laser, electron beam). Their application, however, is limited by the high equipment cost, and material and power consumption.

The paper deals with a technology that combines the essential distinctive features of electric discharge and pulsed-plasma technologies, thus providing formation of alloyed layers at minimal material and power consumption [1–5].

The advantage of pulsed-plasma technology, developed at the PWI, is formation of alloyed layers (10–200 μm) with less stringent requirements to surface preparation and oxidation protection. The technology allows heating over a short time ($3 \cdot 10^{-3}$ s) a surface layer (20–40 μm) up to the melting temperature, thus limiting the HAZ dimensions to 100 μm, and allowing the heat-treated product surface to be alloyed. Metals are added to the plasma jet by sputtering of the end of the rod (wire), thus allowing compact materials and flux-cored wires to be used. The high speed of the metal-containing plasma jet and simultaneous impact of a pulsed electromagnetic field provide mixing of the alloying metal with the molten surface of the item. Gas-dynamic pressure of the plasma promotes compacting the partially-melted surface and closing the pores. Treatment of porous materials, for instance, of iron graphite, is accompanied by the alloying material penetration along the pores to the depth of down to 40 μm.

Features of equipment and technology. Figure 1 gives the schematic of the pulsed-plasma alloying device that consists of a small-sized detonation device *1*, reaction chamber *2*, inner electrode *3*, rod of alloying metals *4*, systems of alloying metal feed *7* and pulsed electric current source *6*. Alloying material in the form of a rod (wire) was connected into the electric circuit as an anode and was fed through electrode *3* into the gap between the walls of the chamber *2* (cathode) and product surface.

Detonation device *1* is used to fill the gap between the electrodes with a combustible gas mixture and initiate the detonation mode of combustion, thus promoting formation of an electrically conducting layer between the electrodes (up to 20 Ohm resistance), switching the circuit of the electric current converter (10–15 kVA power, 3.5 kV voltage). This results in the electric current (up to 20 kA) running behind the detonation wave, inducing additional ponderomotive force and providing additional energy input into the gas.

The theoretical basis of pulsed-plasma alloying is a physico-mathematical model of magnetogasdynamic acceleration of the products of detonation combustion of a combustible gas mixture in the gap between two coaxial bodies of revolution, namely the electrodes [6, 7]. The principle of the plasmatron operation consists in that at electric circuit switching, a kind of a

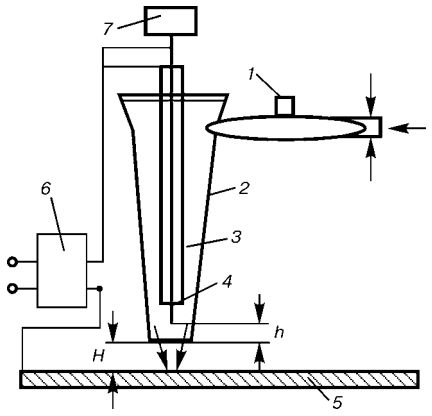

Figure 1. Schematic of a device for pulsed-plasma alloying (for designations see the text): h — distance from plasmatron edge to the rod end; H — distance to item surface

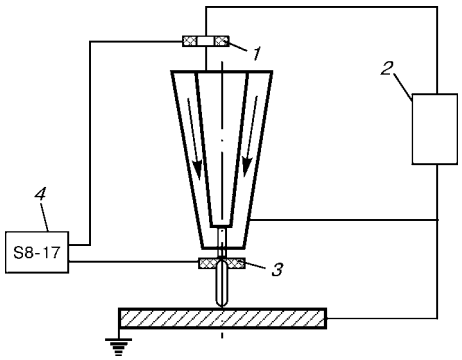

Figure 2. Electric circuit for connection of electrodes and measuring system (for designations see the text)

plasma piston forms in the point of the detonation gun inlet (Figure 1), the piston being accelerated between electrodes *2, 3* and closing the circuit between the end of rod *4* and surface of product *5*.

The electric power from the capacitor bank is distributed for heating and acceleration of the plasma piston in the interelectrode gap; melting, dispersion of the rod end and acceleration of the vapour-drop phase of the alloying material; melting of the product surface and formation of the alloying layer.

Figure 2 gives the electric circuit for measuring the amplitude-time current dependencies in the pulsed plasmatron. It consists of measuring gauges *1* and *3* (Rogowsky belts), two-beam storage-type oscillograph *4* (S8-17), as well as a source of pulsed electric current *2*. Current flowing to the tip of the molten rod is determined by the parameters of external R–L–C electric circuit of the power source and varies by the sinusoidal law [8, 9]. The energy evolved on the conductor (rod tip) can be up to 1/3 of the total power of the electric discharge in the converter.

Depending on the treatment mode, the plasma jet velocity can be in the range of 2–8 km/s [7]. The mass and velocity of the plasma jet determine the gas-dynamic component of metal drops at collision with the item surface.

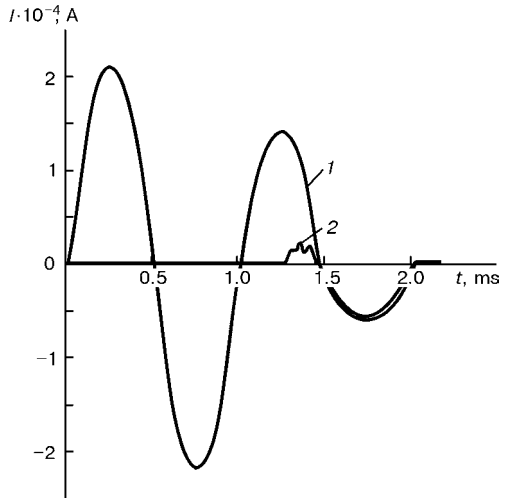

Figure 3. Time diagram of electric current running through the current-conducting wire (*1*) and the plasma jet between the tip of the molten rod and item surface (*2*) at C = 1200 mF, h = 20 mm, H = 40 mm

High energy density promotes overheating of the rod tip, dispersion and introduction of metal into the plasma jet in the condition of the vapour and drops [8]. The high-velocity plasma jet accelerates the motion of the metal drops and guides them to the item surface (up to 30 μm thickness of the surface-melted layer). The volume of the molten metal depends on such factors, as time, heat transfer coefficient, thermo-physical characteristics of metals and heating energy [9].

Energy characteristics of plasma. Different energy characteristics of the plasma pulse were achieved by varying capacitance C of capacitors (200–1200 mF), voltage U_{ch} on capacitor blank plates (2.5–3.5 kV), induction L in the discharge circuit (20–60 mH), distance to item surface (30–120 mm), as well as the size of the spot of plasma interaction with the surface (8–30 mm).

Measurement of time variation of electric current in the interelectrode gap, between the rod tip and the solid surface was performed by Rogowsky procedure (Figure 2) [10, 11].

Analysis of the results given in Figure 3, showed that pulse duration is adjustable by varying the values of bank capacitance and discharge circuit inductance. In the considered case $t_p \approx 0.5$ ms, amplitude of electric current between the rod tip and surface can be up to 5 kA at 8 mm diameter of the spot of current channel coupling.

Studying the time of current distribution showed that the breakdown of the shock-compressed layer occurs only after 1.2 ms. This time is sufficient for the capacitors to be recharged, and the consumable rod will first become the anode for 0.1 ms and then again the cathode for 0.6 ms. Current amplitude values are decreased with the increase of the distance to the item surface. This is attributable to lowering of the plasma jet conductivity.

The selected parameters of the converter provide formation of an electric circuit in the plasma jet between the tip of the melted off rod and the item surface. During time $(0.1–0.3)\cdot10^{-3}$ s at current density of up to $(1–7)\cdot10^{7}$ A/m^2 the end of the rod is overheated, thus providing for metal addition in the form of vapour or drops into the plasma jet.

Structure of alloyed layers. Alloying of sample surface was performed with a single pulse of the energy of 3000 J. Diameter of surface, alloyed with one pulse was 15 mm, pulse repetition rate being 1.5 Hz.

Experiments were conducted on steel samples with 0.3 % carbon. The surface was not cleaned to remove contamination before alloying. Alloying was performed using metals and alloys in the form of rods of 4–5 mm diameter, having different density, melting temperature, reactivity for oxygen and iron (brass, copper, titanium, aluminium, chromium, molybdenum, tungsten and nichrome). Distance from the plasmatron chamber edge to the sample was equal to 50 mm, that from the plasmatron edge to the tip of the electrode rod being 20 mm.

Alloying with copper and aluminium. Investigations demonstrated that a layer of non-uniformly mixed material of the base and copper forms on the sample surface in single-pulse alloying with copper. The alloyed layer thickness is up to 60–100 μm (Figure 4, *a*). It consists of the following phases: Cu, α-Fe, FeO, CuO. Grey-coloured inclusions are present in the alloyed layer along Cu–Fe boundary, their hardness being 20000 MPa. A bluish-coloured monolithic phase of about 800 MPa hardness was found in the surface layer. The hardness of the alloyed layer matrix was 2000 to 2700 MPa. Numerous monolithic light-blue grains of 6100 MPa hardness are present in the layer adjacent to the base. Hardness of copper inclusions is 580 MPa, and that of the base metal samples is 1700 MPa. Coarsening of the base grains due to thermal impact of the heat flows is recorded at the depth of about 100 μm from the sample surface.

When aluminium is used as the filler, a layer, consisting of aluminium (Figure 4, *b*) forms on the sample surface, the layer thickness varying from 60 up to 120 μm. Formed directly under this layer is a diffusion layer of intermetallics of monolithic light-grey grains, that is the result of interaction of liquid aluminium and iron. Underneath is the HAZ metal about 40 μm thick with a structure, consisting of martensite (within the boundaries of former pearlite) and ferrite. In etching some pearlite grains clearly show the HAZ boundary, dividing them into the regions of martensite (light part of the grain) and pearlite (dark part of the grain). The base metal structure consists of pearlite and ferrite.

The alloyed layer consists of the following phases: Al, α-Al_2O_3, α-Fe, FeAl, $FeAl_3$. Aluminium hardness in this layer is equal to 800 MPa, that of Fe–Al intermetallics is 6000–9000 MPa. Hardness of steel in the base layer is 1500 for ferrite and 2500 MPa for pearlite.

Alloying with titanium and tungsten. After single-pulse alloying with titanium the following phases form on the steel sample surface: α-Ti, α-Fe and FeO. Alloyed layer hardness is 4000–8000, that of the transition layer being 4000–5000 MPa. X-ray microprobe analysis revealed on the boundary in the base layer (Figure 5, *a*) the presence of an interlayer with up to 60 % Ti and 26–27 % Fe, above which is a layer of a titanium alloy with up to 2.5 % Fe. A narrow diffusion zone is located between these layers. Yellowish inclusions of a laminated structure with bluish boundaries (possibly Fe–Ti intermetallics, as well as nitrides) are also visible in the outer layer, as well as intermetallics of iron oxides (of light-grey colour).

Single-pulse alloying with tungsten produces a layer up to 80 μm thick (Figure 5, *b*). Light-coloured tungsten inclusions and dark oxide inclusions were found in it. Located underneath is the HAZ metal, consisting of martensite within the boundaries of former pearlite and structurally-free ferrite. The coating contains α-Fe, γ-Fe and tungsten phases. Hardness of the coating is 4100–4500, that of light-coloured inclusions in the coating is 5400 and that of HAZ metal — 3300–2500 MPa. Tungsten particles are present on the alloyed layer surface (Figure 5, *b*). Tungsten weight fraction in the particles is 95 %. It is probable that these particles (drops) penetrated into the molten surface of the sample in the liquid condition practically without diffusion or mixing. Adjacent to them is a layer up to 22 μm thick, where the content of tungsten changes smoothly up to 6–10 % and then drops to 0.5 %. This is followed by an interlayer up to 6 μm thick, enriched with tungsten (up to 8 %), then tungsten concentration again drops towards the base surface (to 0.5 %). A large elongated particle (up to 20 μm thick) of pure tungsten (100 % W) (Figure 5, *b*) is found in the layer on the boundary with the base, that has passed through the molten layer without mixing and became solidified on the boundary with the substrate. It is assumed that non-uniform variation of tungsten content in the coating

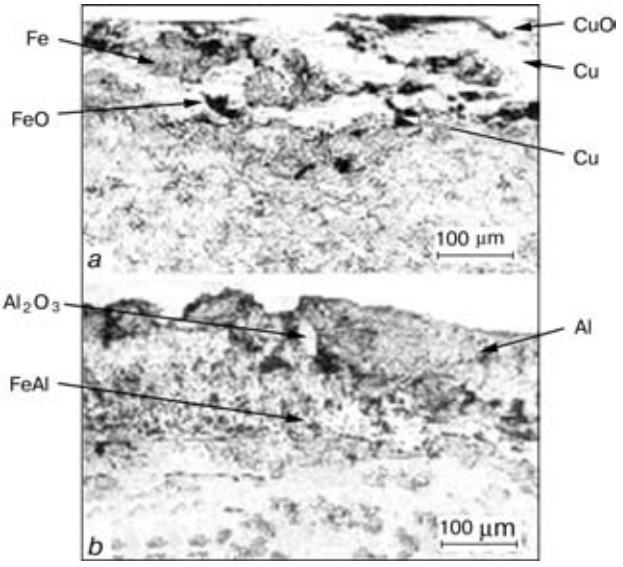

Figure 4. Section of the surface layer of St.3 steel samples after alloying with copper (*a*) and aluminium (*b*)

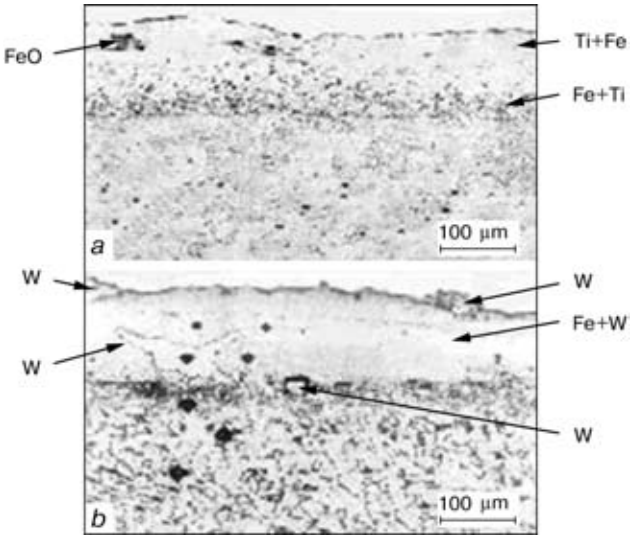

Figure 5. Section of the surface layer of the sample of St.3 after alloying with titanium (*a*) and tungsten (*b*)

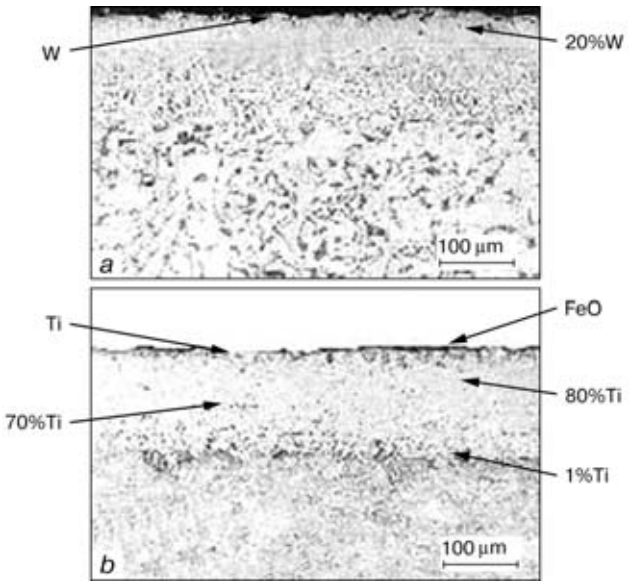

Figure 6. Section of the surface layer of St.3 sample after five plasma pulses, containing tungsten (*a*) and titanium (*b*)

is due to its non-uniform distribution in the plasma jet.

Increase of the number of pulses (up to five) promotes a greater uniformity of the alloying element distribution in the surface layer and HAZ increase up to 60 μm (Figure 6), with the possibility of the alloying element content being rather high. For instance, after five pulses of plasma, containing a drop phase of tungsten (Figure 6, *a*), finely dispersed inclusions with up to 98 % W content can be found on the boundary with the base metal. Particles of a block structure that is Fe–W intermetallics were mainly found on the boundary with the base. A thin interlayer of α-Fe, enriched with tungsten, is adjacent to the boundary. This is followed by a layer with a smooth increase of tungsten content from 8 to 16 %, and, finally, a layer, containing up to 18 % W. Adjacent to the surface is a layer with up to 20 % W. This coincides with the results of spectral analysis, according to which the weight fraction of tungsten in the subsurface layer is 11–20 %.

Multiple treatment by pulsed plasma, containing titanium, also leads to distribution of alloying elements (Figure 6, *b*). A layer of an Fe-based alloy (99 % Fe, 1 % Ti) is found on the boundary with the base. Located above is a wide diffusion interlayer of a cast dendritic structure. Dendrite axes are enriched with titanium (77–78 % Ti, 12–13 % Fe), the interdendritic space contains less titanium than the axes (61–62 % Ti, 28–29 % Fe), and fine (<< 1 μm) inclusions of a light-grey phase (70 % Ti, 12 % Fe) are found. The alloyed layer hardness is 6000–10000 MPa [12].

Alloying of iron-graphite material. Alloying of samples of an iron-graphite material was performed with one pulse. Rods of chromium, nickel-chromium alloy, titanium, molybdenum, tungsten, etc. were used as electrodes.

At single-pulse alloying with titanium, up to 80 μm layer formed on the iron-graphite sample. Coating hardness was 2100 MPa (Figure 7, *a*). Titanium penetrated along the pores into the base material to 25 μm depth. HAZ thickness was 50 μm, base hardness in this zone being 4700 MPa.

Alloying by a single-pulse of a Mo-containing plasma (Figure 7, *b*) produces a layer 9–33 μm thick. Molybdenum penetrates into the alloy along the pores to a depth of down to 35 μm, and the HAZ reaches to the depth of 36–56 μm. The metal of this zone has the hardness of 5480–6740 MPa.

Similar alloying with the Ni–Cr alloy provides an intermittent layer from 4 to 45 μm thick. The alloying material penetrates into the base to the depth of down to 45 μm. The hardness of this layer is 5000 MPa. In alloying with brass (62 % Cu, 38 % Zn) a thin dense layer of brass was produced with its penetration into the sample metal pores to the depth of down to 25 μm.

Alloying by a single pulse of plasma, containing tungsten and chromium, results in formation of an up to 40 μm layer on its surface. The depth of tungsten penetration along the pores in iron-graphite is down to 35 μm (Figure 7, *c, d*).

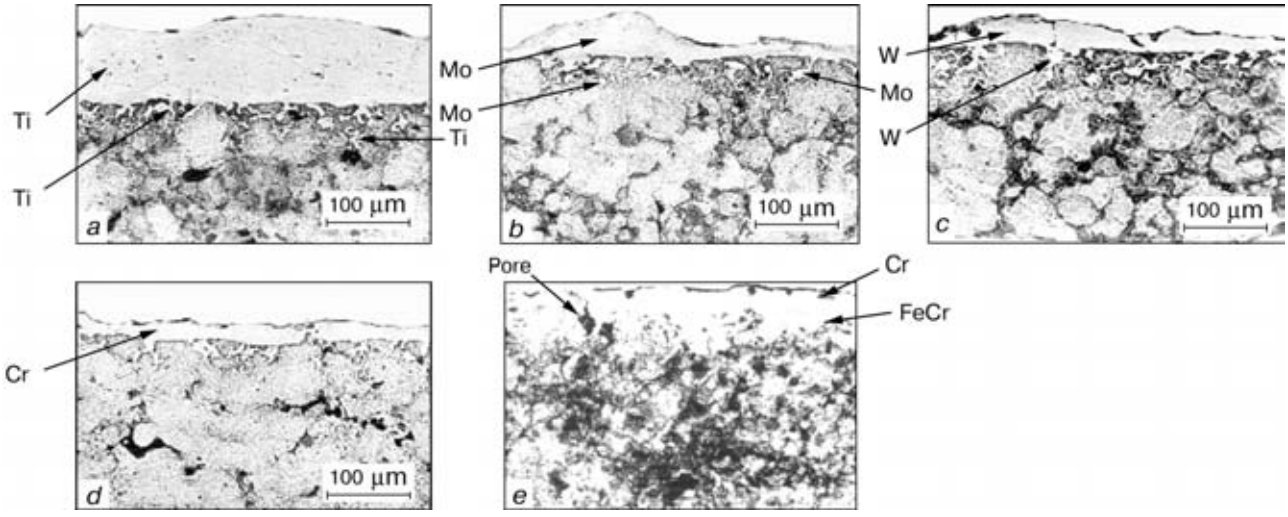

Figure 7. Alloying of iron-graphite sample with titanium (*a*), molybdenum (*b*), tungsten (*c*), chromium (*d, e*): *a–d* — single-pulse alloying; *e* — five-pulse alloying

Multiple pulsed-plasma alloying, for instance, by five pulses, allows a uniform layer to be produced (Figure 7, *e*). The thickness of the alloying layer is up to 90 μm; also a mixing zone 15 to 40 μm thick, consisting of the alloyed and base materials, is present.

The alloyed layer is found to have oxide inclusions. Defects in the form of pores are present under this layer. The alloying material penetrates to the iron-graphite sample base along the open pores and cracks. Use of lower-melting materials (aluminium) as the electrode produces thicker layers (60–150 μm) of the hardness of 700 MPa (aluminum) and 5000–7000 MPa (Fe–Al intermetallics).

Discussion of the results. Experimental results demonstrated that at pulsed alloying the solid surface at the first moment of time experiences an elastic-deformation interaction with the shock wave and the pulsed-plasma jet, and then electric current is applied to the surface. The amplitude value of current can be up to 7 kA. The sample surface melts and the plasma, containing drops of liquid metal (alloy), flows over it at a high speed. Plasma interaction with the sample surface proceeds for $(2–5)\cdot10^{-3}$ s, thus resulting in its short-time heating. Integrated gas-dynamic and electromagnetic impact on the molten surface ensures mixing of the alloying metal with the base metal and its faster solidification [13, 14].

The technology provides alloying of the item surface with formation of a layer 5 to 150 μm thick that consists of elements which are the components of the metal electrode, plasma and base metal. Single-pulse alloying leads to formation of sections of a layer of non-uniform hardness and distribution of alloying elements (electrode metal). Multiple-pulse alloying produces a layer of a sufficiently uniform composition.

HAZ metal thickness is not more than 50 μm. Practically any metals or alloys produced in the form of wire or rod, can be introduced into the plasma. After multiple mixing, the formed alloyed layer has no pores or boundaries with the sample base.

The properties of the metal layers depend on the electrode metal composition and number of plasma pulses. It is possible to alloy the working surfaces of parts, made of structural steels, as well as items produced by powder metallurgy processes. Considering that alloying is performed with separate pulses, it can be applied to produce a uniform layer on the entire working surface of the item or just on its local sections.

1. Grigoriants, A.G. (1989) *Fundamentals of laser treatment of materials*. Moscow: Mashinostroyeniye.
2. Mirkin, L.I. (1975) *Physical fundamentals of laser beam treatment of materials*. Moscow: MGU.
3. Valyaev, A.N., Progrebnyak, A.D., Kishimoto, N. et al. (2000) *Modification of properties of materials and synthesis of thin films in exposure to illumination by electron and ion beams*. Ust-Kamenogorsk: Vostochnokazakhstan. Techn. Univ.
4. Yakushin, V.L., Kalinin, B.A., Polsky, V.I. et al. (1994) Surface alloying of metals, using high-temperature pulse plasma. *Metally*, **6**, 74–81.
5. Parshin, A.M., Kirillov, N.V. (1995) Physical and structural aspects of treatment of alloys by concentrated energy sources. *Ibid.*, **3**, 122–127.
6. Raizer, Yu.P. (1992) *Physics of gas discharge*. Moscow: Nauka.
7. Tyurin, Yu.N. (1999) Improvement of equipment and technology of detonation coating deposition. *Avtomatich. Svarka*, **5**, 13–18.
8. Vorobiev, V.S. (1996) Dynamics of conductor heating and evaporation by high density pulse current. *Zhurnal Tekhnich. Fiziki*, **1**, 35–48.
9. Drapkin, B.M., Rudenko, V.A. (1992) On determination of energy of metal sublimation. *Ibid.*, **9**, 125–129.
10. Lebedev, A.D., Uryukov, B.A. (1990) *Pulse accelerators of high pressure plasma*. Novosibirsk.
11. Sultanov, M.A. (1981) *Shock-compressed plasma in high-power discharges*. Dushanbe: Donish.
12. Tyurin, Yu.N., Adeeva, L.I. (1999) Pulsed plasma strengthening of titanium-base alloys. *Avtomatich. Svarka*, **1**, 32–36.
13. Anastasiadi, G.P. (1992) *Formation of chemical microheterogeneity in cast alloys*. St.-Petersburg: Politekhnik.
14. Gertsriken, D.S., Kostyuchenko, V.G., Tishkevich, V.M. et al. (1997) Influence of plastic strain in a pulsed magnetic field on migration of atoms in metals. *Doklady NAN Ukrainy*, **3**, 37–39.

JAPAN DETERMINES ITS PRIORITIES IN THE FIELD OF WELDING FOR XXI CENTURY

V.N. BERNADSKY
The E.O. Paton Electric Welding Institute, NASU, Kyiv, Ukraine

The paper presents systematised comments of specialists of the Japan Welding Society on determination of the national priorities in the field of welding science and technology at the beginning of the XXI century. Considering the «technological saturation» of the majority of the welding processes, applied on a mass scale, the recommendations are to predominantly develop those technologies, that have a significant potential, in particular, an arc welding process — A-TIG, friction stir welding (FSW), laser and laser-hybrid technologies. The main scientific problem, namely weldability and nature of cracking, is still urgent. The determinant role of computer modelling in research, design and development of welded structures, technologies and welding consumables, has been established unambiguously.

Key words: *welding, science, high technologies, welding production, research, priorities, Japan, XXI century*

At the present threshold of the centuries specialists from the leading countries of the world pay considerable attention to evaluation of the achievements of welding science and technology in the past century, as well as selection of priority and promising trends of development of welding and allied technologies in the interests of industry at the start of the XXI century. National and international conferences, numerous publications of leading scientists and specialists in the world periodicals on welding have been devoted to these issues over the last years. The practice of conducting the working meetings of experts to outline the strategy of the advance of welding science and welding fabrication, as well as of welding equipment market over the next 10 to 20 years, is becoming ever wider accepted. As a rule, the range of interests of the experts, both scientists and production specialists covers the issues of assessment of the effectiveness of high technologies, management of welded structure quality, professional training and certification of personnel, welding production ecology, etc.

Outlining and selection of priority areas for advanced and basic research, as well as transfer of science-intensive welding technologies into industry and construction are based on a number of factors of a general nature. First of all, this is the tendency of continuous reduction of government funding of research and of the means, allocated by industry for specific research. Secondly, this is the need to reduce investments into research and development of those technologies of welding and processing of materials, that have already reached the critical «saturation point» and are widely represented in the world welding market. In addition, the growing globalisation of world economy, accompanied by increased transnational transfer of high technologies and integration of welding equipment manufacturing, predetermines the need to eliminate an unjustified duplication of national research and development. The world market of science and technology products also grows under the globalisation conditions, this influencing selection of national priorities [1].

Welding specialists are already familiar from the local and foreign publications with the change of the paradigm of welding science and new priorities for the start of the XXI century in the USA, Germany, Great Britain and other Western counties. Much less accessible is the information on the very active attitude of the Japanese welding community to selection of the priorities of development of the welding science, equipment and technology. This has a clear explanation: the Japan Welding Society (JWS) believes that an extremely limited access to information in Japanese, unlike the practically unrestrained access to, for instance, information in English, cannot be ignored [2]. This paper is an attempt at somewhat filling this gap for the benefit of the Russian-language readers, by presenting a review of a Japanese publication in the «Journal of the Japan Welding Society» [3].

Such a review is the more timely, as modern Japan is the world's largest capital exporter, the second industrial country of the world. Japan's gross domestic product ($4749.6 bln in 2000) is half of that of the US and is larger, than that of Germany, France, and Great Britain taken together. At present Japan, together with the USA and Western Europe, make up the «leading» three most important economic regions of the world that have the determinant role in globalisation of the world economy. Of 500 major transnational companies 141 are Japanese.

Japan has also been steadily holding one of the leading positions in the world welding fabrication [4, 5]. Output and consumption of welding equipment (machines and welding consumables) can be regarded to be the basic criteria in evaluation of the Japanese welding fabrication. At the end of this century the annual output of a quite modern welding equipment (without robots or laser systems) was more, than 120,000 pcs for a sum of more, than $420 mln, and the output of welding consumables was on the level of 320,000–350,000 t. The scope of application, in particular, of electric arc welding in Japan can be

assessed also by the volume of the deposited metal that in 1999 was equal to 236,000 t. For comparison, this index in the same year 1999 was 422,000 t for Western Europe and 344,000 t for the USA [6]. The most characteristic tendency in the Japanese production of welding consumables is a continuous lowering of the share of manual welding coated electrodes and a stable tendency for a continued growth of the share of flux-cored wire manufacture. Starting from 1994, flux-cored wire manufacturing in Japan has been ahead of that of coated electrodes in terms of volume and in 1996 it reached 90,000 t [4–6].

Japanese welding fabrication has one of the world's highest levels of welding operations mechanization. The continuously growing volume of industrial robots (IR) application has a significant role. In 1999 the total fleet of operated IR of all types was more than 400,000 pcs, this being equal to almost half of the world's IR fleet. Most of IR (238,200 pcs) are installed and operated in the Japanese welding fabrication to perform such process operations as assembly, cutting, welding, spraying, non-destructive testing, billet transportation in welding lines, etc. [5].

The article «Technologies of welding and joining in the XXI century» [3] in its content is a report on a «round table» discussion on the same subject, conducted by the JWS. Leading experts of such research centers as Osaka University, Institute of Materials Science, Center for Development of Technological and Production Systems and of a number of leading Japanese companies: Kobe Steel, Sumitomo Heavy Industries, Nippon Kokan and Nippon Steel (welding equipment manufacturing) participated in this meeting. This review presents in the systematized form some estimates of the achievements of modern welding fabrication over the past century and some comments on the most urgent and priority problems of Japanese welding science and technology at the start of the new century, expressed at the «round table» meeting. Also a procedure from one more article [2] from the same journal is used in this review.

A universally known fact is that XX century was the determinant period for establishment and development of the welding process as a high technology of permanent joining of metallic and non-metallic materials. As noted by the Japanese specialists, experience of the previous century demonstrated that, irrespective of the fluctuations of the world and national economies, investments into welding and allied technologies were, as a rule, justified and yielded the anticipated technico-economic results. Development of welding equipment and technology was accompanied by natural selection of individual technologies. The following technologies of fusion welding have stable positions in welding fabrication: electric arc welding (MIG/MAG, TIG), SAW, electroslag welding (ESW), electron beam welding (EBW) and laser welding (LW). The Japanese experts considered it necessary to note that they are very grateful to the former Soviet Union for the know-how that they were able to borrow at a certain time from the CO_2 welding technology and consumable electrode ESW. They also believe that the technologies of pulsed-arc welding have largely been taken over from the British welding experts.

Practice showed that not all of the currently applied specific welding technologies are promising in view of the requirements of the XXI century, while a number of them have reached their technological limit. So, out of various technologies of SAW, the most extensive development is conducted in Japan in the field of improvement and application of welding from one side with a high heat input on a flux pad. Growing scope of application is characteristic of flux-cored wire gas-shielded welding, using inverter power sources. The scale of EBW application is increasing due to its use for joining plate materials, especially, when it is necessary to ensure a high impact toughness of welds. Over the last 20 years LW did not yet find a wide enough application in industry, despite a large volume of the performed research in this field. A wide enough use of this advanced technology is still anticipated in the next few years and, primarily, in automotive, ship- and bridge-building sectors.

Two promising welding processes are of great practical interest for welding fabrication of Japan at present and in the near future:

- A-TIG, electric-arc welding with application of activating fluxes, developed at the E.O.Paton Electric Welding Institute;
- FSW of extended joints, developed at The Welding Institute (TWI).

It is intended to study and develop the FSW process, accompanied by a low heat input and residual deformation of the welded joint, for butt welding of sheets of high-strength aluminium alloys.

When the status and prospects for industrial application of the currently available and advanced technologies of welding and joining were analysed, none of the participants of the «round table» discussion suggested the possibility of emergence of a fundamentally new, breakthrough technology in the near future.

Over the last decade Japanese welding science has made the most substantial contribution to development of such areas as welding processes, materials and phenomena, weldability and fatigue of welded structures, while the industry created one of the world's most efficient systems of quality assurance, based on these investigations. No matter how paradoxical it may seem, but the JWS believes that such a level of quality would be completely impossible without the Osaka University investigations in the field of cracking. Investigations of various welding processes, namely MIG, MAG, TIG, plasma, electric arc, laser and hybrid processes have been and are currently conducted with the same aim. Industry is actively utilising the new scientific products for optimisation, mechanisation, automation and robotisation of technological processes. More than one third of the total volume of investigations falls to the share

of brazing, diffusion bonding and other processes of pressure welding. The scope of investigations in the field of thermal spraying of coatings and laser spraying for surface modification is becoming wider every year. Another, equally important area, is studying the processes, occurring on the interface in joining ceramics and composite materials; the processes on the interface have been studied especially intensively beginning from 1996. In order not to duplicate the investigations of the American Welding Society in the field of arc welding of ferrous and non-ferrous metals, in Japan studying the nature of joining non-ferrous metals to ceramics has been determined to be the priority area [2].

Such an area of research as studying the weldability of advanced functional materials with the focus on development of production technologies has been accepted as the most promising for the near-term period. This is a broad subject, covering development of joining processes, automation of the technological process, development of highly mechanised equipment with feedbacks, etc. This area is focused on solving the problem of manufacturing finished weldments with a guaranteed quality, not requiring any subsequent treatment [2].

The cardinal problems, faced by humanity and world economy at the start of the XXI century, can be grouped into the following areas: power generation, raw materials and other resources; human factor; ecology.

All these problem areas pertain to welding science, equipment and fabrication to varying degrees, as welding and allied technologies are the basic technological process in material production in the modern society.

A tendency to cost-effective and efficient use of power and raw material resources means not only transition to the resources- and power-saving technologies of welding and joining, but also improvement of the «resources efficiency» in modern production.

Basic development has been started to apply renewable energy sources for welding process in welding fabrication.

The human factor in welding fabrication means improvement of the system of professional training and certification of engineering, technical and production personnel. Qualification of specialists and welding operators in terms of assurance of the quality of welded structures and products has acquired a decisive role after introduction of a system of quality management (ISO 9000) into the world industry. Japan, with its chronic deficit of qualified welding operators, intends to go over to the system of training and certification according to the international standards and norms of IIW. In particular, the focus is on widely using the training materials on CD-ROM, developed by TWI.

Welding fabrication with good reason is considered to be a quite «harmful» production in terms of its influence on personnel health and environmental impact. Today Japanese scientists and developers of welding technologies and filler materials regard their ecological safety and minimal impact on the working zone and personnel as the highest priority. Indirect evidence of the focus on ecology in welding fabrication is a stable tendency of the Japanese manufacturers to reduce the output of coated electrodes for manual welding. Not less urgent for welding fabrication are the problems of reduction and management of wastes, increasing the volume of recycling of welded structures and products after their service life is over. It should be noted that as regards solving this problem, Japan took a leading position already at the end of the last century. So, in 2000 about 2500 enterprises in Japan have passed the audit and received ISO 14001 certification, this being ≈ 20 % of all the enterprises of the world, having international ecological certification by an appropriate international standard.

Scientists of the Osaka University believe, that at this new stage of development of fabrication of highly reliable and cost-effective welded structures in different sectors of industry and construction, the problem of weldability and, primarily, more precise definition of the causes for cracking in welding, still remains to be the fundamental and priority issue. Such investigations are required, primarily to find the methods for improvement of weldability of the currently available steels and development of new readily weldable steels, in particular, high-strength steels, including two-phase steels, IF- and TRIP-steels, stainless and other special steels and alloys of non-ferrous metals. Another problem in this area is development of structural materials, capable of preserving high properties in the HAZ at a high and low heat input in welding.

Computer modelling of the process of welding and formation of the welded joint is considered to be a priority trend in development of specific welding technologies. Such a modern procedural approach will allow creation of a system of selection of the optimal welding parameters, on-line control and active monitoring. Resistance spot welding and TIG-process particularly need that. Not less complicated is the problem of modelling drop transfer of metal in the welding arc, depending on the wire and shielding medium composition and shape of welding current curve. Also urgent is the problem of electronic modelling and simulation of the processes in the liquid metal pool and its subsequent solidification in electric arc welding, EBW and LW.

Specialists noted the need to exercise an integrated approach to selection and optimization of the technology of fusion welding, including selection of an optimal combination of the base and filler material, composition of the shielding gases or their mixture, cost-effective power source and an effective system of control of the joining process. This is the only approach that currently provides a high-quality joint with a «super» weld. Nippon Steel representative recommended the developers to ask the question: «Is Japan following the path that has already been or is being covered by other countries of the world?», when

developing a new welding technology, including the equipment and materials.

In the field of automation of welding fabrication Japan still focuses on robotisation of welding and allied technologies both in large-scale production (car-making, ship-building, etc.), and in medium- and small-sized businesses. The diversity of robot designs is growing and their technological functionality is widening. Robotic production lines, complexes and welding cells are to be created. First generation robots began to be replaced by more advanced systems, of the type of ROBUDEX-2000, fitted with advanced software, sensors, a self-teaching system and having a high efficiency. In the near future the robot fleet is to be complemented by robots, controlled by the operator's voice, and capable of analytical evaluation of the progress of the technological process.

The majority of the participants of the «round table» discussion in their presentations and during the discussion emphasized the determinant role of computerization in research and at all the stages of welding fabrication. There is every ground to believe that in XXI century most of the scientific and production problems can be resolved on the basis of the appropriate computer models. This should be promoted by creation of an all-purpose software and the ability to pull the required DB and other information out of the Internet. The final aim of modelling is reduction of labour consumption in research and development of welding technologies and materials. As the model levels become higher, the scope of the required theoretical and experimental investigations is, as a rule, reduced. It is stated that both modelling of the technological process, and design of welding consumables and welded structures, irrespective of the nature and parameters of the modeled object, will be based on application of neutral networks.

Japanese experts included the problem of harmonizing the national standards, norms and rules with the international (ISO), European (ZEN) standards, as well as IIW recommendations into the priority areas for the national welding fabrication in the first decade.

1. Bernadsky, V.N., Makovetskaya, O.K. (1999) Current tendencies of organization and financing of research and development abroad. *Obzornaya Informatsiya IES.* Kyiv: PWI.
2. (1999) Role of the Japan Welding Society in different fields of welding science and manufacturing. *J. JWS*, **1**, 6–24.
3. (2001) Technology of welding and joining in XXI century. *Ibid.*, **3**, 6–18.
4. Bernadsky, V.N., Dmitrieva, N.A. (1997) State-of-the-art and development of welding manufacturing in Japan. *Svarochn. Proizvodstvo*, **9**, 39–45.
5. (2001) *SVESTA-2001. Economic-statistical data on welding manufacturing*. Kyiv: PWI.
6. Pekkari, B. (2000) Framtida svetsmetodez j en uthallin Miljo. *Svetsen*, **6**, 11.

UNIT FOR RESISTANCE WELDING OF NUCLEAR REACTOR FUEL ELEMENTS

I.N. SIDOROV[1], **A.A. GRADOVICH**[1], **A.A. KISLITSKY**[1], **V.V. ROZHKOV**[1], **A.V. STRUKOV**[1], **I.G. CHAPAEV**[1] and **P.I. LAVRENYUK**[2]

[1] OJSC «Novosibirsky Zavod Khimkontsentratov», Novosibirsk, Russia,
[2]OJSC «Twel», Moscow, Russia

The paper analyses the experience of development and application of highly efficient equipment for sealing fuel elements in WWER type reactors, using resistance welding. A two-position unit, that simultaneously processes two fuel elements in the automatic mode, has been developed on the basis of ASSK automatic welding machines and is being used successfully. The operation of the unit is provided by control system, pneumatic system, system of pumping down and filling the fuel elements with helium, as well as welding power source that are common for both the welding heads. These units were the basis to develop highly efficient automated lines for welding and sealing the fuel elements.

Key words: *resistance welding, fuel element, sealing, automatic machine, unit*

Fuel elements in WWER type reactors are long thin-walled tubes of a zirconium alloy of about 9 mm diameter, filled with ceramic nuclear fuel in the form of cylindrical tablets and increased-pressure helium. To provide the required purity of the atmosphere, the inner volume of the fuel elements is pumped down prior to sealing. Sealing is performed by resistance welding of tube-plugs from the element end faces, forming the fuel element shell. Most of the fuel elements are currently made with application of resistance welding. For this purpose the local industry has mastered the manufacture of automatic welding machines of ASSK type. During their introduction in the Novosibirsk Plant of Chemical Concentrates, development work has been performed to improve the stability and reliability of functioning of individual components and the automatic machines, as a whole, which were based on ASSK 4001 automatic welding machines. One of the problems that the plant experts faced during pumping down, was intensive removal of finely-dispersed abrasive particles of the fuel from under the fuel element shell, these particles being

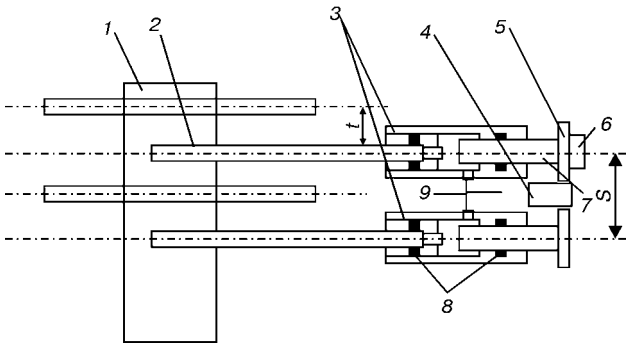

Figure 1. Schematic of a unit for resistance welding of fuel elements of power reactors (for designations see the text)

formed as a result of mechanical friction of fuel tablets against each other in transportation and loading into the fuel element.

The pumping down process is the longest operation in sealing of the fuel elements, so attempts were made to shorten it as much as possible during development of the automatic machines. For this purpose special vacuum plenums were mounted on the automatic machines, providing a fast pumping down of the fuel elements at the first moment after connection of the automatic machine chamber to the vacuum system. A fast connection of the inner volume of the fuel element of several tens of cubic centimeters to a vacuum line of a volume that is many times larger, than the free volume under the shell, led to an instant pressure drop in the welding chamber of the automatic machine (from the atmospheric to ≈ 13.3 Pa) and removal of dustlike particles of fuel into the chamber. With time the fuel particles, removed by an air flow from under the fuel element shell accumulated in the seats of the mobile parts of the automatic machine, causing their jamming and failure, and deposited on the contact surfaces of the welding fixture, thus lowering its resistance.

In order to reduce the contamination of the welding chamber with the fuel particles, the possibility of using throttling orifices, automatic valves with a variable open flow area was studied. In all the cases, however, either the pumping down time was increased significantly, or it was not possible to reduce the removal of the fuel particles to acceptable limits. Optimal results were derived after the vacuum plenum switching off and connection of the vacuum system to the atmosphere for 0.5–1.0 s at the moment of the start of pumping down. In addition, different tubing began to be used for pumping down and filling the fuel element and the welding chamber with helium, thus preventing additional transfer of fuel particles within the welding chamber. Thus, the reliability and stability of the automatic machine operation were ensured as a result of optimising the technology of pumping down the fuel element with an atmosphere of the specified composition and pressure, and the design and circuit variants of the automatic machine. The efficiency of the above process, however, still remained low. According to the certificate data, the efficiency of the automatic machine, taking into account the performance of operations, providing the specified atmosphere under the shell, is 60 items per hour [1]. The main time of the automatic machine process cycle is taken up by parts feeding into the welding zone, pumping down and filling of the inner volume with helium, as well as taking the sealed fuel element out of the automatic machine. The welding process proper takes fractions of a second. Insufficient efficiency results either in more complicated process sequences or increase of their number.

In order to fulfil the production tasks at minimal expense, a two-position resistance welding unit, with its schematics shown in Figure 1, has been developed on the base of ASSK type automatic machines, incorporating the retrofits, and is used at the Novosibirsk Plant of Chemical Concentrates to manufacture the fuel elements in WWER-1000 and WWER-440 type reactors. The unit consists of conveyer *1* for lateral displacement of fuel element *2* with step t, two (minimum) welding heads *3* of ASSK-4001(4002) automatic machines with upgraded designs and circuits. The inter-axial spacing of welding chambers S was determined from the following relationship:

$$S = t(mk + 1),$$

where m is any integer number, beginning from a unity; k is the number of welding heads in the unit, equal to the number of the conveyor belt steps at each single travel.

Elongation of the busbars in connection with relocation of transformer *4* of the power source, compared to automatic machines ASSK, is partially compensated by the increase of their cross-section. The dimensions of the busbars and their relative location were selected, taking into account the recommendations of [2]. One of the heads is fitted with a device for breaking secondary circuit *5* of the transformer, that is connected to electrode *7* via the rod of welding force drive *6*. Seals *8* are used for sealing the welding chambers. Welding heads have a common control system, pneumatic system, system of pumping down and filling the fuel element with helium *9*, as well as the welding source. Fuel elements are fed to the welding heads by a conveyor with single travel $2t$. Thus, positioning of new fuel element blanks, not subjected to welding, opposite each welding head, is provided. All the operations with the fuel element blanks, loaded into the welding chambers of the unit, are carried out in parallel, except for welding proper, performed in minimal time sequentially. The general view of the unit is shown in Figure 2.

ASSK automatic machines have capacitor-type power sources that are sufficiently critical to the welding circuit impedance parameter. Design of the busbars and selection of the location of the welding transformer relative to the welding heads, provided the modes of welding in the two-position units, close to the modes in ASSK automatic machines (increase of

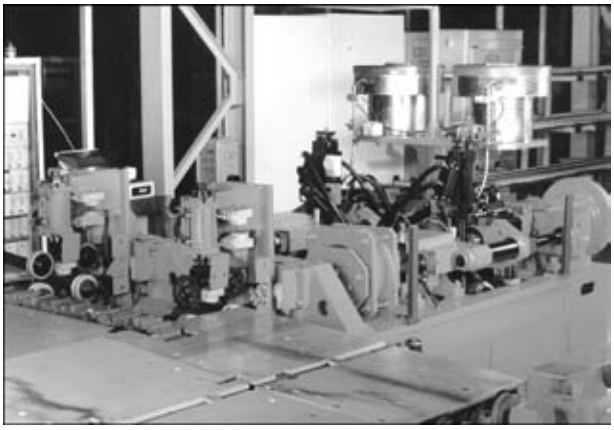

Figure 2. Unit for resistance welding of fuel elements

the capacitor bank charging voltage was less than 10 %). For a more flexible adjustment of the welding modes, changes were made in the control system of the welding bank charging, that provided a separate adjustment of this parameter for each welding head. Air pressure in the welding force drives also has a separate adjustment. Welding positions are fitted with sensors of the plug displacement.

Later on three more similar units were made in the plant, that were the basis for developing compact highly efficient automated lines for fuel element welding and sealing (Figure 3), not requiring more shop space, and also allowing reduction of the capital cost of the power sources and the control system.

CONCLUSIONS

1. Upgrading of automatic machines of ASSK type has been conducted in order to increase the reliability and stability of their operation.

Figure 3. Automated line for fuel element sealing, based on the resistance welding unit

2. Automatic machines of ASSK type were the basis to develop and master a two-position unit for resistance welding of fuel elements.

3. The above units were the basis for development of compact highly efficient lines for manufacturing fuel elements for WWER type reactors.

4. Use of the developed units improves the operational capabilities of production owing to their high efficiency, reduces the required shop space and lowers the equipment cost.

1. Reshetnikov, F.G., Bibilashvili, Yu.K., Golovnin, I.S. et al. (1995) *Development, production and operation of fuel elements of power reactors*. Moscow: Energoatomizdat.
2. Ryskova, Z.A. (1988) T*ransformers for electric resistance welding*. Leningrad: Energiya.

LASER CLADDING OF HYPOEUTECTOID COMPLEXLY-ALLOYED STEELS

V.Yu. KHASKIN and **V.P. GARASHCHUK**
The E.O. Paton Electric Welding Institute, NASU, Kyiv, Ukraine

Process of laser alloying of steels 25Kh1M2FTR and 40KhN2MFA was investigated. Technology for strengthening surfaces of workpieces operating at high temperatures in aggressive environments was developed, providing an extension of their service life by more than 1.5–2 times. It was established that the laser alloying with a mixture of chromium and relite powders provided an increase of several times in wear resistance of hypoeutectoid complexly-alloyed steels and in their heat resistance from 400 to about 1000 °C.

Key words: *laser radiation, cladding, complexly-alloyed steels, wear resistance, filler materials, microcracks, HF-preheating*

One of the rarely used laser technologies of strengthening is alloying. It is used only in manufacture of new products and not often withstands the competition with traditional volume thermal technologies. However, the laser strengthening is best in those cases when the conventional technologies are not acceptable due to the geometry of the part being strengthened and inadmissibility of distortion at certain stages of manufacture [1].

The technology of strengthening surfaces of rotation workpieces operating at high temperatures in aggressive media was developed to increase their service life by more than 1.5–2 times. Example of the part with such surface (∅ 60×800 mm) is a rod of a starting-control valve of the steam turbine. It operates at temperature of about 560 °C in the atmosphere of overheated water vapour. The process of laser alloying of steels of 25Kh1M1FTR and 40KhN2MFA type was investigated. It was suggested to deposit an alloyed layer in the form of a path of 5 mm width and 1.0–1.5 mm depth, coming in a spiral with a 1–2 mm pitch between turns. Similar conditions were earlier [2] realized in the technological process of a laser cladding.

Experiments were made in the equipment described in [3]. Due to a large width of the path and radiation capacity $P = 5$ kW, the rate of alloying was in the ranges of 20–40 m/h. When selecting the filler material, satisfying the technical requirements, the powders of self-fluxing alloys PG-12N-01, PG-12N-02, PG-N1, PG-AN3, PG-AN6, PG-10N-04, Hastelloy (50–160 μm granule size), mechanical mixtures of powders PG-AN6 and PG-10N-04 with tungsten carbide VK6, titanium nitride, chromium, relite and also their combination were considered. Chemical composition of the materials used is given in the Table.

Due to comparatively low speeds of the process a large HAZ (100–200 % of the alloyed layer depth) was observed in all the cases of the laser alloying. It represents a fine-acicular martensite with microhardness $HV1$ 580–670 for the selected class of steels. There is α- and γ-iron, i.e. martensite and ferritic phases, in a large amount (30–40 %) in the alloying paths. Structure of the alloying layer in the lower part (near the parent metal) is the relatively fine-dispersed crystallites which are oriented normal to the transition zone. In the upper part of the alloying layer a comparatively equilibrium fine-dispersed structure is observed.

The typical defect of the alloying layer is microcracks. In all cases of alloying with powders of alloys of Ni–Cr–B–Si system the presence of a brittle eutectics forming at the grain boundaries can be considered as a cause of their initiation. It is more probable that these are borides or silicides. Moreover, the

Chemical composition of materials used, wt.%

Material	*C*	*Mn*	*Si*	*Cr*	*Ni*	*Mo*	*Ti*	*V*	*W*	*B*	*Fe*
25Kh1M1FTR	0.25			1.0		1.0	0.3	0.6	0.3		
40KhN2MFA	0.4			1.0	2.0	0.6		0.6			
St.3	0.14–0.22	0.3–0.6									Balance
St.45	0.45										Same
PG-AN3	0.8–1.2		2.0–3.0	14.0–18.0	Base					1.0–1.9	Up to 3.0
PG-AN6	0.9–1.8		2.5–3.5	14.0–18.0	Same					2.5–3.5	Up to 3.0
PG-N1	0.8–1.2		2.0–4.0	10.0	30.0					2.0–4.0	Base
PG-10N-04	0.2–0.6		2.3–2.8		Base					1.2–1.8	Up to 0.1
PG-12N-01	0.3–0.6		1.25–3.25	8.0–14.0	Same					1.75–2.5	1.25–3.25
PG-12N-02	0.4–0.8		3.0–5.0	10.0–16.0	»					2.0–4.0	3.0–5.0

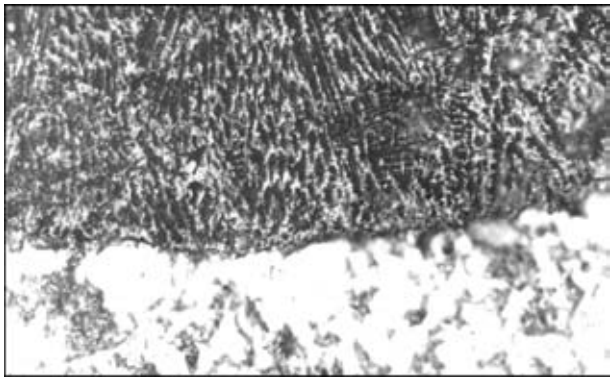

Figure 1. Microstructure of area of a laser alloying path at an auxiliary HF-preheating of sample made from St.3 using materials PG-N1 (×400)

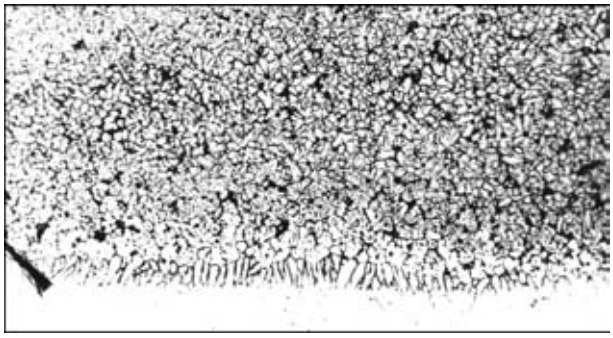

Figure 2. Microstructure of area of a laser alloying path of sample made from steel 40KhN2MFA using a mixture of powders of chromium and VK6 (×200)

cracks can initiate due to high temporary stresses occurring because of a volume effect of a fast formation of martensite in cooling the molten region of metal down to the temperatures of about 300 °C.

To prevent the crack formation the auxiliary high-frequency (HF) preheating of cylindrical samples up to surface temperatures of about 800 °C was used. Here, the rates of alloying are significantly increased (from 20–40 to 160–180 m/h), while the capacity of the laser radiation is remained at the same level (≈ 5 kW).

The laser alloying with HF-preheating of St.3 was performed using the powder PG-N1 of Fe-based alloy. The hardness of the produced layer was *HRC* 20–40, while the certificate hardness of the used alloy was *HRC* 50–55. The depth of the alloyed layer was 0.5 mm. There were no microcracks typical of the conventional laser alloying. Microstructure of the alloyed layer is close to the structure of layers of a laser cladding with a subsequent high tempering: it has a clearly expressed dendritic nature, the large dendrites are observed. The transition zone was 5–8 μm (Figure 1).

The selection of chemical composition of the filler material was made taking into account the service requirements to the alloyed layers. The wear resistance of the latter was determined by a dry friction using the method «pin–cylinder» in the specially-manufactured friction machine, while the high-temperature strength was determined by measurements of microhardness before and after heating of microsections in the furnace. Mating bodies for the friction machine were manufactured from St.45 with a subsequent hardening to the hardness of about *HRC* 55 and about *HRC* 60 in a hard alloy T-15. The specific pressure was set within the ranges of 10–16 MPa, the rate of test sample rotation is changed in the range of 50–1600 min^{-1}, linear rates of friction were 1600–54000 m/h. The wear of samples was measured by changing the diameter using a micrometer with a scale factor 0.01 mm and also changing the mass by weighing in beam balances MTZ No.206 (1965) with ±1 mg accuracy. To increase the accuracy the time of friction was increased.

The experiments showed that the alloying with powders of self-fluxing alloys (for example, PG-N1, PG-AN3, PG-AN6, PG-12N-02, PG-10N-01) gives a negligible (by 10 %) increase in wear-resistance in combination with a high-temperature strength (up to 700–800 °C). The hardness of alloyed layers depends on the initial hardness of the filler material and amounts to *HRC* 50–55 for materials of *HRC* 50–65 hardness. To increase the wear-, thermal and corrosion resistance the alloying with chromium was investigated. Here, the wear-resistance was increased by 4 times and hardness of the produced layers was about *HRC* 36. The high technological properties are provided by mixture of powders of chromium and relite or chromium and tungsten carbide VK6 (Figure 2) in an appropriate ratio. The best results were obtained by mixture of chromium and relite. The alloying of steels of the above-mentioned class using this mixture makes it possible to increase their resistance by an order. The hardness of the produced layers is *HRC* 50–56, their depth — 1.0–1.5 mm at the 5 mm path width (paths of alloying were deposited in spiral at 1.0–1.5 mm pitch). High-temperature strength of the layers was about 1000–1100 °C.

CONCLUSIONS

1. Laser alloying with a mixture of powders of chromium and relite provides the several times increase in the wear-resistance of hypoeutectoid complexly-alloyed steels and in their high-temperature resistance from 400 to about 1000 °C.

2. Microcracks are typical defect of the paths of alloying steels of the class being considered. To prevent them it is necessary to use preliminary or auxiliary heating of the workpiece. The best results are provided by the auxiliary HF-preheating to the temperatures of about 800 °C.

3. Except the crack formation prevention, the HF-preheating makes it possible to increase by 3–5 times the linear rate of the process without changing the laser radiation power. The peculiar features of structures of the alloyed layers enable us to state that this combined process can present interest as a separate technology.

1. Abilsiitov, G.A., Golubev, V.S., Gontar, V.G. et al. (1991) *Technological lasers*. Handbook. Ed. by G.A. Abilsiitov. Moscow: Mashinostroyeniye.
2. Velichko, O.A., Avramchenko, P.F., Molchan, I.V. et al. (1990) Laser cladding of cylindrical parts with flux-cored materials. *Avtomatich. Svarka*, **1**, 59–65.
3. Garashchuk, V.P., Shelyagin, V.D., Nazarenko, O.K. et al. (1997) Technological CO_2-laser LT 104 of 10 kW capacity. *Ibid.*, **1**, 36–39.

MICROPLASMA SPRAYING USING WIRE MATERIALS

Yu.S. BORISOV and **A.N. KISLITSA**
The E.O. Paton Electric Welding Institute, NASU, Kyiv, Ukraine

A microplasma method of coating deposition using wires has been developed. Specifications of the MPN-004 unit with an attachment for microplasma spraying using wires are presented. Parameters of the process of microplasma spraying depending on the wire material are determined. Microstructures of tungsten and copper coatings, obtained by this method, are given.

Key words: *microplasma method of coating deposition, plasmatron, spraying, plasma jet, wire materials, mechanism of wire feed, coating, microstructure*

One of the types of plasma-arc spraying is the method of coating deposition using wires as initial material [1].

Until now this coating was performed using powerful plasmatrons. For example, the plasmatron of 40 kW capacity in the UPU-8M unit performs spraying from wire materials of 0.8–1.2 mm diameter. In this case the risk of a local overheating and distortion of the item of a wall thickness ≤ 1 mm occurs. The need of plasma spraying on narrow ribs or paths leads to large losses in the material sprayed (diameter of spraying spot is usually 15–30 mm).

Analyzing the existing units [2, 3] and theoretical evaluation of feasibility of spraying wires using a microplasma jet, an attachment to the plasmatron for microplasma spraying, which makes it possible to perform process using the wire materials, has been developed at the E.O. Paton Electric Welding Institute. The attachment was used in a set with the existing MPN-004 unit designed for spraying coatings from flux-cored wires [4]. It includes a power source with a control panel, plasmatron and special device for powder feeding. Design and parameters of the plasmatron operation enable the formation of a laminar plasma jet (Raynolds number is 0.10–0.55), that specifies the peculiar features of the process:

• feasibility of decrease in size of spraying spot to 1–5 mm (angle of opening of plasma jet is only 2–6° instead of 10–18° for turbulent plasma jets and nozzle diameter ≤ 1–2 mm);

• feasibility of coating deposition on small-sized items with thin walls without excessive local overheating and distortion (low heat capacity of microplasma jets decreases the base heating);

• low level of a laminar plasma jet noise (only 30–50 dB).

Characteristic of the modified unit MPN-004 for microplasma spraying of coatings using wire materials is as follows:

Operating gas	argon
Shielding gas	argon
Capacity, kW	up to 3.0
Current, A	10–50
Voltage, V	up to 60
Consumption of plasma gas, l/h	10–150
Consumption of shielding gas, l/h	60–240
Wire diameter, mm	0.15–0.30
Wire feed speed, m/min	0.5–10.0
Dimensions, mm	390×225×205
Mass, kg	14

The peculiar feature of this unit is the presence of a compact mechanism of wire feed into the interelectrode region of the plasma jet. The wire is fed by the DC drive with the help of friction rollers. The feeding mechanism has a step (by changeable rollers) and smooth (by changing number of rotations on the electric motor shaft) adjustment of wire feed speed. It was established as a result of experiments that the stable process of spraying neutral wire by the microplasma jet is observed at higher (by 3–5 times) speeds of wire feeding as compared with traditional methods of plasma spraying using the wire materials [1, 3].

Experiments on microplasma spraying of coating were made using wires of different diameters and from different materials. Dependences of required speeds of wire feed, its diameter, consumption of plasma and shielding gases, voltage and current on the wire material were established to provide optimum conditions of spraying and formation of coatings.

Thus, for example, for steel wire of 0.3 mm diameter the optimum conditions of spraying are attained at lower values of wire feed speed, voltage, current and gas consumption as compared with a copper and nichrome wires of the same diameter. For the copper and nichrome wires the parameters of the mi-

Parameters of microplasma spraying using wire materials

Parameter	*Wire material*			
	Steel	*Copper*	*NiCr*	*W*
Wire diameter, mm	0.3	0.3	0.3	0.2
Wire feed speed, m/min	4.0–5.0	5.0–6.0	4.5–5.5	8.0–9.0
Voltage, V	30	32	32	32
Current, A	45	48	48	50
Consumption of plasma gas, l/h	90	100	100	120
Consumption of shielding gas, l/h	180	200	200	240

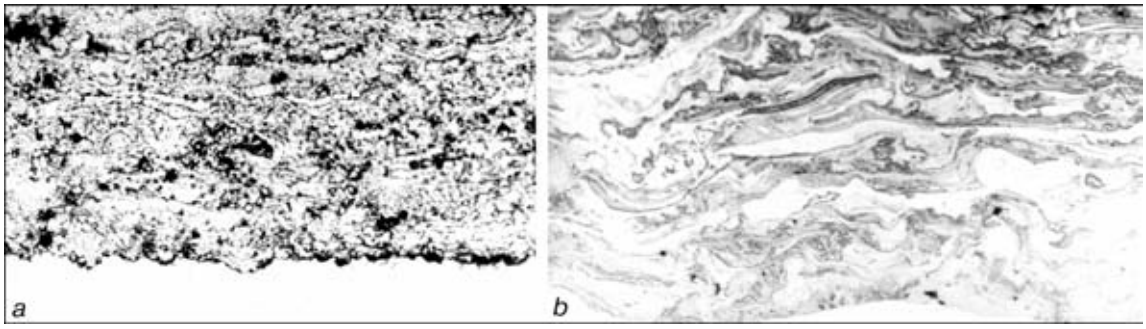

Figure 1. Microstructure of plasma coatings produced by the method of microplasma spraying of wire materials: *a* — tungsten on steel base (etched microsection) (×200); *b* — cooper on steel base (non-etched microsection) (×200)

croplasma spraying are almost similar. It was established that to provide a stable process of a microplasma spraying of wire from tungsten it is necessary to use wire of a smaller diameter (0.2 mm) and higher values of wire feed speed, voltage, current and gas consumption due to higher temperature of melting of tungsten (3395 °C) (Table)

Microstructure of plasma coatings produced in spraying tungsten and copper wires is given in Figure 1.

Coating from tungsten (Figure 1, *a*) of 1.0 mm thickness has a sufficiently dense structure, without spallings and cracks, a good adhesion to the base. The structure is lamellar. The inner structure of lamellas is fine-dispersed, columnar in some places, thickness of lamella is 5–10 μm. According to data of X-ray diffraction analysis the coating contains one phase, i.e. tungsten. Microhardness of tungsten coating is *HV* 1884–2060 MPa.

Coatings from copper (Figure 1, *b*) of 0.5 mm thickness has, the same as tungsten coating, a dense structure, without spallings and cracks, a good adhesion to the base. Structure is lamellar, heterogeneous, lamella thickness is 5–30 μm. According to X-ray diffraction analysis the basic phase is copper. There are inclusions Cu_2O and areas of eutectics $Cu + Cu_2O$. Microhardness of copper coating: for Cu — *HV* 453–613 MPa; for Cu_2O — *HV* 876–916 MPa; for eutectics $Cu + Cu_2O$ — *HV* 1000–1100 MPa.

CONCLUSIONS

1. Design of unit for microplasma spraying of coating from wire materials has been developed.

2. Complex of experiments on microplasma spraying of coating from steel, copper, tungsten and nichrome wires was made.

3. Peculiar features of microplasma spraying using wire materials were established as compared with traditional plasma spraying where wire is used as spraying material. The main peculiarity is the use of high wire feed speed in microplasma spraying.

4. Feasibility of producing coatings of thickness up to 0.5–1.0 mm with a dense structure and defect-free boundary adjacent to the base by the method of microplasma spraying using wires was shown.

1. Krasnov, A.N., Sharivker, S.Yu., Zilberberg, V.G. (1970) *Low-temperature plasma in metallurgy*. Moscow: Metallurgiya.
2. Bobrov, G.V., Privezentsev, V.I., Umnova, L.V. et al. (1969) Formation of particles in melting wire in a plasma flow. *Poroshkov. Metallurgiya*, **5**, 104–111.
3. Petrunichev, V.A., Titkov, V.V. (1977) About mechanism of plasma spraying of wire. *Fizika i Khimiya Obrab. Materialov*, **1**, 14–16.
4. Borisov, Yu.S., Vojnarovich, S.G., Bobrik, V.G. et al. (2000) Microplasma spraying of bioceramic coatings. *The Paton Welding J.*, **12**, 62–66.

Visit by the Extraordinary and Plenipotentiary Ambassador of the Russian Federation in Ukraine to the STC «E.O. Paton Electric Welding Institute» of the NAS of Ukraine

On the 21st of December 2001 the Extraordinary and Plenipotentiary Ambassador of the Russian Federation in Ukraine Mr. V.S. Chernomyrdin visited the Scientific-and-Technical Centre «The E.O. Paton Electric Welding Institute» of the NAS of Ukraine. Mr. Chernomyrdin was welcomed by the Director of the Institute Prof. B.E. Paton.

V.S. Chernomyrdin visited the PWI before, and he is well aware of many achievements of scientists of the Institute. Therefore, his primary interest was in new developments which were shown to him at the demonstration hall of the Institute. The distinguished guest expressed a great interest in samples of equipment and new technologies to be used for construction and service of main oil and gas pipelines, in space, aerospace engineering, power generation, general machine building, etc.

Mr. Chernomyrdin visited the Pilot Plant for New Technologies of the PWI, in one workshop of which the Joint Venture «Pratt & Whitney–Paton» associates demonstrated to the guests the latest of their developments in the field of electron beam deposition of thermal barrier coatings. Up to date the JV «Pratt & Whitney–Paton» has been the only enterprise in the territory of Ukraine, certified according to the international standard ISO 9001. The JV is involved in EB PVD of ceramic thermal barrier and metal protective coatings on blades of gas turbines for power and gas-pumping stations, aircraft engines, etc. In addition, the Company performs repair of blades of various-application gas turbine engines and produces ceramic and metallic materials for EB PVD.

Of high interest for the guests were the works performed by the Department for Electron Beam and Laser Welding Technology and Equipment, which, in collaboration with a number of industrial companies, develops, manufactures and supplies to different countries all over the world the advanced versatile and specialised units for EBW, and develops technologies for EBW of new materials and structures.

Then Mr. Chernomyrdin was introduced to the activities of the Institute Engineering Centres «Pressure Welding» and «Titan». The first of them is widely known for its developments in the field of flash butt welding of large-diameter pipes, railway rails, aerospace application items, etc., and the second is noted for the modern production of high-quality round ingots and slabs of titanium and its alloys by the method of electron beam melting.

Participating in the detailed discussions taking place at the EC «Titan» between Prof. B.E. Paton and the Extraordinary and Plenipotentiary Ambassador in Ukraine Mr. Chernomyrdin were Deputy Directors of the PWI Prof. S.I. Kuchuk-Yatsenko, Prof. L.M. Lobanov, Prof. K.A. Yushchenko, Prof. M.L. Zhadkevich, Dr. G.S. Marinsky, and a number of leading scientists and experts of the Institute and managers of the Pilot Pant for New Technologies.

As pointed by Prof. B.E. Paton, the last decade was noted by a marked reduction of traditional business and creative contacts of the PWI with Russian enterprises. Some movement in these contacts has shown up in the last two years. Associates of the Institute have resumed work on welded pipes at the Open Joint-Stock Companies «Chelyabinsk Pipe Rolling Factory» and «Vyksunsk Metallurgical Factory». Based on requirements of Russian enterprises of oil and gas industry, specialists of the Institute carry out works at the Khartsyzsk Pipe Plant on widening of the range and improving the quality of welded large-diameter pipes. At the end of 2001 the Institute was visited by a delegation from the Magnitogorsk Metallurgical Works headed by chief engineer E.V. Karpov. The specific plan for joint activity in different areas between PWI and MMW was developed by the results of that visit.

Although there are examples of successful cooperation with other enterprises of the Russian Federation, this is obviously not enough. Prof. B.E. Paton

expressed confidence that the visit by Mr. Chernomyrdin to the PWI would not only help to promote developments made by scientists of the Institute into the Russian market, but also would favour increase in demand of Russian enterprises for the scientific potential of the Institute.

In the course of the discussions the Parties tackled the issue of participation by the Institute scientists in events of the Year of Ukraine in Russia announced by Presidents of the two counties. It is planned that scientists of the Institute in close collaboration with the Russian Welding Society and the International Welding Council will take an active part in conferences and exhibitions held in different regions of the Russian Federation.

The Extraordinary and Plenipotentiary Ambassador of the Russian Federation in Ukraine Mr. V.S. Chernomyrdin noted a high level of innovations of R&D of the E.O. Paton Electric Welding Institute and expressed conviction that they would find application in industry of the Russian Federation. Also he expressed his sincere appreciation to Prof. B.E. Paton for the reception, discussions and the opportunity of having seen for himself the latest achievements of the STC «The E.O. Paton Electric Welding Institute».

Dr. I.A. Ryabtsev
(PWI Press Group)